Effect of Pyridine and Imidazole Functionality on Chiral Resolution, Solution Spin State and Electrochemistry within Ni (II) and Fe (II) Complexes

A

Thesis Submitted

in Partial Fulfilment of the Requirement

for the degree of

DOCTOR OF PHILOSOPHY

By

Sounak Bhattacharya

Department of Chemistry

Indian Institute of Technology Guwahati

Guwahati-781039

Dedicated to my Parents

… Sounak Bhattacharya

INDIAN INSTITUTE OF TECHNOLOGY GUWAHATI

Department of Chemistry

STATEMENT

I hereby declare that the matter embodied in this thesis is the result of investigations carried out by me in the Department of Chemistry, Indian Institute of Technology Guwahati, India under the supervision of Prof. Manabendra Ray, Professor, Department of Chemistry, Indian Institute of Technology Guwahati, India.

In keeping with the general practice of reporting observations, due acknowledgements have been made wherever the work described is based on the findings of other investigations.

May, 2021

I. I. T. Guwahati Sounak Bhattacharya

Prof. Manabendra Ray
Professor
Indian Institute of Technology Guwahati
Department of Chemistry
Tel. 91 361 258 2310
Fax.91 361 258 2349

CERTIFICATE

This is to certify that **Mr. Sounak Bhattacharya** has been working under my supervision since July 2015. I am forwarding his thesis, entitled, "**Substitution of pyridine with imidazole derivatives within Ni (II) and Fe (II) complexes and their effect on chiral resolution, solution spin state and electrochemical properties"** being submitted for the degree of Doctorate of Philosophy of this Institute. I certify that he has fulfilled all the requirements according to the rules of this Institute, and that the investigations embodied in this thesis have not been submitted elsewhere for a degree.

May, 2021
I. I. T. Guwahati

Prof. Manabendra Ray
Supervisor

Acknowledgements

I take this opportunity to express my deep sense of gratitude and indebtedness towards my supervisor Prof. Manabendra Ray, Department of Chemistry, IIT Guwahati for his guidance, tireless efforts, perpetual encouragements and moral supports at each and every step of my research work, which enable me to complete my thesis work. He helped me to recognize what was important, and made many contributions to this work. I am fortunate enough to have his teaching about how to cultivate scientific thoughts.

I would like to acknowledge my sincere gratitude to all my doctoral committee members, Prof. Gopal Das, Prof. Chandan. K. Jana and Dr. Animesh Das for their insightful advices and valuable suggestions.

I express my sincere appreciation to Prof. Biplab Mondal and his student Rakesh Mazumdar, for helping out with Variable Temperature UV-Visible using his setup.

I express my sincere appreciation to Professor C. S. Yadav and Ms. Sheetal, School of Basic Science, IIT Mandi for solid state temperature dependent magnetic measurements using AMRC facility of IIT Mandi and SAIF, IIT Bombay and Biotech Park, IIT Guwahati for the elemental analyses and other measurements.

I also express my sincere thanks to all faculty members, Department of Chemistry, IIT Guwahati for their help and encouragement.

I am thankful to the Institute, Indian Institute of Technology Guwahati for providing me with the state-of-the-art infrastructure and facilities for advanced research.

I am grateful to all non-teaching staffs of the Department for their technical support.
I would like to thank DST under FIST program for providing single crystal XRD instrument facility and Babulal Das and Prasenjit Sarkar for mounting the crystal.

The financial support from Department of Science and Technology (DST), New Delhi is duly acknowledged.

I would like to thank my former and present lab members for their timely help, support and for the wonderful time we shared during this period.

I extend my sincerest special thanks to Saikat Pal, Prasenjit Sarkar, Pritam Gupta, Shubhajit Dhara, Avik Bhanja and Shuvankar Dey, Sumanta Let, Dipanjan Bhattacharyya, Keshab Mondal, Shubra Kanti Roy, Pradip Das and Jinat Aktar for their constant help, motivation, enthusiastic company and all the wonderful time we spent in various events ever since.

At last but not least, I want to express my sincere thanks to all of my family members, especially to my Father (Mr. Debasish Bhattacharya) and Mother (Mrs. Soma Bhattacharya) for their constant encouragement, moral support during my research work and throughout life.

Sounak Bhattacharya

This thesis work stems from our quest to find a simple way to recognize an enantiomer from a racemic mixture using coordination bond. To do that, we choose to use Ni (II)(high-spin) and Fe (II) (low-spin) complexes of chiral bidentate Schiff-base ligands. Observations on Fe (II) complexes led to finding complexes that show high-spin <–––> low-spin transitions in solution. Digging deeper with more complexes along with a host of electrochemical and spectrometric tools, we ended up finding an intimate relationship between donor groups, redox potential, and spin-state. The effect of replacing pyridine with imidazole on redox and the spin-state properties discussed in the thesis is relevant to biomimetic chemistry. Imidazole group is a part of L-histidine amino acid, ubiquitous in metalloenzyme active sites. On the other hand, pyridine donor is typical in ligands related to biomimetic chemistry.

Chapter I. This chapter briefly summarizes metal complexes with Schiff bases as ligands have been playing an important part in the development of coordination chemistry as a whole and embraces very wide and diversified subjects comprising vast areas of organometallic compounds and various aspects of bioinorganic chemistry and also in the field of asymmetric catalysis. The importance of chemistry between Pyridine and Imidazole as part of an organic molecule and when coordinated to metal atom. The role of Imidazole in catalysis in various metalloenzymes and metalloproteins while pharmaceutical relevance and biomimetic complexes having Pyridine donor groups is proved to be an important area of study. Narrowing it down to Fe complexes as it changes spin-state with a change in ligand environment, geometry and temperature. Recognition in biology using non-bonded interaction as well as recognition in coordination complexes using bonded interaction is also discussed. A summary of literature on the metal complexes mostly having imidazole

and pyridine group their effect on chiral resolution, spin-state phenomena, spectroscopic and electrochemical properties have been presented and the objective of the thesis was defined.

Chapter II. In this chapter, we have transformed the racemic 1-phenylethylamine into a bidentate ligand (*rac*-L2) **1a** through Schiff-base condensation (Scheme 1). We allowed this to bind to a Ni (II) complex with other enantiopure co-ligands (*S*-L1), yielding enantiopure crystals of *fac*-Δ- $[Ni(S\text{-}L1)_2(S\text{-}L2)](ClO_4)_2$ (**1b**) in which all the chiral centers at C7, C21, and C35 have the *S*-conformation. This means that out of two enantiomers of *rac*-L2, only the *S*-L2 was found to bind in the complex. Centroid to centroid distance between phenyl rings, and either pyridine or imidazole is less than 4 Å showing π...π stacking. Groups on the chiral center are still free to interact with neighboring groups through non-covalent interactions. We expected that the coordination bond would enhance the fitting of one enantiomer better than the ionic interaction employed earlier.

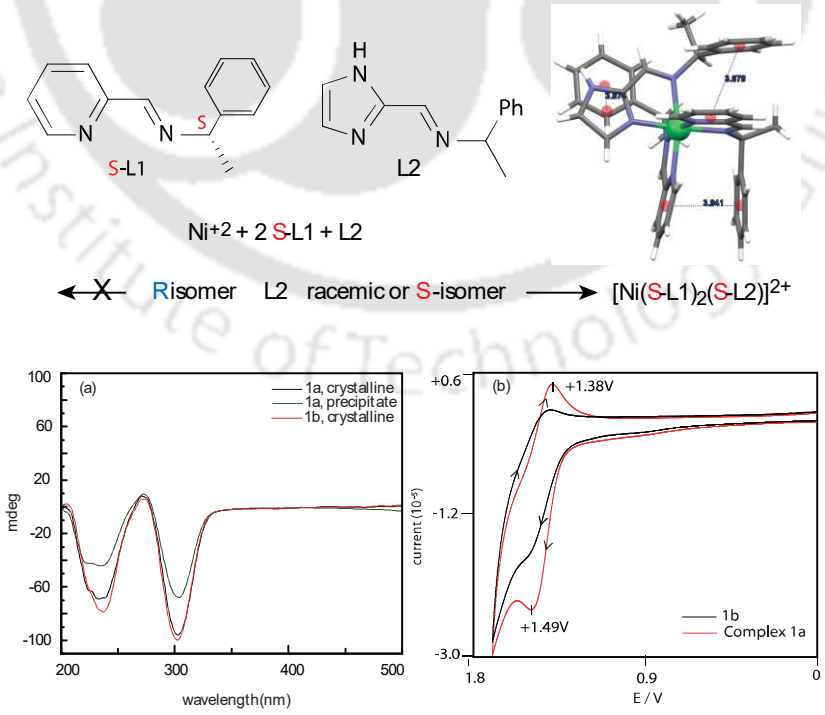

Scheme 1. Schematic representation of the reaction pathway and its circular dichroism studies showing enantiomeric excess.

Substituting *rac*-L2 with *R*-L2 in the reaction did not yield the diastereoisomer **1c** [Ni(*S*-L1)$_2$(*R*-L2)](ClO$_4$)$_2$ (Scheme 1). Instead we got an amorphous solid which was not structurally characterized. This could be due to the following possibilities; (a) loss of phenyl…imidazole interaction or (b) it is more likely that the unfavourable interactions between sterically demanding -CH$_3$ … -C-H interactions. We tried to detect the two diastereoisomer (**1b** and **1c**) electrochemically. The cyclic voltammogram of **1b** and **1c** are at the same concentration (4.2 mg/5 mL) compared (Scheme 1). The complex **1c** did not show the oxidation couple clearly perhaps due to the fact that it is a mixture. Thus, the discrimination of one enantiomer is visible in the CV, but not a clear on-off type. In the past, we used HPLC and chiral columns to calculate the enhancement in bulk, but it proved to be difficult for the Schiff base ligands in the chiral column that we have used. So, to calculate chiral enhancement, we used circular dichroism and optical rotation on **1a** [Ni(*S*-L1)$_2$(*S*-L2)](ClO$_4$)$_2$ (from racemic) using **1b** having the same molecular formula [Ni(*S*-L1)$_2$(*S*-L2)](ClO$_4$)$_2$ as an enantiopure reference compound. We observed ~91 % ee in the crystalline state and ~59% ee in the precipitated form using bulk compound measured using optical rotation and circular dichroism studies. Compared to this, only 40-60% ee in bulk crystals and no enhancement in precipitated form was achieved in our earlier report.

Chapter III. In the previous chapter, we used a kinetically labile Ni (II) complex for the chiral resolution of 1-phenylethylamine using direct metal coordination bond (Scheme 1). We observed % ee in bulk crystals within complex **1a** was found to be ~ 91% and in bulk amorphous form was found to be ~ 59%. Continuing the work, we wanted to observe the changes in enantiomeric enhancement that could happen on moving from a labile to inert complex. In this chapter we have used kinetically inert Fe (II) complexes which are diamagnetic at room temperature so we could use the

additional advantage of NMR spectroscopy in this case to monitor the speciation in solution. We have prepared the mixed ligand complex having the formula [Fe(*S*-L1)$_2$(*S*-L2)](ClO$_4$)$_2$ from three different synthetic pathways (Scheme 2). Products from reaction I and II have been structurally characterized as well.

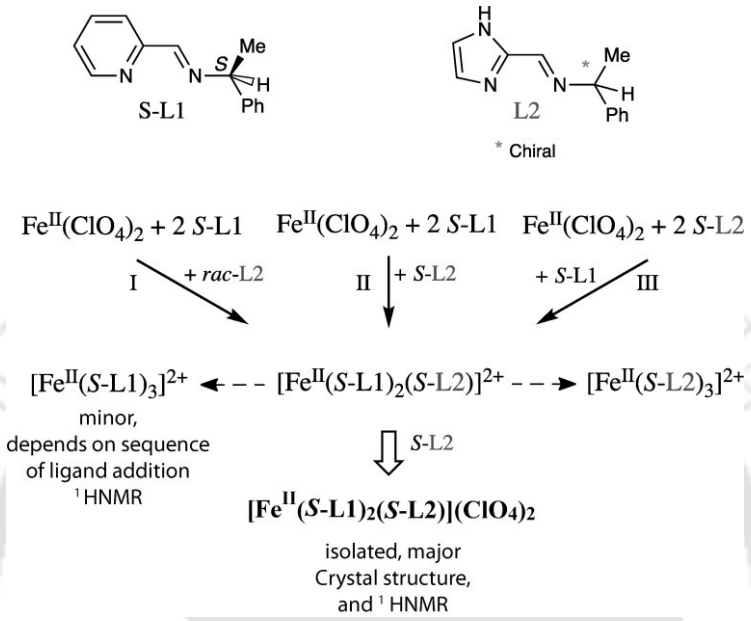

Scheme 2. Reactions I – III varying the sequence of ligand addition along with possible products.

From circular dichroism studies, chiral enhancement (*ee*) of bulk crystals of **2a** was found to be ~ 66 %, and that of the precipitated form isolated by rapid precipitation was ~ 54 %. The enhancement from bulk crystallization was relatively less than our previous report using Ni (II) complex. Analysis of ^{1}H NMR and ESI-MS of **2b** showed the presence of [Fe(*S*-L1)$_3$](ClO$_4$)$_2$, which was not observed from single crystal analysis. This could be due to the presence of homoleptic [Fe(*S*-L1)$_3$](ClO$_4$)$_2$ in equilibrium with [Fe(*S*-L1)$_2$(*S*-L2)](ClO$_4$)$_2$ in solution. The electrochemical study of this complex also showed an additional peak corresponding to the presence of [Fe(*S*-L1)$_3$](ClO$_4$)$_2$. To avoid this, we employed reaction III (Complex **2c**) by changing the synthetic sequence. This yielded the same product as **2a** and **2b**. ^{1}HNMR and cyclic voltammetric studies revealed a substantial decrease in the presence of the

homoleptic complex $[Fe(S\text{-}L1)_3](ClO_4)_2$ but we were not able to eliminate it completely from the solution (Figure 1). We infer that spin-state plays an important role in enantiomeric enhancement. We have covered the relationship of spin-state with varying donor atoms and effect on spectroscopic and electrochemical properties in a set of mononuclear Fe (II) complexes in the next two chapters.

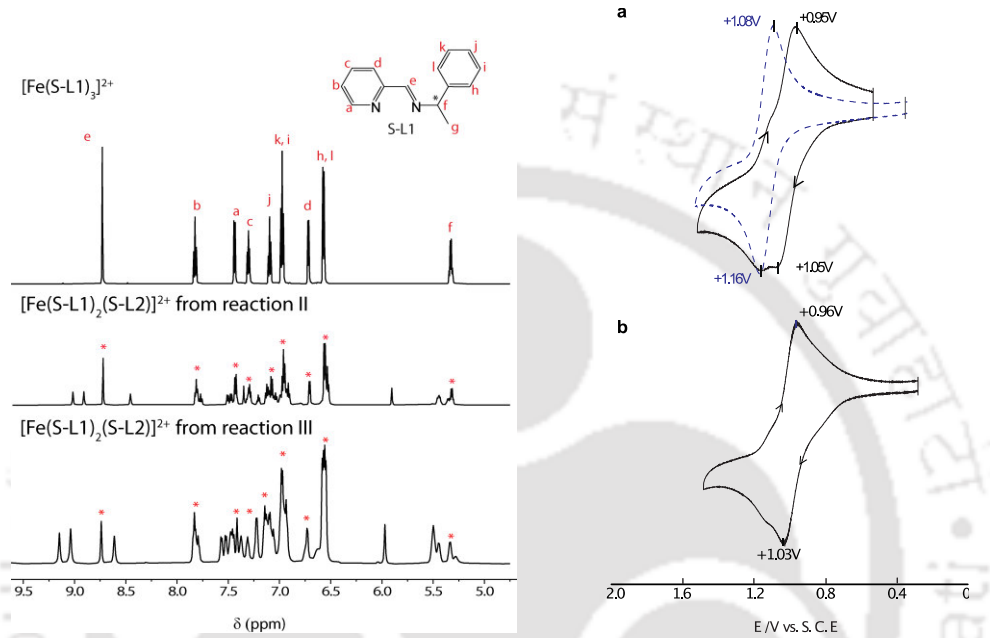

Figure 1. ^{1}H NMR spectra of homoleptic $[Fe(S\text{-}L1)_3]^{2+}$ complex and isolated products from reactions II and III of Scheme 2 in CD_3CN. The '*' marked peaks have contribution from $[Fe(S\text{-}L1)_3]^{2+}$ present in heteroleptic complex. Cyclic voltammetry of isolated products of (a) reaction I, (b) reaction II of Scheme 2 in MeCN. The redox couple of $[Fe(S\text{-}L1)_3]^{2+}$, dashed plot in (a), is overlapped to show its presence.

Chapter IV. From the previous chapter, we inferred that chiral enhancement has decreased from a high-spin labile complex to a low-spin inert complex. Solution studies have revealed a relationship between magnetic and electrochemical properties with donor atoms present. But the analysis of the Fe-mix ligand complex having the formula $[Fe(S\text{-}L1)_2(S\text{-}L2)](ClO_4)_2$ was not easy, to begin with. To simplify it and understand the dependence of donor atoms on the spin-state and electrochemical properties, we chose to synthesize and study three homoleptic tris Fe (II) complexes.

Complex **1** having pyridine-based ligand *S*-L1, Complex **2** having 2-imidazole based ligand *S*-L2 and Complex **3** having 4-imidazole based ligand *S*-L3 (Scheme 3). Out of these three, Complex **2** have been structurally characterized as well. We studied how substituting pyridine with imidazole analogues has a considerable effect on its solution magnetic and electrochemical properties. Based on this, we report that the change in redox potential is associated with an accompanying spin-state change. The difference between pyridine and imidazole analogue is quite noticeable.

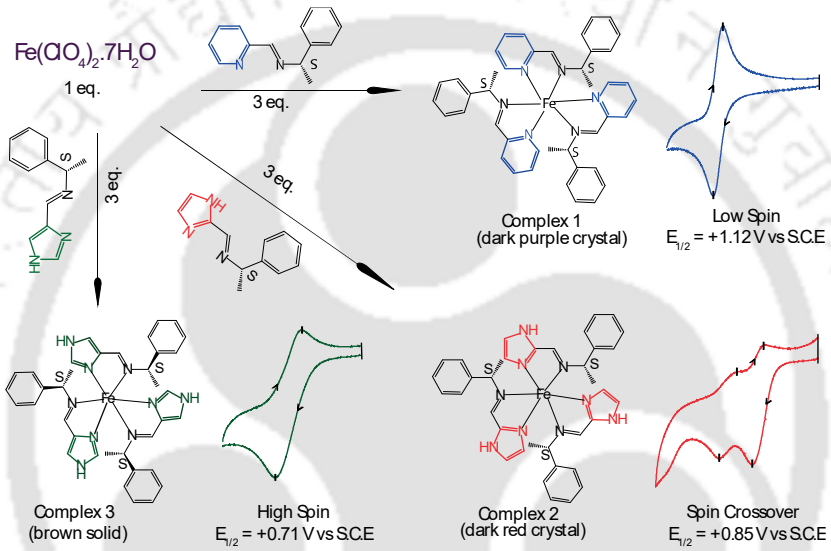

Scheme 3. Schematic representation of the homoleptic tris complexes along with their spin state and cyclic voltammograms.

X-ray structure of **2** showed that Fe-N (imidazole) bond lengths are slightly shorter than Fe-N (imine), showing a stronger interaction between the iron and the imidazolate rings. Lattice interactions included the imidazole-NH, which is H-bonded to the surrounding perchlorate anions and weakly interacted to an imidazole carbon of the neighboring molecule. Further, **2** (Figure 2b) shows two redox couples for low-spin and high-spin forms. Complex **2**, having the 2-imidazole group, showed a noticeable difference in the magnetic moment between the solid (μ_{eff} = 2.54) and solution state (μ_{eff} = 4.8). Variable temperature magnetic study in solid and in solution

revealed the spin crossover property of **2** throughout the given temperature range (4-350) K (Figure 2a).

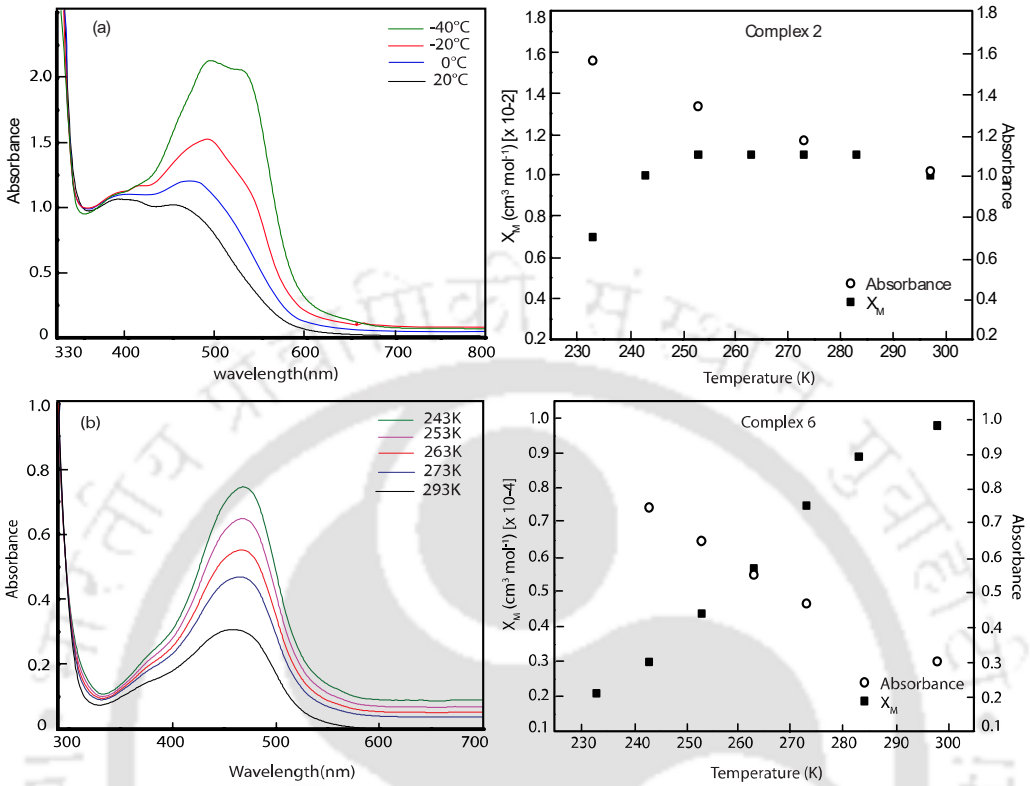

Figure 2. Complex **2** plot of **(a)** Temperature-dependent magnetic susceptibility within the range (4-350) K, **(b)** cyclic voltammogram and differential pulse voltammogram plot, **(c)** Temperature-dependent UV-visible spectrum and **(d)** comparison between temperature dependence χ_M and absorbance of the same respectively.

UV-visible studies have shown intense, less intense MLCT bands in **2** and the forbidden (*d-d*) transition corresponding to the high spin state in the solution. With a decrease in the temperature, **2** showed an increase in the MLCT band intensity, with a blue shift of ~ 40 nm (Figure 2c). The change in the spin state has been detected electrochemically as well. **2** showed two redox peaks, one at +0.85V corresponding to the high spin and one at +1.11 V corresponding to the low spin species. ΔE_p value suggests that **2** is chemically reversible but electrochemically irreversible (Figure 2d).

Chapter V. Previously we have discussed the trends in magnetic and electrochemical behavior of complexes **1-3**. Switching from pyridine to imidazole functionality, we have observed a significant change in the spin-state in solid and solution as well. **1** (pyridine donor) was found to be low-spin in solid and solution. **3**(4-imidazole donor) was found to be high-spin both in solid and solution as well. **2**(2-imidazole donor) had an intermediate spin-state in solid and a predominantly high-spin species in solution. Temperature dependant (VT-UV-visible, VT-Evan's NMR and VT- ^{1}HNMR) studies revealed the spin-crossover property of **2** both in solid and solution but it had no such effect on the spin-state of **1** and **3**. Continuing from this study, we wanted to check the validity of this study over few other set of Fe (II) complexes keeping the pyridine, 2-imidazole and 4-imidazole donor group intact and changing the amine group. This chapter has expanded our work to other compounds (**4, 7, 8** and **9**) previously synthesized by Brewer, Struch, and Howson. Complex **5** and **6** has been newly synthesized, characterized, and studied as well (Scheme 4).

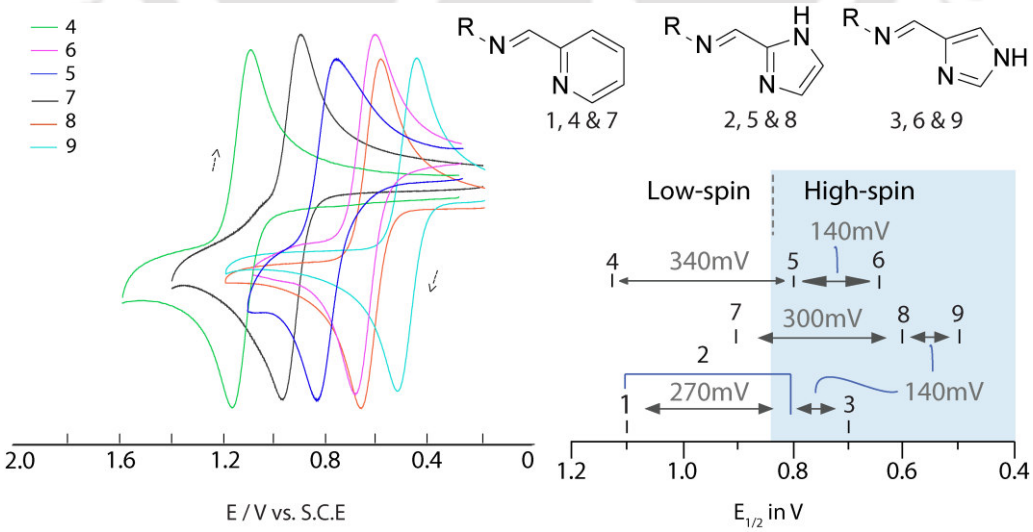

Scheme 4. The redox potential (E½) of the complexes plotted diagrammatically and, on a scale, illustrates the donor atom's effect. Complexes **1**, **4** & **7** contains pyridine, **2, 5** & **8** has 2-imidazole, and **3**, **6** & **9** has 4-imidazole donor.

Here, we discuss the spectroscopic properties of the complexes (**1**-**9**) in solution and the relationship of the redox potential with the accompanying spin-state change. 1**, 4** and **7** having the pyridine group were low spin in solution. Complex **2**, **3**, **5**, **6, 8** and **9** having 2 and 4-imidazole group were said to have more high-spin species in solution. **5, 6, 8** and **9** showed crossover property in solution as well. However, the noticeable difference from **2** is that the electronic spectra showed an increase in intensity without a shift in wavelength, and spin crossover change in solution is much faster and occurs at a relatively higher temperature (Figure 2d). We drew a relationship between potential and spin-state by plotting the potentials on a scale (Scheme 4). High-spin and low-spin complexes are in two widely different region. Differences between pyridine (low-spin) and 2-imidazole (high-spin) is accounted for a shift of ~ 300 mV and between 2-imidazole and 4-imidazole analogue, both of which are high-spin at room temperature, are lower at ~140mV. These have been reproducible for different sets (**1**-**3**, **4**-**6** and **7**-**9**) of Fe (II) complexes. Few parameters of the magnetic, spectroscopic and electrochemical data of **1**-**9** have been summarized in (Table 5.1).

Contents

Chapter I

Introduction

Schiff bases are imines having a hydrocarbyl group on the nitrogen atom $R_2C=NR'$ ($R' \neq H$) and is formed by the condensation reaction between a primary amine and an aldehyde or ketone. The metal complexes with Schiff bases as ligands have been playing an important part in the development of coordination chemistry as a whole.[1] Professor H. Schiff reported on the first synthesis of Schiff base metal complexes as early as the 1860s.[2] In the early days the main efforts were directed toward synthesis and characterization of rather fundamental complexes, which do not look striking nowadays but were strongly needed earlier. Some of typical examples included metal complexes M(II)(X-Sal-NR)$_2$, M(III)(X-Sal-NR)$_3$, and so on, where X-Sal-NR (formula II) denotes bidentate Schiff bases.[3] To cite another example, it was regarded as significant to synthesize complexes of the formula Co(X-Sal-NR)$_3$, R-i-Pr, where X = 5-Br and 5-NO_2.[4] West and coworkers synthesized heteronuclear oxo-bridged compounds of the type (porphyrin)Cr–O–M(L) from the one-electron redox reactions of CrO(porphyrin) and Fe(II), Mn(II) or Mo(IV) complexes containing ligands such as salicylideneaminates and dithiocarbamates.[5] Nowadays, the research field dealing with Schiff base metal complexes has expanded enormously, and embraces very wide and diversified subjects comprising vast areas of organometallic compounds and various aspects of bioinorganic chemistry and also in the field of asymmetric catalysis.[6]

1.1 Chiral metal salen ligand catalyst.

Salen ligands bind metal ions securely through four atoms. This tetradentate binding motif is reminiscent of the porphyrin framework in heme base oxidative enzymes. The design of the chiral manganese-salen complex was originally inspired by consideration of the oxo-transfer mechanism of heme-containing enzymes such as cytochrome P-450. However, salen derivatives are more easily synthesized than porphyrins, and their structures are more easily manipulated to create an asymmetric environment around the metal active site.[7] A few examples of chiral Metal-salen complex (M = Mn^{III}, Co^{III} and Cu^{II}) catalyst (Figure 1.1) and their functions are discussed in brief. Zhang and coworkers reported a chiral Mn^{III}-salen catalyst for the asymmetric epoxidation of simple olefins yielding both cis and trans epoxides with cis-epoxide as the major product (Figure 1.1a).[8] Chang and group thereafter prepared another chiral Mn^{III}-salen catalyst for the epoxidation of olefins but this time with

trans-epoxide as the major product (Figure 1.1b).[9] While conversion of olefins has been successful but progress in the development of catalysts for enantioselective nitrogen-group transfer to alkenes has been slow.[10] Zhen Li and coworkers prepared Cu^{II}-salen complexes for alkene aziridination with good enantioselectivity. They even showed an increase in enantioselectivity up to 90% by using Cu^{I}-Otf as a catalyst (Figure 1.1c).[11] Thomas Belser incorporated into self-assembled thiolate monolayers (SAMs) on gold colloids and coated with Co^{III} salen ligands which was an efficient method of catalytic conversion of hydrolytic kinetic resolution (HKR) of 1,2-epoxyhexane to the respective diol (Figure 1.1d).[12] Annis and coworker the synthesis of polystyrene- and silica-bound chiral Co^{III}(salen) complexes catalyzing highly efficient and enantioselective ring opening of terminal epoxides (Figure 1.1e).[13]

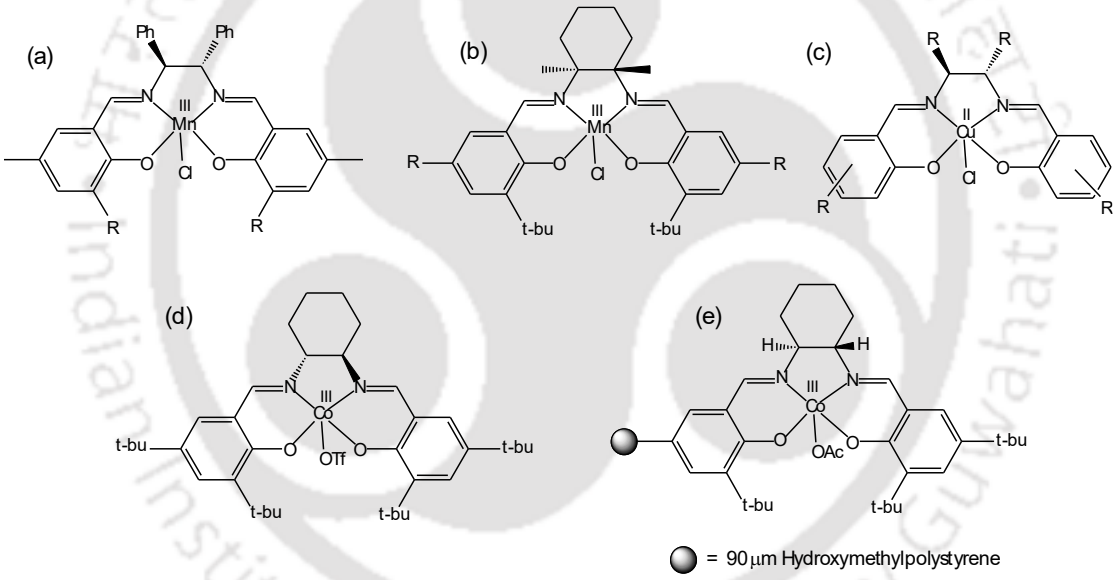

Figure 1.1. Examples of chiral Salen Schiff Base ligand metal (Mn^{III}, Cu^{II} and Co^{III}) complexes used as asymmetric catalyst.

1.2 Importance of Imidazole and Pyridine groups as a part of ligands.

1.2.1 Role of Imidazole in some metalloenzymes and metalloproteins.

The field of bioinorganic chemistry is at a propitious stage of development. R. H. Holm and E. I. Solomon classified different metalloproteins and metalloenzymes based on their structure/function analysis (e.g dismutases, oxidases and oxygenase,

nitrogenases and hydrogenases, oxotransferases, hydrolases etc.).[14] As a part of histidine, imidazole is one such functional group which is present in the active site of these proteins either as a coordinating group to the metal atom or helps in catalyzing a specific reaction.[15] This ring system is present in important biological building blocks, such as histidine and the related hormone histamine. Many drugs contain an imidazole ring, such as certain antifungal drugs, the nitroimidazole series of antibiotics, and the sedative midazolam.[16] This is the reason why it behaves both as an acid and a base at different pH range. Some of the examples of the active sites having single metal atom (e.g. Fe^{II}, Fe^{III}, Cu^{II}, Mn^{II}, Mg^{II} and Zn^{II}) is shown in (Figure 1.2.1). All of these contain Imidazole donor atom which actively takes part in catalyzing a reaction specific to that enzyme.[14]

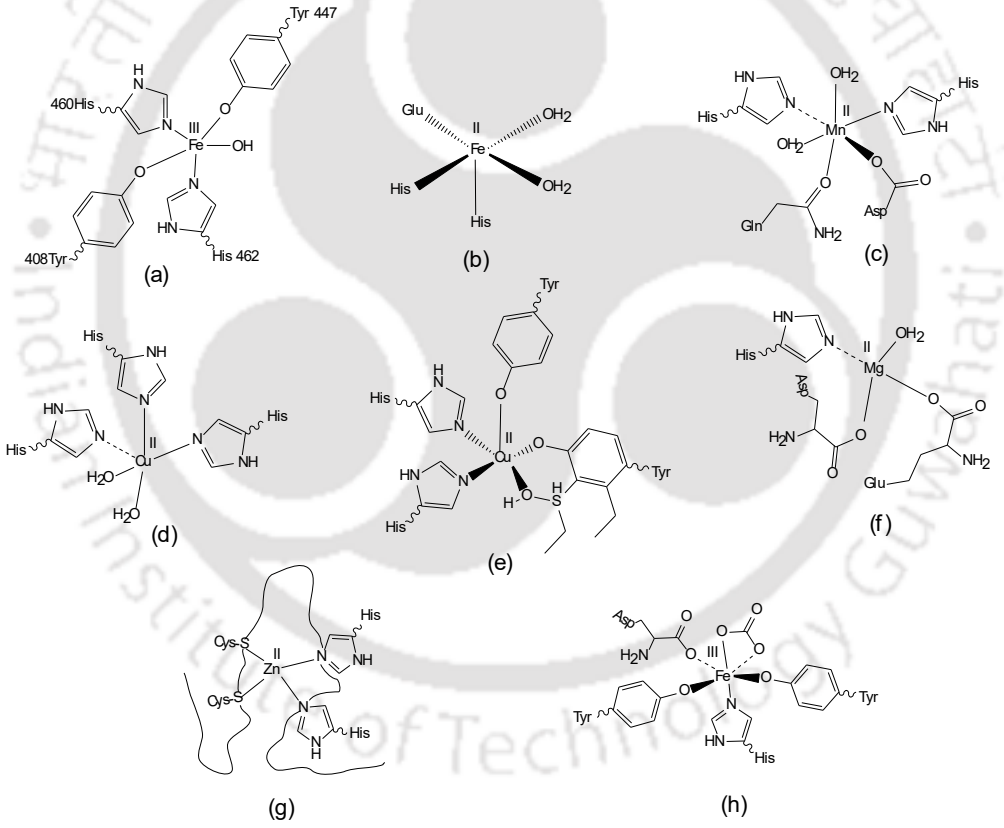

Figure 1.2.1. The active site of **(a)** protocatechuate 3,4-dioxygenase, **(b)** 2,3-dihydroxybiphenyl 1,2-dioxygenase, **(c)** isopenicillin N-synthase, **(d)** amine oxidase, **(d)** galactose oxidase, **(e)** bovine heart, **(f)** Zn-finger protein and **(g)** transferrin.

We take a few examples of biomolecules with mononuclear metal centers and discussed about their function. Protocatechuate 3,4-dioxygenase and 2,3-dihydroxybiphenyl 1,2-dioxygenase belong to the group of intramolecular

dioxygenase type of enzyme which catalyzes the oxidation of catechol to acid through dioxygen intermediate. Iron in both +2 and +3 has been used to catalyze similar reactions (Figure 1.2.1a, 1.2.1b).[17-20] Isopenicillin N-synthase, amine oxidase and galactose oxidase all belong to the oxidase type of enzymes. Their function is cyclization of secondary amine[21] (Figure 1.2.1c) and oxidation of the primary amine to respective aldehyde (Figure 1.2.1d).[22-23] It also selectively catalyzes one of the -OH of the catechol group to ketone.[24-25] Bovine heart serum which has substituted Mg^{II} where two proton transfer pathways, one for protons consumed in water formation and one for proton pumping are discussed (Figure 1.2.1e).[26] Zn(II) has a very significant, purely structural role in metallobiomolecules in addition to serving as a catalytic metal. Zinc finger proteins is one such example. Tetrahedral coordination Zn(II) results in the folding of protein minidomains which are recognized and bound to DNA. In addition to the foregoing site, $[Zn(N\hat{a}His)_2\text{-}(S\hat{a}Cys)_2]$ is a frequent structural unit in zinc fingers (Figure 1.2.1f).[27] Transferrin belong to the class of storage and transport protein whose function is to solubilize, transport, and deliver Fe^{III} ions to cells (Figure 1.2.1g).[28]

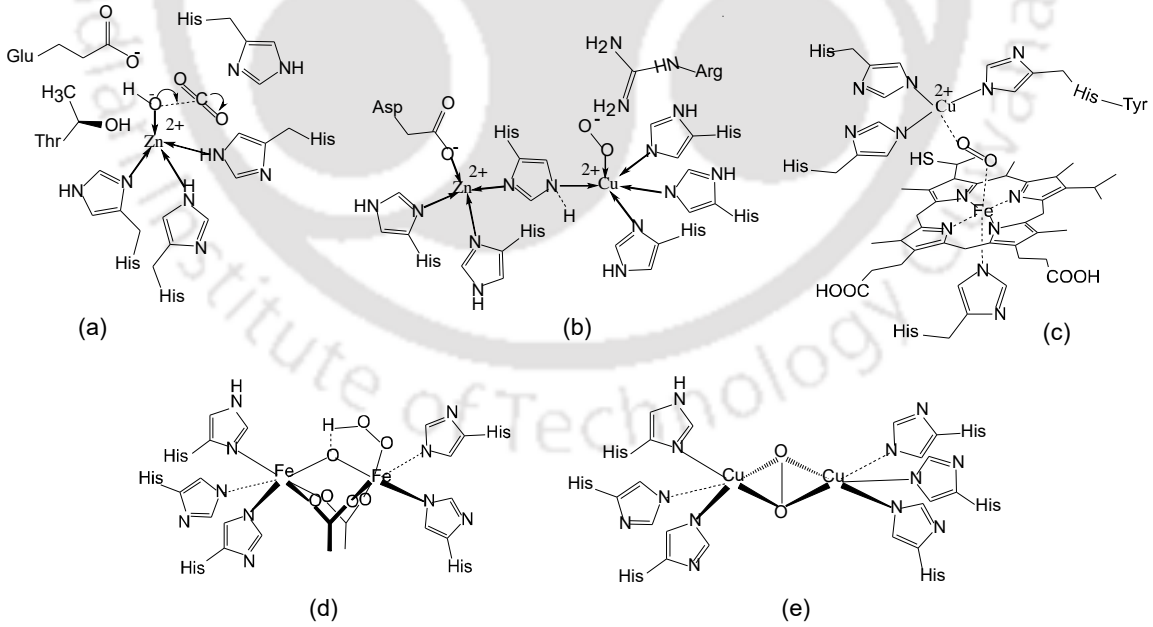

Figure 1.2.2 The active site of **(a)** carbonic anhydrase, **(b)** Cu-Zn Superoxide dismutase, **(c)** cytochrome C oxidase, **(d)** hemerythrin and **(e)** hemocyanin.

Here are some of the examples of active site of biomolecules having binuclear metal centers where we see the catalytic activity as well. Electron transfer is also an important factor in these types of mechanism. The basic nitrogen of histidine abstracts a proton from serine, threonine, or cysteine to activate it as a nucleophile. For instance, in carbonic anhydrase, a histidine proton shuttle is utilized to rapidly shuttle protons away from a zinc-bound water molecule to quickly regenerate the active form of the enzyme. (Figure 1.2.2a) Cu-Zn Superoxide dismutase Dismutation involves the conversion of superoxide into O_2 and H_2O_2. During the catalytic cycle, imidazole attracts the proton working as a base and then later on supplies the proton to ensure the release of peroxide. (Figure 1.2.2b) Imidazole group also helps in electron transfer reactions. In cytochrome C oxidase, the central Fe is hexa-coordinated with porphyrin ring equatorially and two histidine residues at the axial positions. The electron transfer redox process is assisted by the flow of electron from the t_2g orbitals of Low spin Fe (II) to π^* orbitals of the porphyrin ring. (Figure 1.2.2c) Imidazole is not only present in vertebrates but also very common in invertebrates. Hemerythrin and Hemocyanin are oxygen storage and transport proteins that are found in some invertebrates. In these proteins, metals are directly coordinated only to the imidazole group of histidine residues. This core helps the metal to directly bind with oxygen and with its transport as well in difficult conditions as well as compared to the vertebrates.[29] (Figure 1.2.2d and 1.2.2e)

1.2.2 Role of pyridine in biomimetic complexes and pharmaceutical drugs.

Simultaneously, there was development in the field of functional synthetic models and the consequent application of various spectroscopic techniques to elucidate the active site structure and the role of the metal center in catalysis.[30] Complexes with ligands containing pyridine donor are more common in biomimetic chemistry presumably due to the structural similarity between imidazole and pyridine and the ease of incorporating pyridine unit within a ligand framework.[31-32] These pyridine model complexes can also be achieved through synthesis and can be optimized to a broader range of physical conditions (pH and temperature) than more or less be quite effective to mimic with biological systems. The complexes exhibit a range of

spectroscopic parameters has been critical to assigning metalloenzyme structural and spectroscopic features. However, most of the characterized synthetic Fe complexes have used primarily N-donor supporting ligands such as tertiary amines and pyridines and O-donors like carboxylate and alkoxide functional groups to mimic the active sites respectively. Some of the ligands were designed such that it occupies most of the coordination site of the metal leaving cis positions labile sites to bind solvent and/or oxygen.[33] Lippard and coworkers reported a Fe (III)-complex which contains the quadrilateral {Fe2(μ-O)2} core believed to be present in the diiron (IV) intermediate Q of sMMOH, a remarkable enzyme that is capable of transforming methane group to methanol (Figure 1.2.3a).[34] Rybak-Akimova and group introduced electron donating substituents onto the pyridine donors a previously reported compound with the goal of stabilizing higher-valent intermediates in the catalytic cycles of these complexes, an approach previously demonstrated in diiron (IV) chemistry. Here they describe new intermediates generated from H_2O_2, and RCOOH (Figure 1.2.3f).[35] Que and group have reported a-KG-dependent enzyme taurine dioxygenase (TauD), the oxoiron(IV) moiety is postulated to be ligated by two carboxylate ligands cis to the oxo ligand while for phenylalanine hydroxylase (PheH, a pterin-dependent hydroxylase) the oxoiron(IV) species is believed to have a single bidentate carboxylate ligand cis to the oxo (Figure 1.2.3d).[36] Structural changes accompanying substrate binding to an extradiol dioxygenase. Catechol chelates asymmetrically to the iron center, a binding mode found for a mono-anionic catecholate. This feature has been assigned to one of the catecholate oxygens by comparison to the structural data for the first example of a synthetic Fe^{II} catecholate complex (Figure 1.2.3c).[37] The R-keto acid-dependent enzymes require an R-keto acid cofactor as well as Fe^{II} and O_2 for reactivity. The R-keto acid moiety can coordinate to the iron either as a monodentate or bidentate ligand. The reaction is also monitored spectroscopically with UV/vis spectra for the bidentate-bound Fe^{II}(6-Me3-TPA)-BF (Figure 1.2.3e) complex has absorbances at 544 nm (ε = 690 M^{-1} cm^{-1}) and at 590 nm (ε = 600 $M^{-1}cm^{-1}$) which are attributed to (ε = Fe (II)-to-BF) charge transfer transitions.[38] A Bleomycin model complex is proposed to coordinate to the Fe (II) center via five ligands, as shown in (Figure 1.2.3g). The sixth coordination site is therefore available to bind O_2. Spectroscopic studies following the reaction of Fe^{II}-BLM and O_2 have identified two transient species. Upon exposure to O_2, the EPR-silent, high-spin Fe^{II}-BLM.[39,40] is rapidly

converted to Fe^{II}-BLM-O_2, the Mossbauer parameters of which are most consistent with an Fe^{III}-superoxide species.[41] The advantage of using Iron is that switching of its spin-state throughout the catalytic reaction helps us to identify the intermediates and monitor the course of the reaction. Due to the flipping of the spin state $Fe^{II/III}$ positively responds to some spectroscopic techniques and negatively to others simultaneously.

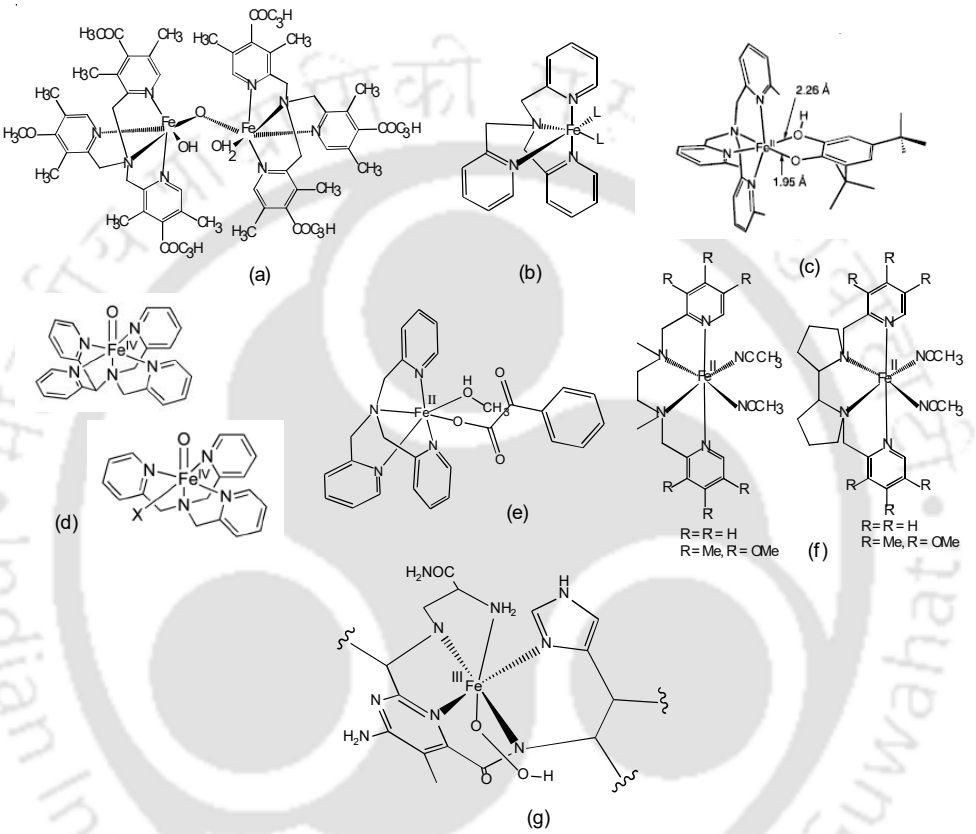

Figure 1.2.3. Pyridine incorporated ligand framework of a few biomimetic Fe-complexes.

N-containing heterocycles has been reported to be associated with a wide range of biological activity.[42] In the field of six membered heterocyclic structures, pyridine nucleus shows various properties. The high therapeutic properties of the Pyridine related drugs have encouraged the medicinal chemists to synthesize a large number of chemotherapeutic agents.[43] Flupirtine is an aminopyridine that functions as a centrally acting non-opioid analgesic that for acute and chronic pain. It is used in case of moderate to severe pain. It's muscle relaxant properties make it popular for back pain and other orthopaedical uses, but it is also used to medicate migraine pain (Figure 1.2.4a).[44] Enpirolin is used as an anti-malarial drug (Figure 1.2.4b).[44] Nikethamide is a

stimulant which mainly affects the respiratory cycle. It was used before as a medical countermeasure against tranquilizer overdoses. It is available as a short-acting over-the-counter drug combined with glucose in form of lozenges especially useful for mountain climbers to increase endurance at high altitudes (Figure 1.2.4c).[45] Indinavir does not cure HIV/AIDS, but it can extend the length of a person's life for several years by slowing the progression of the disease (Figure 1.2.4d).[46]

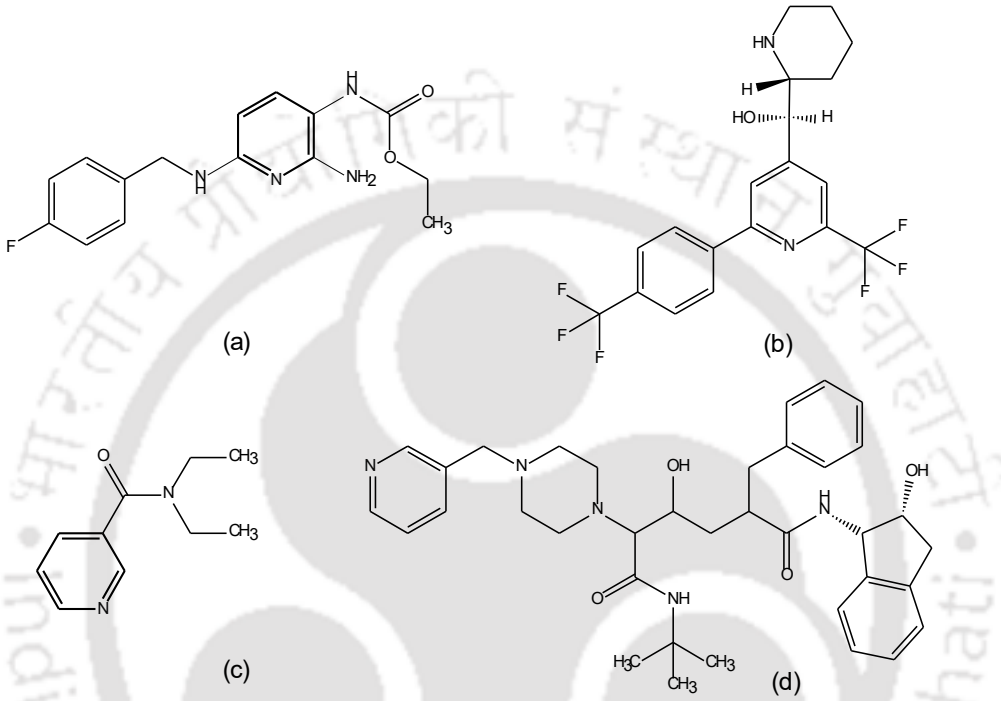

Figure 1.2.4 Pyridine containing therapeutic drugs **(a)** Flupirtine, **(b)** Enpirolin, **(c)** Nikethimide and **(d)** Indinavir.

1.3. Spin-crossover phenomena in some mononuclear Fe (II) complexes.

Spin-crossover compounds are becoming increasingly popular for device and sensor applications, and in soft materials, that make use of their switchable colour, paramagnetism and conductivity. Spin-crossover is most commonly observed in six-coordinate iron (II) complexes.[47] As we intend to use simple metal complexes of Schiff-base ligands, we have narrowed down our focus on mononuclear Fe (II) bidentate and tridentate Schiff base complexes (Figure 1.3). We found that some of the iron complexes with these ligands have interesting electrochemical, spin-state, and spectroscopic properties.

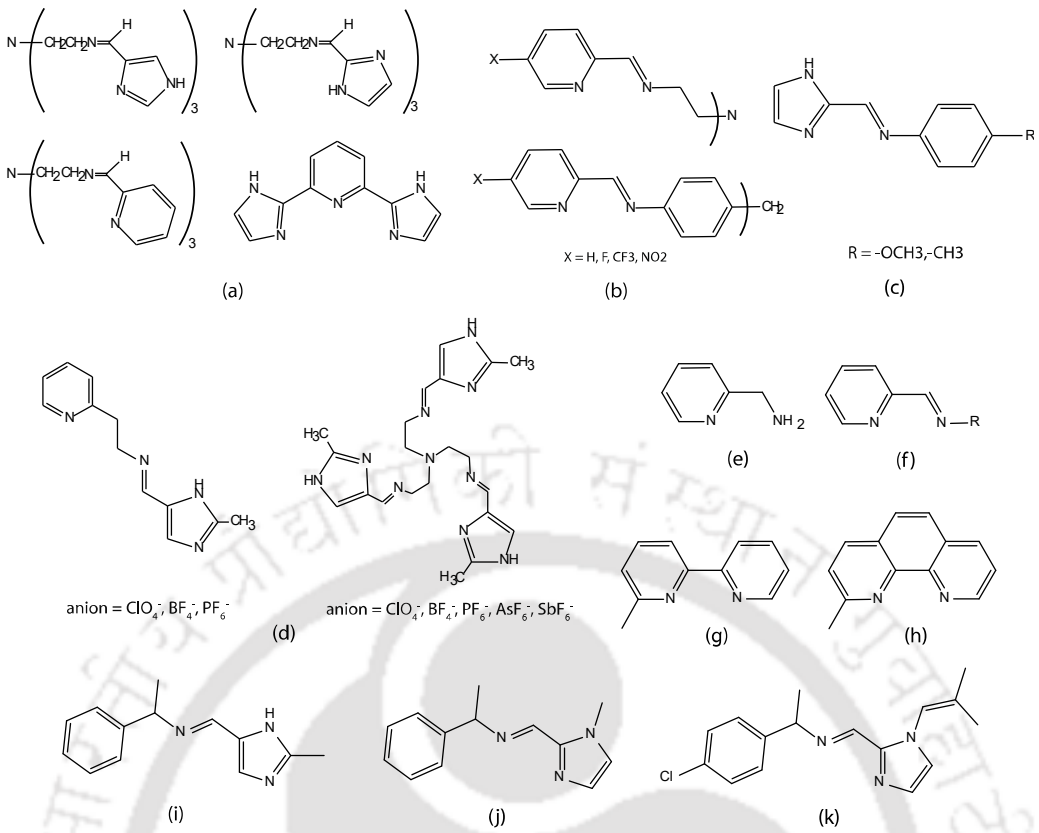

Figure 1.3. A few examples of mononuclear spin crossover Fe (II) complexes with Schiff Base ligands having imidazole and pyridine donors.

Katz and co-worker reported a room temperature crystal structure determination of mononuclear [Fe(II)aminoethylpyridine]I_2 showed that its asymmetric unit contains a 1:1 mixture of the fac and mer isomers of the complex (Figure 1.3e).[48] The mer molecule in the crystal is high-spin, while the Fe–N bond lengths in the fac molecule imply that it is predominantly low-spin. Maeda and group prepared compound $[Fe^{II}(L)_3][ClO_4]_2$ shows a gradual thermal spin-transition centred near 160 K, that is 70% complete at 5 K from susceptibility and Mossbauer measurements (Figure 1.3f).[49] Onggo and Harris and their coworkers altered the reduction in ligand field required to afford a spin-transition centre with this ligand type by substitution at the 6-position of one of the pyridyl rings, as in $[FeL_3]^{2+}$ (Figure 1.3g, 1.3h).[50-51] This induces steric repulsion within the coordination shell, making the high-spin state (with its longer Fe–N bonds) more favourable. Sunatski and group reported a homochiral spin crossover iron (II) complex, fac-Λ was synthesized and its crystal structures in both the high-spin (HS) and low-spin (LS) states were determined which showed abrupt crossover at $T_{1/2}$ ~ 195 K (Figure 1.3i).[52] Gu and coworkers on the other hand

reported a similar ligand with a different substitution yielding both fac-Λ (using S-isomer)and fac-Δ (using R-isomer) homochiral crystals which showed crossover property at $T_{1/2}$ ~ 370 K (Figure 1.3g).[53] Ling also reported a Fe (II) SCO fac complex with $T_{1/2}$ ~ 375K (Figure 1.3k).[54] Struch and coworkers showed that changing electronic properties and tuning the spin-state set of Fe (II) with electron-deficient pyridylimine ligands have resulted in a change in their supramolecular chemistry (Figure 1.3a).[55] Naohide and coworkers showed anion-dependent one-dimensional and two-dimensional Spin-Crossover in Iron (II) complexes bridged by cooperative intermolecular interactions (Figure 1.3b).[56] Brachňaková and coworkers Low-spin and spin-crossover Iron (II) complexes with pyridyl-benzimidazole ligands. They have reported thermal and light-induced spin-state switching of the compounds in solid-state accompanied with their redox potential (Figure 1.3d).[57] Kruger and coworkers had reported the solvent-dependent spin-crossover in Imidazolylimine Fe (II) Complexes and the effect on its photomagnetic properties (Figure 1.3c).[58] Solid-state studies on these have been quite common and well documented. Solution properties especially spin-state in solution, and electrochemical properties on these complexes, are fewer.

1.4 Importance of Chirality and how recognition in Biology

Stereoisomers are isomers that differ in spatial arrangement of atoms, rather than order of atomic connectivity. One of their most interesting type of isomer is the mirror-image stereoisomers, a non-superimposable set of two molecules that are mirror image of one another. The existence of these molecules is determined by concept known as chirality (Figure 1.4.1).

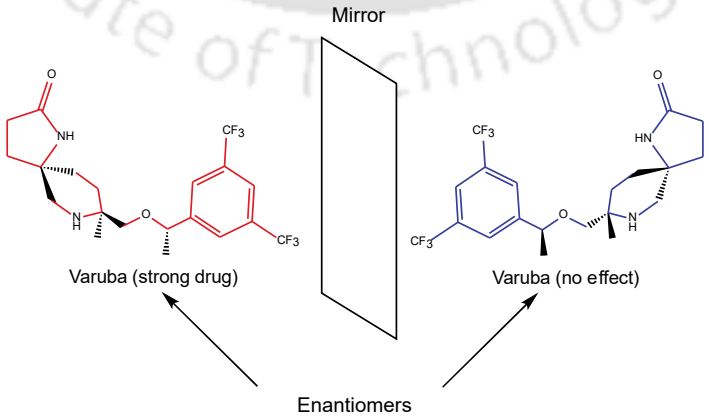

Figure 1.4.1. A pair of enantiomers where one is more potent drug than the other.

Recognition in biology is omnipresent as a result of interactions occur between a host and an incoming guest molecule. It takes place when one of the enantiomers is preferred over the other due to the formation of a favored host-guest adduct. The interactions between host guest is mainly due to a combination of strong and weak non-covalent interactions. Theoretically recognition results because of the differences in Gibbs free energy between the two diastereoisomeric enantiomer-selector complexes.[59-62] In recognition, there are four types commonly known non-bonded interactions.[63-65] namely hydrogen bonds, ionic bonds, van der Waals forces and hydrophobic interaction. These are mostly responsible for the three-dimensional structure of large molecules, such as proteins and enzymes. A recognition site of adrenaline molecule shows a combination of electrostatic interactions, H-bonding and aromatic π-interactions with the β_2-adrenergic receptor comprising of amino acid residues (Figure 1.4.2).[66-70]

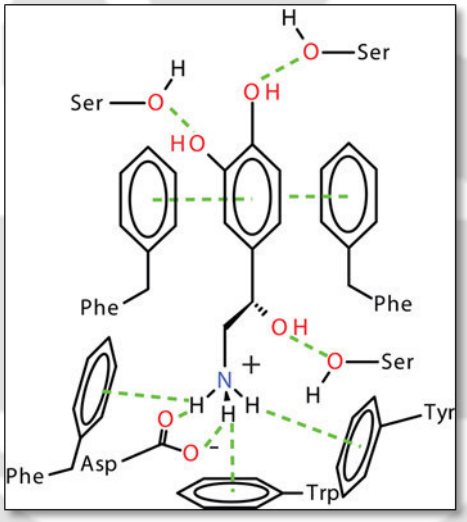

Figure 1.4.2. Non-covalent interactions between noradrenaline and the β_2-adrenergic receptor.[68]

1.5 Chiral Recognition by supramolecular cages and Host-guest complex using non-bonded interactions.

Synthetic supramolecular assemblies have demonstrated their ability to encapsulate organic guests based on their size, shape, and functional group complementarity.[71-74] The encapsulation of chiral organic guest molecules into chiral cage like host structures has been reported to proceed with moderate to good diastereoselectivity.[75-78]

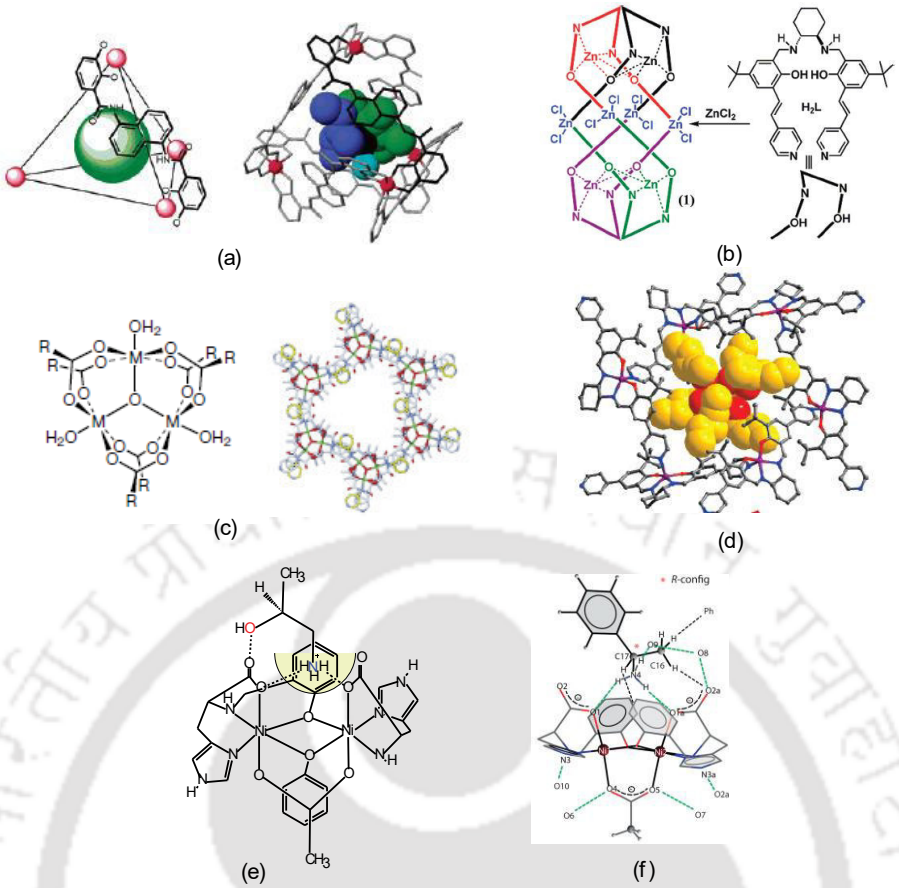

Figure 1.5. Chiral recognition of few metal complexes using bonded interactions.

Raymond and group report here the encapsulation of organometallic complexes which have been reported to be catalytically active, into a chiral, well-defined cavity. The encapsulations of the chiral ruthenium complexes proceed with diastereoselectivities up to 70% (Figure 1.5a).[79] Yong Cui an coworkers report here the assembly of a homochiral helicate cage from the pyridyl-functionalized salen ligand and $ZnCl_2$. The cage exhibits enantioselective luminescence enhancement by chiral amino acids, and its crystalline samples can serve as hosts for adsorption separation of racemic organic molecules (Figure 1.5b).[80] Kim and group reported an enantiopure chiral organic building block, which can be easily synthesized from D-tartaric acid, reacts with Zn^{2+} ions to produce a homochiral open-framework solid whose formula is given as $[Zn_3(\mu_3\text{-}O)(1\text{-}H)_6].2H_3O.12H_2O$ (Figure 1.5c).[81] Gao Li and group reported the efficient assembly of a nanotubular supramolecular structure based on hexametallic Zn-macrocycles. Chiral channel and hydrophobic functionality make it an excellent host to recognize and separate racemic alcohols with high enantioselectivity up to 99.5% (Figure 1.5d).[82] Ray and group showed the chiral

resolution of 1-phenylethylamine with an enhancement of (40-60 % *ee*) in bulk crystals and amino alcohol with an enhancement of (93-100 % *ee*) using a binuclear Ni (II) anionic host (Figure 1.5e, 1.5f).[83]

1.6 Chiral Recognition by metal complexes through bonded interactions.

While more focus has been given to recognition through non-covalent interactions as it is closer to what happens in biology, examples of recognition using covalent interactions is less in comparison. However, in recent years transition-metal complexes have been extensively used in recognition and asymmetric catalytic transformations of racemic, prochiral, and optical substrates to yield single-enantiomer compounds through bonded interactions.[84-86] Chin and others used kinetically inert cobalt (III) complexes to show different chiral interactions that change the rate of epimerization(Figure 1.6e).[87] Willock and coworkers reported the asymmetric interaction of the chiral amines (R-/S-methylbenzylamine) with the chiral [Cu(1,2)] complexes was revealed by CW EPR and DFT. The spectroscopic data revealed that only one MBA substrate bound weakly to the copper complexes having 86:14 preference for the heterochiral adducts (RR-S and SS-R) in [Cu(1)] (Figure 1.6b).[88] Imai and group reported a chiral water-soluble Zn-porphyrin was optically resolved, and the binding data with amino carboxylates indicated that this porphyrin shows chiral recognition (Figure 1.6a).[89] Shionoya and others recognized D-phenylglycine over corresponding L-enantiomer (20 % ee) within a mixed ligand environment around cobalt (III) complex (Figure 1.6c).[90] Ye and others recognized chiral bidentate sulphoxides using an enantiopure Ir (III) complex (Figure 1.6f).[91] Li and group reported A pair of 2D chiral coordination polymers were constructed through the self-assembly of a chiral metal-camphor-10-sulfonate salt and a bidentate linker, which show selective inclusion of S and R enantiomers of 1-phenylethanol respectively with an enantioselectivity of 9:1 (Figure 1.6d).[92]

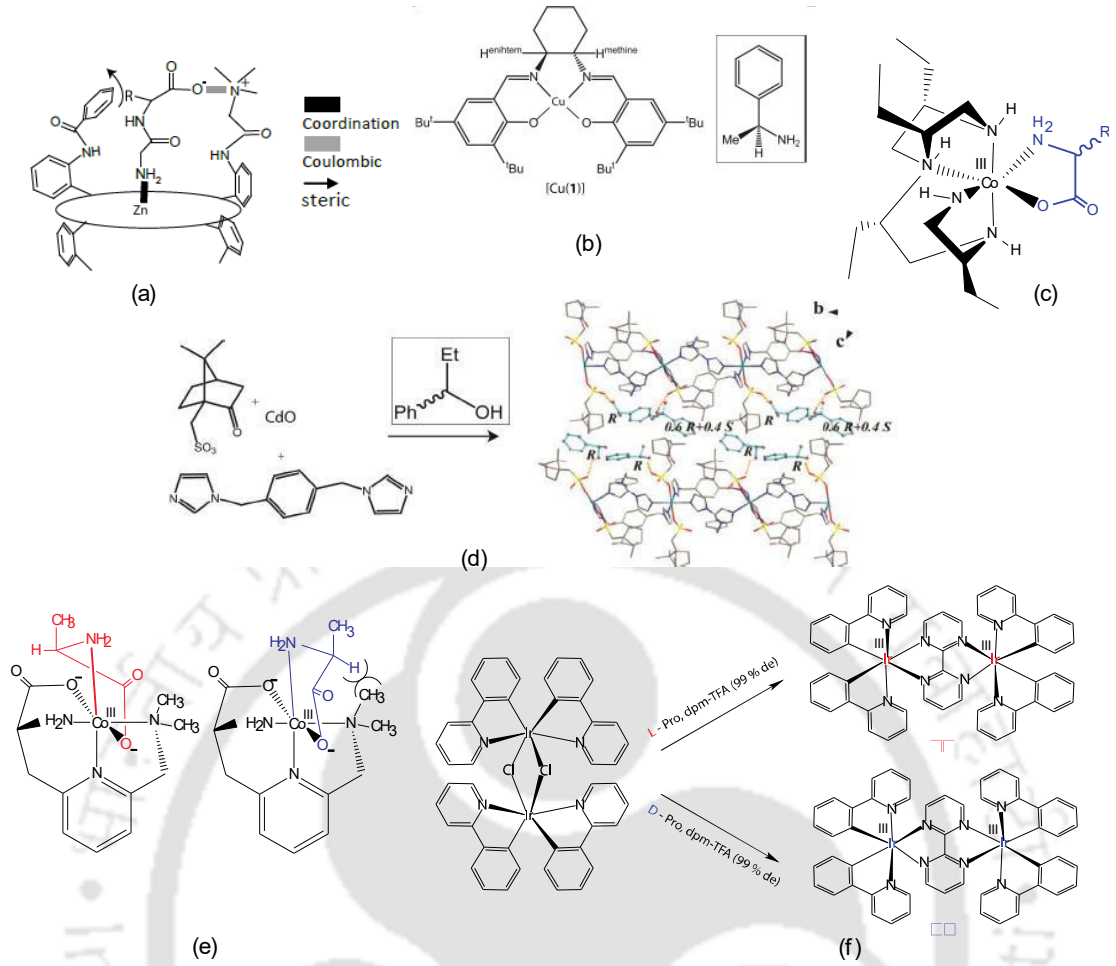

Figure 1.6. Chiral recognition of few metal complexes using bonded interactions.

1.7. Conclusions from the literature survey and objectives of the thesis

From the survey of literature, Firstly, we observed the importance of Schiff base ligand complexes with transition metals and understanding their cooperative relationship in catalysis. During many biocatalytic reactions, Fe-complexes especially Fe (II) changes its spin-state (HS⇌LS) based on the ligand environment, geometry and other thermodynamic parameters. Secondly, imidazole functionality is very important in biological active sites.[14-15] Many pyridine and imidazole containing biomimetic intermediate have been stabilized and studied extensively. Pyridine has been a part of many clinical drugs and still used as precursors in preparing drug molecule.[30-32, 42-43] Lastly, recognition of a single enantiomer from their racemic mixture through non-covalent interaction is also very important in biology and drug industry.[59-65] Recognition metal complexes using bonded interaction in biology might be less important but its an important tool to understand the binding mode, geometry and mechanism. Combining these factors, we chose to understand the chemistry

between imidazole and pyridine donor group as a part of chiral Schiff Base ligands with their respective mononuclear Ni(II) and Fe(II) complexes. The literature survey lacks a comparative study between imidazole and pyridine functionality in coordination complexes. A detailed study on their chiral recognition, spin-crossover and spectroscopic behavior within metal complexes having similar coordination environment were found to be rare in literature.

Based on these facts, the set objectives of this thesis are:

- Synthesizing both chiral and achiral bidentate Schiff base having either pyridine or imidazole group as the donor atom with their respective sets of Ni(II) and Fe(II) mononuclear complexes for our study.

- We tried to improve the enantiomeric enhancement of 1-phenylethylamine by using a different approach and transformed the chiral amine into its Schiff base form using both imidazole and pyridine aldehyde. Keeping the pyridine containing imine and the metal as the host, we tried to recognize the incoming imidazole containing imine from its racemic mixture using covalent bond formation. Not only this we even tried to understand the difference and assign the problems that have raised between a kinetically labile Ni (II) complex and a kinetically inert Fe (II) complex in a mixed ligand environment.

- From the chiral resolution studies, we infer that chiral enhancement does depend on the spin-state of Fe (II) inert complexes. We prepared a set of homoleptic Fe (II) complexes having different spin-state (LS, HS and SCO) based on different coordination environment (keeping pyridine and imidazole intact). Our main focus was as to how these complexes' magnetic, electronic and electrochemical behave in solution with respect to the change in donor atom and temperature. This study is also complimented by solid state magnetic study as well.

References

1. Yamada, S. Advancement in stereochemical aspects of Schiff base metal complexes. *Coord. Chem. Rev*. **1999**, *190*, 537.

2. (a) Schiff, H. *Ann. Chem. Suppl*. **1864**, *3*, 343. (b) Schiff, H. *Ann. Chem*. **1869**, *150*, 193. (c) Schiff, H. Ann. Chem. **1869**, *151*, 186.

3. (a) West, B. O. Rev. Pure Appl. Chem. **1960**, *10*, 207. (b)West, B. O. *J. Chem. Soc.* **1952**, 3115. (c) West, B. O. *J. Chem. Soc*. **1960**, 4944. (d) Van den Bergen, A.; Murray, K. S.; O'Connor, M. J.; West, B. O. *Aust. J. Chem*. **1969**, *22*, 39.

4. Yamada, S.; Ohno, E.; Yamanouchi, K.; *Bull. Chem. Soc. Jpn*. **1968**, *41*, 535.

5. (a) Elliott, R. E.; Nichols, P. J.; West, B. O. Synthesis of Heterobinuclear Oxo-Bridged Compounds of Chromium, Iron, Manganese and Molybdenum. *Aust. J. Chem*. **1986**, *39*, 975. (b) Elliott, R. E.; Nichols, P. J.; West, B. O. The synthesis of heterobinuclear μ-oxo complexes containing Cr–O–Mn, Cr–O–Mo, Mo–O–Fe, and Cr–O–Fe combinations. *J. Chem. Soc. Chem. Commun*. **1986**, 840.

6. Toscano, P. J.; Marzilli, L. G. *Prog. Inorg. Chem*. **1984**, *31*, 105.

7. P. Yoon, T.; Jacobsen, E. N. Privileged Chiral Catalysts. *Science*, **2003**, *299*, 1691.

8. Zhang, W.; Jacobsen, E. N. Asymmetric Olefin Epoxidation with Sodium Hypochlorite Catalyzed by Easily Prepared Chiral Mn (III) Salen Complexes. *J. Org. Chem*. **1991**, *56*, 2296.

9. Chang, S.; Galvin, J. M.; Jacobsen, E. N. Effect of Chiral Quaternary Ammonium Salts on (salen)Mn-Catalyzed Epoxidation of cis-Olefins. A Highly Enantioselective, Catalytic Route to Trans-Epoxides. *J. Am. Chem. Soc*. **1994**, *116*, 6937.

10. (a) Deyrup, J. A. In Heterocycles·, Hassner, A., Ed.; Wiley: New York, **1983**; Vol. *42*, Part 1, p 1. (b) Padwa, A.; Woolhouse, A. D. In Comprehensive Heterocyclic Chemistry·, Lwowski, W., Ed.; Pergamon Press: Oxford, **1984**; Vol. *7*.

11. Li, Z.; Conser, K. R.; Jacobsen, E. N. Asymmetric Alkene Aziridination with Readily Available Chiral Diimine-Based Catalysts. *J. Am. Chem. Soc*. **1993**, *115*, 5326.

12. Belsera, T.; Jacobsen, E. N Cooperative Catalysis in the Hydrolytic Kinetic Resolution of Epoxides by Chiral [(salen)Co(III)] Complexes Immobilized on Gold Colloids. *Adv. Synth. Catal.* **2008**, *350*, 967.

13. Annis, D. A.; Jacobsen, E. N. Polymer-Supported Chiral Co(Salen) Complexes: Synthetic Applications and Mechanistic Investigations in the Hydrolytic Kinetic Resolution of Terminal Epoxides. *J. Am. Chem. Soc*. **1999**, *121*, 4147.

14. Holm, R. H.; Kennepohl, P.; Solomon, E. I. Structural and Functional Aspects of Metal Sites in Biology. *Chem. Rev.* **1996**, *96*, 2239.

15. Ingle, R. A.; Histidine Biosynthesis. 2011 The Arabidopsis Book Vol. 9.

16. (a) Karitzky, A. R.; Rees, C.W.R.; Scriven, E.F.V. Comprehensive Heterocyclic Chemistry. 1984, 469. (b) Grimmett, M. R. Imidazole and Benzimidazole Synthesis. 1997, Academic Press. (c) Brown, E. G. Ring Nitrogen and Key Biomolecules. 1998, Kluwer Academic Press. (d) Pozharskii, A. F.; et al. Heterocycles in Life and Society. 1997, John Wiley & Sons. (e) Gilchrist, T. L. (1985). Heterocyclic Chemistry. 1985, Bath Press.

17. Ohlendorf, D. H.; Lipscomb, J. D.; Weber, P. C. Structure and assembly of protocatechuate 3,4-dioxygenase. *Nature*, **1988**, *336*, 403.

18. Howard, J. D.; Rees, D. C. Perspectives on Non-Heme Iron Protein Chemistry. *Adv. Protein Chem*. **1991**, *42*, 199.

19. Ohlendorf, D. H.; Orville, A. M.; Lipscomb, J. D. Structure of Protocatechuate 3,4-Dioxygenase from Pseudomonas aeruginosa at 2.15 Å Resolution. *J. Mol. Biol*. **1994**, *244*, 586.

20. Han, S.; Eltis, L. D.; Timmis, K. N.; Muchmore, S. W.; Bolin, J. T. Crystal structure of the biphenyl-cleaving extradiol dioxygenase from a PCB-degrading pseudomonad. *Science*. **1995**, *270*, 976.

21. Roach, P. L.; Clifton, I. J.; Fu¨ lo¨p, V.; Harlos, K.; Barton, G.; Hajdu, J.; Andersson, I.; Schofield, C. J.; Baldwin, J. E. Crystal structure of isopenicillin N synthase is the first from a new structural family of enzymes. *Nature*. **1995**, *375*, 700.

22. Parsons, M. R.; Convery, M. A.; Wilmot, C. M.; Yadav, K. D. S.; Blakeley, V.; Corner, A. S.; Phillips, S. E. V.; McPherson, M. J.; Knowles, P. F. Crystal structure of a quinoenzyme: copper amine oxidase of Escherichia coli at 2 Å resolution. *Structure*, **1995**, *3*, 1171.

23. Cumar, V.; Guss, J. M.; McGuirl, M. A.; Dooley, D. M.; Freeman, H. C. *Structure*.

24. Ito, N.; Phillips, S. E. V.; Stevens, C.; Ogel, Z. B.; McPherson, M. J.; Keen, J. N.; Yadav, K. D. S.; Knowles, P. F. Novel thioether bond revealed by a 1.7 Å crystal structure of galactose oxidase. *Nature*. **1991**, *350*, 87.

25. Messerschmidt, A.; Ladenstein, R.; Huber, R.; Bolognesi, M.; Avigliano, L.; Petruzzelli, R.; Rossi, A.; Finazzi-Agro´, A. Refined crystal structure of ascorbate oxidase at 1.9 Å resolution. *J. Mol. Biol.* **1992**, *224*, 179.

26. Tsukihara, T.; Aoyama, H.; Yamashita, E.; Tomikazi, T.; Yamaguchi, H.; Shinzawa-Itoh, K.; Nakashima, R.; Yaono, R.; Yoshikawa, S. Structures of Metal Sites of Oxidized Bovine Heart Cytochrome c Oxidase at 2.8 Å. *Science*. **1995**, *269*, 1069.

27. Fairall, L.; Schwabe, J. W. R.; Chapman, L.; Finch, J. T.; Rhodes, D. The crystal structure of a two zinc-finger peptide reveals an extension to the rules for zinc-finger/DNA recognition. *Nature*. **1993**, *366*, 483.

28. Bailey, S.; Evans, R. W.; Garratt, R. C.; Gorinsky, B.; Hasnain, S.; Horsburgh, C.; Jhoti, H.; Lindley, P. F.; Mydin, A.; Sarra, R.; Watson, J. L. Molecular Structure of Serum Transferrin at 3.3-Á Resolution. *Biochemistry*. **1988**, *27*, 5804.

29. Bertini, I.; Gray, H. B.; Lippard, S. J.; Valentine, J. S. *Bioinorganic Chemistry*. **1994**. University Science Books, Mill Valley, CA.

30. Que, L. Jr.; Raymond, Y. N. Ho. Dioxygen Activation by Enzymes with Mononuclear Non-Heme Iron Active Sites. *Chem. Rev*. **1996**, *96*, 2607.

31. Costas, M.; Mehn, M. P.; Jensen, M. P. Que, L. Jr. Dioxygen Activation at Mononuclear Nonheme Iron Active Sites: Enzymes, Models, and Intermediates. *Chem. Rev.* **2004**, *104*, 939.

32. Jasniewski, A. J.; Que, L. Jr. Dioxygen Activation by Nonheme Diiron Enzymes: Diverse Dioxygen, Adducts, High-Valent Intermediates, and Related Model Complexes. *Chem. Rev*. **2018**, *118*, 2554.

33. Zang, Y.; Kim, J.; Dong, Y. H.; Wilkinson, E. C.; Appelman, E. H.; Que, L., Jr. Models for Nonheme Iron Intermediates: Structural Basis for Tuning the Spin States of Fe (TPA) Complexes. *J. Am. Chem. Soc*. **1997**, *119*, 4197.

34. Do, L. H.; Xue, G.; Que, L. Jr.; Lippard, S J. Evaluating the Identity and Diiron Core Transformations of a (μ-Oxo) diiron (III) Complex Supported by Electron-Rich Tris(pyridyl-2-methyl) amine Ligands. *Inorg. Chem*. **2012**, *51*, 2393.

35. Makhlynets, O. V.; Oloo, W. N.; Moroz, Y, S.; Belaya, I, G.; Palluccio, T. D.; Filatov, A. S.; Mu¨ller, P.; Cranswick, M. A.; Lawrence Que, L. Jr.; Rybak-Akimova.; E V. H2O2 activation with biomimetic non-haem iron complexes and AcOH: connecting the g = 2.7 EPR signal with a visible chromophore. *Chem. Commun*., **2014**, *50*, 645.

36. McDonald, A. R.; Guo, Y.; Vu, V. V.; Bominaar, E. L.; M€unck, E.; Que, L. Jr. A mononuclear carboxylate-rich oxoiron(IV) complex: a structural and functional mimic of TauD intermediate 'J'. *Chem. Sci.,* **2012**, *3*, 1680.

37. Chiou, Y. M.; Que, L., Jr. Structure of a Mononuclear Iron (II)-Catecholate Complex and Its Relevance to the Extradiol-Cleaving Catechol Dioxygenases. *Inorg. Chem.* **1995**, *34*, 3577.

38. Ha, E. H.; Ho, R. Y. N.; Kisiel, J. F.; Valentine, J. S. Modeling the Reactivity of alpha-Ketoglutarate-Dependent Non-Heme Iron (II)-Containing Enzymes. *Inorg. Chem.* **1995**, *34*, 2265.

39. Burger, R. M.; Peisach, J.; Horwitz, S. B. Activated bleomycin. A transient complex of drug, iron, and oxygen that degrades DNA. *J. Biol. Chem.* **1981**, *256*, 11636.

40. Burger, R. M.; Horwitz, S. B.; Peisach, J.; Wittenberg, J. B. J. Oxygenated iron bleomycin. A short-lived intermediate in the reaction of ferrous bleomycin with O_2. *J. Biol. Chem.* **1979**, *254*, 12299.

41. Burger, R. M.; Kent, T. A.; Horwitz, S. B.; Munck, E.; Peisach, J. Mössbauer study of iron bleomycin and its activation intermediates. *J. Biol. Chem.* **1983**, *258*, 1559.

42. Patil, P.; Sethy, S. P.; Sameena, T.; Shailaja, K. Pyridine and Its Biological Activity: A Review. *Asian J. Research Chem*. **2013**, *6*, 888.

43. Swedberg M. D.; Shannon H.E.; Nickel B.; Goldberg S. R. Pharmacological mechanisms of action of flupirtine: a novel, centrally acting, nonopioid analgesic evaluated by its discriminative effects in the rat. *J. Pharmacol. Exp. Ther*. **1988**, *246*, 1067.

44. Lipman, A. G. Martindale - the Extra Phar- macopoeia' (30th ed), edited by J. E. F. Reynolds. 1993. London: The Pharmaceutical Press.

45. Pandya, S. N. A Test Book of Medicinal Chemistry. Vol 1, 610.

46. Pandya, S. N. A Test Book of Medicinal Chemistry Vol 1, 713.

47. Halcrow, M. A. Structure:function relationships in molecular spin-crossover complexes. *Chem. Soc. Rev*., **2011**, *40*, 4119.

48. Katz, B. A.; Strouse, C. E. Spin-state isomerism of tris(2-picolylamine)iron(II). The diiodide and the hydrated dichloride. *Inorg. Chem*. **1980**, *19*, 658.

49. Maeda, Y.; Shite, S.; Takashima, Y.; Nishida, Y. Magnetic Cross-over in Hexa-coordinate Iron(II) Complexes of Several Schiff Bases. *Bull. Chem. Soc. Jpn*. **1977**, *50*, 2902.

50. Onggo, D.; Goodwin, H. A. Steric Effects of the Spin State of Iron(II) in Complexes of Substituted Bipyridine Derivatives. *Aust. J. Chem*. **1991**, *44*, 1539.

51. Harris, C. M.; Kokot, S.; Patil, H. R. H.; Sinn, E.; Wong, H. High- and low-spin complexes with similar, ligands. II. Iron(II) complexes with sterically hindered analogues of 2,2'-bipyridyl. *Aust. J. Chem.* **1972**, *25*, 1631.

52. Hashibe, T.; Fujinami, T.; Furusho, D.; Matsumoto, N.; Sunatsuki, Y. Chiral spin crossover iron(II) complex, fac-Λ-[FeII(HLR)3](ClO4)2·EtOH (HLR = 2-methylimidazol-4-yl-methylideneamino-R-(+)-1-methylphenyl). *Inorganica Chim. Acta*. **2011**, *375*, 338.

53. Gu, Z, -G.; Pang, C. -Y.; Qiu, D.; Zhang, J.; Huang, J, -L.; Qin, L, -F.;Sun, A, -Q.; Li, Z. Homochiral iron(II) complexes based on imidazole Schiff-base ligands: Syntheses, structures, and spin-crossover properties. *Inorg. Chem. Commun.* **2013**, *35*, 164.

54. Ling, G.; Dong-Hong, R.; Zhi-Ming, L.; Xiao-Li, S.; Dan, Q.; Zhi-Guo, G.; Zai-Jun, L. *Chin. J. Inorg. Chem*. **2015**, *31*, 1357.

55. Struch, N.; Topić, F.; Schnakenburg, G.; Rissanen, K.; Lützen, A. Electron-Deficient Pyridylimines: Versatile Building Blocks for Functional Metallosupramolecular Chemistry. *Inorg. Chem.* **2018**, *57*, 241.

56. Nishi, K.; Arata, S.; Matsumoto, N.; Iijima, S.; Sunatsuki, Y.; Ishida, H.; Kojima, M. One-Dimensional Spin-Crossover Iron (II) Complexes Bridged by Intermolecular Imidazole-Pyridine NH…N Hydrogen Bonds, [Fe(HLMe)3]X2 (HLMe = (2-Methylimidazol-4-yl-methylideneamino-2-ethylpyridine; X = PF6, ClO4, BF4). *Inorg. Chem*. **2010**, *49*, 1517, (b) Yamada, M.; Ooidemizu, M.; Ikuta, Y.; Osa, S.; Matsumoto, N.; Iijima, S.; Kojima, M.; Dehan, F.; Tuchagues, J.P. Interlayer Interaction of Two-Dimensional Layered Spin Crossover Complexes [FeIIH3LMe][FeIILMe]X (X- = ClO4-, BF4-, PF6-, AsF6-, and SbF6-; H3LMe = Tris[2-(((2-methylimidazol-4-yl)methylidene)amino)ethyl]amine). *Inorg. Chem.* **2003**, *43*, 8406.

57. Brachňaková, B.; Kožíšková, J. A.; Kožíšek, J.; Melníková, E.; Gál, M.; Herchel, R.; Dubajb, T.; Šalitroš, I.; Low-spin and spin-crossover iron (II) complexes with pyridyl-benzimidazole ligands: synthesis, and structural, magnetic and solution study. *Dalton Trans*., **1989**, *49*, 17786.

58. Archer, R. J.; Scott, H. S.; Polson, M. I. J.; MathoniHre, C.; RouziHres, M.; Clerac, R.; Kruger, P. E. Solvent Dependent Spin-Crossover and Photomagnetic Properties in an Imidazolylimine FeII Complex. *Chem. Asian J.* **2019**, *14*, 2225.

59. Berthod. A. Chiral recognition mechanisms. *Anal.Chem*, **2006**,*78*, 2093.

60. Bernhardt, P.V.; Comba, P.; Gyr, T. Predictions and methods of separation of racemic bidentate ligands via stereoselective ligand exchange reactions. *Inorg. Chem*.**1992**, *31*, 1220.

61. Carrillo, R.; Martin, V. S.; Martin, T. Quantification of a CH-pi interaction responsible for chiral discrimination and evaluation of its contribution to enantioselectivity. *Angew. Chen. Int. Ed*. **2009**, *48*, 7803.

62. Keurentjes, J. T. F.; Nabuurs, L. J. W. M.; Vegter, E. A. J. Membr. Liquid membrane technology for the separation of racemic mixtures. *Sci*. **1996**, *113*, 351.

63. Nishio, M.; Hirota, M.; Umezawa, Y. **1998**. The CH…π interaction; Wiley-VCH: New York.

64. Desiraju, G.R.; Steiner, T.; **1999**. The weak hydrogen bond; Oxford University Press: New York.

65. Desiraju, G. R. Hydrogen Bridges in Crystal Engineering: Interactions without Borders. *Acc. Chem. Res*. **2002**, *35*, 565.

66. Ahlquist, R. P. A Study of the Adrenotropic Receptor. *Am. J. Physiol*. **1948**, *153*, 586.

67. Nisoli, E.; Tonello, C.; Landi, M.; Carruba. Functional studies of the first selective beta 3-adrenergic receptor antagonist SR 59230A in rat brown adipocytes. *M. Mol. Pharmacol*. **1996**, *49*, 7.

68. Schrader, T. Toward Synthetic Adrenaline Receptors: Strong, Selective, and Biomimetic Recognition of Biologically Active Amino Alcohols by Bisphosphonate Receptor Molecules. *J. Org. Chem*. **1998**, *63*, 264.

69. Schrader, T. Towards synthetic adrenaline receptors—Strong binding of amino alcohols by bisphosphonates. *Angew. Chem. Int. Ed.* **1996**, *35*, 2649.

70. Strader, C.D.; Fong, T.M.; Tota, M.R.U. D. Structure and function of G protein-coupled receptors. *Annu. Rev. Biochem*. **1994**, *63*, 101.

71. Lehn, J.-M. Supramolecular Chemistry; *Science*, **1993**, *260*, 1762.

72. Rebek, J. Jr. Reversible Encapsulation and Its Consequences in Solution. *Acc. Chem. Res*. **1999**, *32*, 278.

73. Sauvage, J. P. Transition Metal-Containing Rotaxanes and Catenanes in Motion: Toward Molecular Machines and Motors. *Acc. Chem. Res*. **1998**, *31*, 611.

74. Caulder, D. L.; Raymond, K. N. *J. Chem. Soc., Dalton Trans*. **1999**, 1185.

75. Peacock, S. C.; Domeier, L. A.; Gaeta, F. C. A.; Helgeson, R. C.; Timko, J. M.; Cram, D. J. Host-Guest Complexation. 13. High Chiral Recognition of Amino Esters by Dilocular Hosts Containing Extended Steric Barriers. *J. Am. Chem. Soc.* **1978**, *100*, 8190.

76. Zhang, X. X.; Bradshaw, J. S.; Izatt, R. M. Enantiomeric Recognition of Amine Compounds by Chiral Macrocyclic Receptors. *Chem. Rev*. **1997**, *97*, 3313.

77. Scarso, A.; Shivanyuk, A.; Hayashida, O.; Rebek, J. Jr. Asymmetric Environments in Encapsulation Complexes. *J. Am. Chem. Soc.* **2003**, *25*, 6239.

78. Judice, J. K.; Cram, D. J. Stereoselectivity in Guest Release from Constrictive Binding in a Hemicarceplex. *J. Am. Chem. Soc*. **1991**, *113*, 2790.

79. Fiedler, D.; Leung, D. H.; Bergman, R, G.; Raymond. K. N. Enantioselective Guest Binding and Dynamic Resolution of Cationic Ruthenium Complexes by a Chiral Metal-Ligand Assembly. *J. Am. Chem. Soc*. **2004**, *126*, 3674.

80. Xuan, W.; Zhang, M.; Liu, Y.; Chen, Z.; Cui, Y. A Chiral Quadruple-Stranded Helicate Cage for Enantioselective Recognition and Separation. *J. Am. Chem. Soc.* **2012**, *134*, 6904.

81. Seo, J. S.; Whang, D.; Lee, H.; Jun, S. I.; Oh, J.; Jeon, Y, J.; Kim, K. A homochiral metal-organic porous material for enantioselective separation and catalysis. *Nature*, **2000**, *404*, 983.

82. Li, G.; Yu, G.; Cui, Y. A Homochiral Nanotubular Crystalline Framework of Metallomacrocycles for Enantioselective Recognition and Separation. *J. Am. Chem. Soc*. **2008**, *130*, 4582.

83. (a) Sahoo, S.C.; Ray, M.; Three Point Chiral Recognition and Resolution of Amino Alcohols Through Well-Defined Interaction Inside a Metallocavity, *Chem. Eur. J*. **2010**, *16*, 5004. (b) Das, C.R.; Sahoo, S.C.; Ray, M. Chiral Recognition and Partial Resolution of 1-Phenylethylamine through Noncovalent Interactions Using Binuclear Ni (II) Complex as Host, *Cryst. Growth Des*. **2014**, *14*, 3958.

84. Heitbaum, M.; Glorius, F.; Escher, I. Asymmetric Heterogeneous Catalysis. *Angew. Chem., Int. Ed.* **2006**, *45*, 4732.

85. Jacobsen, E. N.; Pfaltz, A.; Yamamoto, H.; Eds.; in Comprehensive Asymmetric Catalysis; Springer: New York, **1999**, Vols. 1-3.

86. Ojima, I. Ed.; In Catalytic Asymmetric Synthesis, 2nd ed.; Wiley-VCH: New York, **2000**.

87. Chin, J.; Lee, S.S.; Lee, K.J.; Park, S.; Kim, D.H. A metal complex that binds α-amino acids with high and predictable stereospecificity, *Nature*. **1999**, *401*, 254.

88. Murphy, D. M.; Caretti, I.; Carter, E.; Fallis, I. A.; G€obel, M. C.; Landon, J.; Doorslaer, S. V.; Willock, D. J. Visualizing Diastereomeric Interactions of Chiral Amine-Chiral Copper Salen Adducts by EPR Spectroscopy and DFT. *Inorg. Chem.* **2011**, *50*, 6944.

89. Imai, H.; Munakata, H.; Uemori, Y.; Sakura, N. Chiral Recognition of Amino Acids and Dipeptides by a Water-Soluble Zinc Porphyrin. *Inorg. Chem*., **2004**, *43*, 1211.

90. Tashiro, S.; Ogura, Y.; Tsuboyama, S.; Tsuboyama, K.; Shionoya, M. Chiral recognition of α-Amino acids by an optically active (2 s, 5 s, 8 s, 11 s)-2, 5, 8, 11-tetraethyl cyclen Cobalt (III) complex, *Inorg. Chem.* **2010**, *50*, 4.

91. Yao, S.-Y.; Ou, Y.-L.; Ye, B.-H. Asymmetric synthesis of enantiomerically pure mono- and binuclear bis (cyclometalated) iridium (III) complexes, *Inorg. Chem.* **2016**, *55*, 6018.

92. Li, Z. J.; Yao, J.; Tao, Q.; Jiang, L.; Lu, T. B. Enantioselective Recognition and Separation of Racemic 1-Phenylethanol by a Pair of 2D Chiral Coordination Polymers. *Inorg. Chem.* **2013**, *52*, 11694.

Chapter II

Chiral resolution of 1-phenylethylamine in Schiff base form using mixed ligand Ni (II) complexes

Introduction

Most chiral amines and amino alcohols are biologically active, and usually, one enantiomer is more active than the other.[1-4] Chiral recognition of amines and amino alcohols in biology works mostly through non-covalent interactions.[5] The earlier report from our group using an anionic host was effective for amino alcohol recognition (> 95 % ee) but not with 1-phenylethylamine (40-60 % *ee*).[6,7] Unlike amino alcohols, amines lack the H-bonding capability of -OH group which makes it harder to recognize.[8] In the present work, we have transformed the racemic 1-phenylethylamine into a bidentate ligand (*rac*-L2) through Schiff-base condensation (Scheme 2.1). We allowed this to bind to a Ni(II) complex with other enantiopure co-ligands (*S*-L1). Groups, on the chiral center, are still free to interact with neighboring groups through non-covalent interactions. We expected that the coordination bond will enhance the fitting of one enantiomer better than the ionic interaction employed earlier.[7,8] The use of coordination bonds in chiral recognition has been used occasionally. Using kinetically inert cobalt (III) complex, within a mixed ligand environment, Chin & others showed that different chiral interaction leads to a different rate of epimerization.[9] Shionoya and others recognized D-phenylglycine over corresponding L-enantiomer (20 % *ee*) within a mixed ligand environment around cobalt (III) complex.[10] At least two groups probed the chiral interactions between chiral guest singly bonded to structurally different zinc (II) porphyrin using spectroscopic techniques.[11,12] Resolutions observed were not very high. Ye and others recognized chiral bidentate sulphoxides using an enantiopure Ir (III) complex.[13] In this case, the resolution was almost quantitative. However, none of this were with a chiral amine. The ligand *S*-L1 and it's complex, $[Ni(S\text{-}L1)_3](ClO_4)_2$ has been structurally characterized by Scott and others.[14] Mixed ligand complexes with the present ligands have not been reported before.

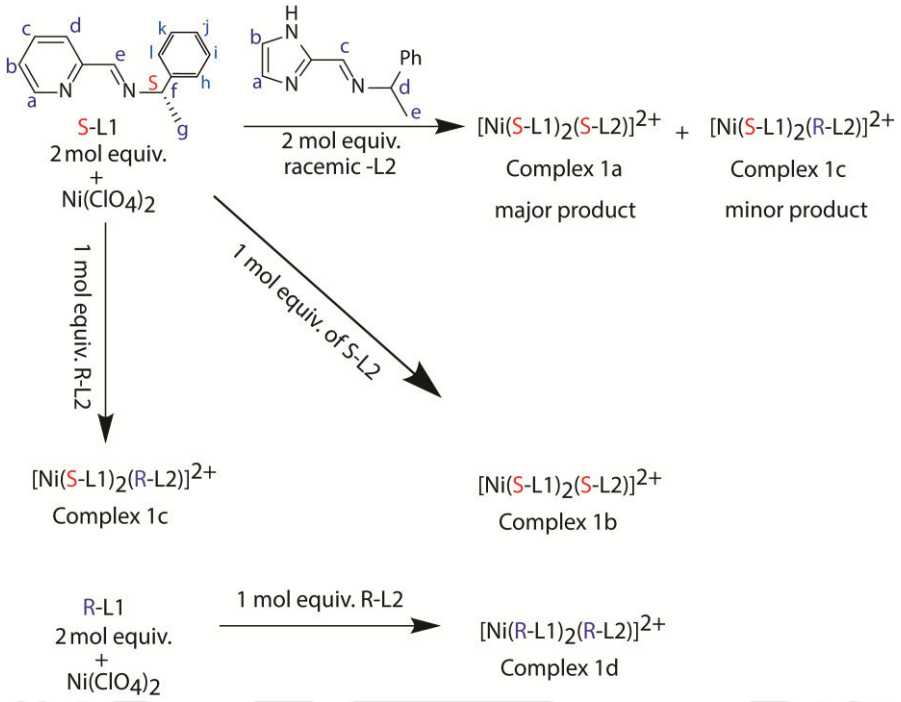

Scheme 2.1. The ligands, their NMR labeling and syntheses of the complexes **1a-1d**. **1b** and **1d** are enantiomers. **1b** and **1c** are diastereomers. **1a** and **1b** are indentical complex but isolated from different reaction sequences.

2. Experimental Section

2.1 Materials and Methods

Solvents were obtained from commercial sources and used without further purifications unless otherwise stated. Imidazole-2-carbaldehyde, pyridine-2-carboxaldehyde, the racemic and both enantiomers of 1-phenylethylamine, electrochemical grade tetrabutylammonium perchlorate (TBAP) and $Ni(ClO_4)_2 \cdot 6H_2O$ purchased from Aldrich Chemical Co. The complex $[Ni(S\text{-}L1)_3](ClO_4)_2$ was prepared following the reported procedure.[14]

The FTIR spectra recorded on PerkinElmer Spectrum One FT-IR spectrophotometer with KBr discs in the range 4000-400 cm^{-1} and electronic spectra on Perkin Elmer Lambda 25 UV-vis spectrophotometers. Solid-state magnetic susceptibility of the complexes at room temperature was recorded using Sherwood Scientific magnetic balance MSB-1. Electrospray Ionization mass (ESI-MS) spectra recorded on AGILENT Q-TOF 6520 High-Resolution Mass Spectrometer. ^{1}HNMR spectra were recorded using Bruker ASCEND-600 600 MHz instruments. Powder X-ray diffraction patterns were recorded using MAKE Bruker, D2 Phaser instrument

with Cu-Kα radiation (λ = 1.5418 Å) equipped with an integrated PC and DIFFRAC.SUITE software. Diffraction patterns were collected over 2θ range between 3-50° at a step scan rate of 0.02°. Samples for powder diffraction were stored inside the vacuum desiccator before measurement. Circular Dichroism measurements were performed using JASCO J-1500 CD Spectrometer and the spectra were analyzed using JASCO spectra manager version 2.0. All the CD spectra were recorded under inert N_2 atmosphere using HPLC grade acetonitrile as a solvent and a High Precision Cell made of Quartz SUPRASIL cuvette having a path length of 1mm. Cyclic Voltammetric measurements were performed using CH instruments Electrochemical Workstation. Potentials are reported at 25 °C relative to a 0.01 M $Ag/AgNO_3$ reference electrode using 0.15 M TBAP as a supporting electrolyte. A glassy carbon electrode used as the working electrode. Measurements in dry acetonitrile solvent under inert N_2 atmosphere and a scan rate of 100 mV s^{-1} was found to give the most appropriate results. The system calibrated against ferrocene $[Fe(\eta^5\text{-}C_5H_5)_2]$ and tris(2,2-bipyridine)-Iron(II) perchlorate $[Fe(bpy)_3](ClO_4)_2$.[15] Using this setup, the $E_{1/2}$ of ferrocene and $[Fe(bpy)_3](ClO_4)_2$ were observed at 0.09 V and 0.75 V respectively. ΔE_p values are calculated by taking the average of cathodic (E_{pc}) and anodic (E_{pa}) peak potentials.

2.2 Syntheses

2.2.1 (S,E)-N-(1-phenylethyl)-1-(pyridin-2-yl)methanimine (S-L1).

(*S*)-α-1-Phenylethylamine (0.500 g, 4.12 mmol) was stirred in 10 mL methanol. A solution of distilled pyridine-2-carbaldehyde (0.441 g, 4.11 mmol) in 10 mL methanol was added dropwise to the first solution. The solution turned yellowish, but no precipitation was formed. It was stirred for 3 h at room temperature. The solvent was evaporated and ~ 10 mL ethyl acetate was added. To remove the unreacted amine, which is soluble in water, the solution was extracted 7-8 times with 20 mL of diluted brine solution (10 mL of saturated brine & 10 mL distilled water) each time. The ethyl acetate layer was dried over anhydrous sodium sulfate for 10-15 min and filtered. The solvent was evaporated under vacuum to obtain the Schiff base as a yellowish-brown oily liquid. The quantity of the oil obtained was measured by the difference in weight with the empty flask. Yield, 0.570 g, 66 %. FTIR (KBr, cm^{-1}): $\upsilon(C{=}N)_{stretch}$ 1646 (s). ^1H NMR (600 MHz, $CDCl_3$, ppm): 8.50 (Imine, s, 1 H), 8.63

(Py-H^a, d, 1 H, J = 6 Hz), 8.12 (Py-H^d, d, 1 H, J = 8 Hz), 7.71 (Py-H^b, t, 1 H, J = 8 Hz), 7.46 (Ph-H^h/H^l, d, 2H, J = 8),7.37 (Py-H^c, t, 1 H), 7.37 (Ph-H^j, t, 1 H), 7.27 (Ph-H^i/H^k, m, 2 H), 4.67 (Chiral-H, q, 1 H, J = 6 Hz), 1.64 (Methyl-H, d, 3 H, J = 6 Hz). ESI-MS ($[M + H]^+$): calcd 211.1235; found 211.1246.

2.2.2 (R,E)-N-(1-phenylethyl)-1-(pyridin-2-yl)methanimine (R-L1).

This was prepared following the same procedure as *S*-L1 using (*R*)-α-1-Phenylethylamine instead of (*S*)-α-1-Phenylethylamine. Yield, 0.535 g, 61 %. FTIR (KBr, cm^{-1}): $\upsilon(C=N)_{stretch}$ 1643 (s). ^1H NMR (600 MHz, $CDCl_3$, ppm): 8.49 (Imine, s, 1 H), 8.65 (Py-H^a, d, 1 H, J = 6 Hz), 8.12 (Py-H^d, d, 1 H, J = 8 Hz), 7.75 (Py-H^b, t, 1 H, J = 8 Hz), 7.46 (Ph-H^h/H^l, d, 2 H, J = 8), 7.37 (Py-H^c, t, 1 H), 7.37 (Ph-H^j, t, 1 H), 7.29 (Ph-H^i/H^k, m, 2 H), 4.67 (Chiral-H, q, 1 H, J = 6 Hz), 1.64 (Methyl-H, d, 3H, J = 6 Hz). ESI-MS ($[M + H]^+$): calcd 211.1235; found 211.1272.

2.2.3 (E)-1-(1H-imidazol-2-yl)-N-(1-phenylethyl)methanimine (racemic-L2).

1-phenylethylamine (0.500 g, 4.12 mmol, 1 eq.) was stirred in 10 mL methanol. A solution of imidazole-2-aldehyde (0.396 g, 4.12 mmol, 1 eq.) in 10 mL methanol was added dropwise to the first solution. The initial colorless solution turned yellowish upon warming in a water bath for 30 mins. The mixture was stirred for 3 h at room temperature. The solvent was evaporated to obtain a white solid. Solid was washed with 10 mL of n-hexane followed by 10 mL of undistilled diethyl ether. The solid was dried overnight in a desiccator to obtain the product as off-white solid. Yield ~ 0.500 g, 60 %. FTIR (KBr, cm^{-1}): $\upsilon(C=N)_{stretch}$ 1648 (s). ^1H NMR (600 MHz, $CDCl_3$, ppm): ^1H NMR (600 MHz, $CDCl_3$, ppm): 8.34 (Imine-H, s, 1 H), 7.26 (Ph-H, m, 5 H), 7.15 (Im-H, s, 1 H,), 6.85 (Im-H, s, 1 H), 4.59 (Chiral-H, q, 1 H, J = 10 Hz), 1.57 (Methyl-H, d, 3 H, J = 10 Hz). ESI-MS ($[M + H]^+$): calcd 200.1187; found 200.1199.

2.2.4 (S,E)-1-(1H-imidazol-2-yl)-N-(1-phenylethyl)methanimine (S-L2).

This was prepared using the same procedure as *racemic*-L2 using (*S*)-α-1-Phenylethylamine instead of racemic amine. Yield ~ 0.600 g, 73 %. FTIR (KBr, cm^{-1}): $\upsilon(C=N)_{stretch}$ 1642 (s). ^1H NMR (600 MHz, $CDCl_3$, ppm): 8.36 (Imine-H, s, 1 H), 7.26 (Ph-H, m, 5 H), 7.15 (Im-H, s, 1 H,), 6.79 (Im-H, s, 1 H), 4.60 (Chiral-H, q, 1 H, J = 10 Hz), 1.58 (Methyl-H, d, 3 H, J = 10 Hz). ESI-MS ($[M + H]^+$): calcd 200.1187;

found 200.1203.

2.2.5 (R,E)-1-(1H-imidazol-2-yl)-N-(1-phenylethyl)methanimine (R-L2).

This was prepared using the same procedure as *racemic*-L2 using (*R*)-α-1-Phenylethylamine instead of racemic amine. Yield 0.506 g, 62 %. FTIR (KBr, cm^{-1}): $\upsilon(C{=}N)_{stretch}$ 1642 (s). ^1H NMR (600 MHz, $CDCl_3$, ppm): 8.26 (Imine-H, s, 1 H), 7.20 (Ph-H, m, 5 H), 7.09 (Im-H, s, 1 H,), 6.81 (Im-H, s, 1 H), 4.52 (Chiral-H, q, 1 H, J = 10 Hz), 1.50 (Methyl-H, d, 3 H, J = 10 Hz). ESI-MS ($[M + H]^+$): calcd 200.1187; found 200.1205.

2.2.6 $[Ni(S\text{-}L1)_2(S\text{-}L2)](ClO_4)_2$ (1a) from racemic L2 .

The ligand *S*-L1 (0.150 g, 0.71 mmol, 2 eq.) was dissolved in 3 mL of acetonitrile and stirred initially at room temperature. To the stirred solution, $Ni(ClO_4)_2{\cdot}6H_2O$ (0.130 g, 0.36 mmol, 1 eq.) in 4 mL of acetonitrile was added dropwise which turned it to slightly reddish clear solution followed by the addition of *racemic*-L2 (0.144 g, 0.71 mmol, 2 eq.) in 3 mL acetonitrile and stirred for 4 h. The solvent was layered with ethyl acetate, covered properly and kept in the refrigerator for crystallization. Reddish-orange crystals appeared after 1-2 days. The complex is soluble in both methanol and acetonitrile. Yield ~ 0.220 g, (68 %). Anal. Calcd. for $[Ni(C_{14}H_{14}N_2)_2(C_{12}H_{13}N_3)]{\cdot}2(ClO_4){\cdot}1.75H_2O$: C, 52.93; H, 4.94; N, 10.81; found C, 53.08; H, 4.76; N, 10.92. FTIR (KBr, cm^{-1}): $\upsilon(C{=}N)_{stretch}$ 1641 (s), 1622 (s) and 1600 (s) . μ_{eff} (powder, 298 K): 2.79. Visible spectra in dry MeCN: λ_{max} in nm (ε, $M^{-1}cm^{-1}$) 539 (13), 878 (10).

2.2.7 Complex 1b from enantiopure *S*-L2 (1b)

This was prepared using the same procedure and quantity as for **1a** but using 1 equiv. of *S*-L2 instead of 2 equiv. of *rac*-L2. Reddish-orange crystals appeared after 3 days. Soluble in methanol, acetonitrile. Yield ~ 0.213 g, (66 %). Anal. Calcd. for $[Ni(C_{14}H_{14}N_2)_2(C_{12}H_{13}N_3)]{\cdot}2(ClO_4){\cdot}2H_2O$: C, 52.67; H, 4.97; N, 10.75; found C, 52.66; H, 4.67; N, 10.78. FTIR (KBr, cm^{-1}): $\upsilon(C{=}N)_{stretch}$ 1641 (s), 1622 (s) and 1599 (s). μ_{eff} (powder, 298 K): 2.89 .Visible spectra in dry MeCN: λ_{max} in nm (ε, $M^{-1}cm^{-1}$) 543 (10), 877 (9).

2.2.8 $[Ni(R\text{-}L1)_2(R\text{-}L2)](ClO_4)_2$ (1d).

This was prepared using the same procedure as for **1b** (Section 2.2.7) but using *R*-L1 and R-L2 instead of *S*-L1 and *S*-L2. The quantities used are *R*-L1 (0.100 g, 0.475 mmol, 2 eq.) , $Ni(ClO_4)_2 \cdot 6H_2O$ (0.087 g, 0.24 mmol, 1 eq.) and *R*-L2 (0.048 g, 0.24 mmol, 1 eq.). Reddish-orange crystals appeared after 2 days. Soluble in methanol, acetonitrile. Yield ~ 0.147 g. (70 %). Anal. Calcd. for $[Ni(C_{14}H_{14}N_2)_2(C_{12}H_{13}N_3)] \cdot 2(ClO_4) \cdot 3.5H_2O \cdot 2CH_3CN$: C, 51.75; H, 5.33; N, 12.35; found C, 51.85; H, 5.40; N, 12.44. FTIR (KBr, cm^{-1}): $\upsilon(C=N)_{stretch}$ 1641 (s), 1622 (s) and 1599 (s).

2.2.9 Reaction with *R*-L2 instead of *S*-L2 (1c).

A reaction identical to the one for **1b** (Section was performed with *R*-L2 substituting the *S*-L2. Unlike **1b**, No precipitation of crystals was obtained even after doubling the amount of precipitant ethyl acetate. The solvent was evaporated to dryness, washed with (2x5 mL) of ethyl acetate followed by 5 mL of diethyl ether. A light brown solid powder was obtained. Soluble in methanol, acetonitrile. (yield ~ 0.141 g starting with 0.100 g of *S*-L1). FTIR (KBr, cm^{-1}): $\upsilon(C=N)_{stretch}$ 1640 (s), 1624 (s) and 1599 (s). ESI Mass is given in Figure S3.

2.3 X-ray Data Collection, Structure Solvation and Refinement

All the crystals show desolvation to a different degree. Thus, the crystals were covered with grease (Vaseline) and mounted on glass fiber for data collection. All geometric and intensity data for the crystals of **1a** and **1b** were collected at a low temperature using a 'CrysAlisPro 1.171.40.23a (Rigaku Oxford Diffraction, 2018)' diffractometer equipped with a fine focus 1.75 kW sealed tube Mo-Kα (λ = 0.71073 Å) X-ray source. The SMART software was used for data acquisition and the 'CrysAlisPro 1.171.40.23a (Rigaku OD, 2018)' software for data extraction and reduction. Absorption corrections were done using spherical harmonics, implemented in SCALE3 ABSPACK scaling algorithm. The final refinements were performed on WinGX[16] environment. The crystals of **1d** were collected at room temperature using a Bruker SMART APEX CCD diffractometer equipped with a fine focus 1.75 kW sealed tube Mo-Kα (λ = 0.71073 Å) X-ray source. The SMART software was used for data acquisition and the 'Bruker SAINT' software for data refinement and reduction. Absorption corrections were done using SADABS. After the initial solution and refinement with SHELXL, the final refinements were performed on WinGX[16] environment. Almost all non-hydrogen atoms in the complexes were refined

anisotropically. In **1a**, **1b** and **1d**, 'SQUEEZE' was performed in order to remove the disordered solvent molecules.[17] All of the hydrogen atoms were added in the refinement stage. The molecular weight from structure and bulk may not match as the dry powdered form of crystals was used for elemental analysis and other studies.

2.4 Results and Discussion

2.4.1 Syntheses

The Schiff base ligands were synthesized by condensing the chiral amine and the aldehyde in methanol. The *S*-L1 or *R*-L1 was isolated as oil while all three Schiff bases containing imidazole were white powder. The FTIR spectra showed a strong vibration near 1650 cm^{-1} assigned as C=N stretch of the imine formed. The ligands were characterized by proton NMR and Mass spectrometry (Experimental section). Proton NMR assignments are consistent with the respective chemical structure. The mixed ligand complexes were synthesized by the sequential addition of the ligands (ref. Scheme 2.1). The enantiopure *S*-L1 was reacted with nickel (II) salt first before the addition of *racemic*-L2 or *S*-L2. For **1a**, the ratio of Ni: *S*-L1: *racemic*-L2 used was 1:2:2. The use of *racemic*-L2 at double the quantity than required for $[Ni(S\text{-}L1)_2(L2)]^{2+}$ was to maximize yield in case only one of the enantiomers of L2 binds. In the case of **1b**, the ratio of Ni: *S*-L1: *S*-L2 was 1:2:1 as required by the formula. For **1d**, everything is identical to **1b** except ligands used are *R*-L1 and *R*-L2. Complex **1a** and **1b** are identical but as they were isolated from difference reaction sequence, bulk compound of **1a** may contain **1c** (Scheme 2.1) as minor product along with **1a** as the major product. The complex **1b** do not have **1c** as synthetic sequence doesn't not involve *R*-L2 and hence considered as enantiomerically pure. The complex **1b** and **1d**, enantiomer to each other (Scheme 2.1), have been used as references in circular dichroism (CD) spectroscopy. The complexes were isolated as crystals with ~70% yield. Reaction identical to that of **1b** with enantiopure *R*-L2 instead of *S*-L2 did not yield crystals of $[Ni(S\text{-}L1)_2(R\text{-}L2)](ClO_4)_2$.

2.4.2 Molecular structures of the complexes

The complex **1a** was crystallized in a chiral space group $P2_1$ with one molecule of the cationic complex, two perchlorate cation, and one acetonitrile molecule in the asymmetric unit. The crystals showed solvent disorder. We applied SQUEEZE on the

data.[17] The final structural parameters are in Table 2.1, and the selected bond and lengths are in Table 2.2. The ORTEP diagram of the complex cation showed it to be an octahedral Ni (II) complex (Figure. 2.1a). The geometry around Ni (II) slightly deviated from the perfect octahedron. This is evident from the deviation of angles from the ideal value of 90º for in-plane angles and 180º for axial angles (Table 2.2). All the Ni-N (pyridine or imidazole) are slightly shorter (<2.09 Å) compared to Ni-N-imine lengths (> 2.1 Å). The other bond lengths are within the expected range.[14] The crystal also contains H-bonded interactions between imidazole NH and one of the perchlorate oxygen. The number of CH...O interactions were observed as well (Table 2.4). The structure of **1b** is identical to that of **1a** (Table S1 and S2, Supplementary data). It further supports that the chirality of L2 in **1** has *S* configuration. The complex **1d**, with the formula $[Ni(R\text{-}L1)_2(R\text{-}L2)](ClO_4)_2$, was prepared using enantiopure ligands *R*-L1 and *R*-L2. The solved structure showed it to be the mirror image enantiomer of **1** (Figure S1). The structural data for **1d** are given in Table S3 and S4.

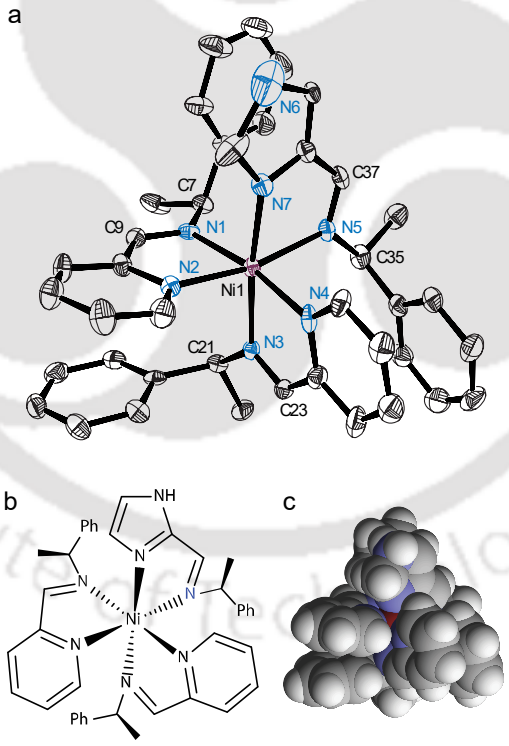

Figure 2.1. (a) ORTEP diagram of the cationic part of Complex **1a**. Thermal ellipsoids are set to 50% probability level. Hydrogens removed for clarity. **(b)** A chemical diagram of the same. **(c)** A spacefilling model highlighting the methyl and C-H groups of the chiral carbon.

The structural data i.e bond lengths and angles, inter and intramolecular interactions of **1b** and **1d** are same as **1a** with no such observable difference to mention. The complex **1a** is a facial (fac) isomer with all three imines are on a triangular face. The pyridines and imidazole are in the opposite triangular face. The complex is an Δ isomer (Figure 2.1b). This is one out of 16 possible isomers (Figure. 2.2a). In all the reported single crystal X-ray structures of $[M(S\text{-}L1)_3]^{2+}$, where M is either nickel (II) or iron (II), have this preference.[14] All the chiral centers at C7, C21, and C35 have the *S*-conformation. This means that out of two enantiomers of *rac*-L2, only the *S*-L2 was found to bind in the complex.[14]

Table 2.1. Crystallographic data and refinement parameters of complexes.

	1a	**1b**	**1d**
Empirical formula	C42 H44 N8 Ni1 O8 Cl2	C42 H44 N8 Ni1 O8 Cl2	C40 H41 Cl2 N7 Ni1 O8
fw	918.46	918.46	877.41
crystal system	Monoclinic	Monoclinic	Monoclinic
space group	$P2_1$	$P2_1$	$P2_1$
a, A°	12.1838(11)	12.1363(5)	12.2356(11)
b, A°	13.3956(8)	13.3803(5)	13.5952(12)
c, A°	15.3606(13)	15.3352(7)	15.5863(14)
$\beta(°)^{\alpha}$	105.753(8)	106.039(5)	105.287(3)
V, Å^3	2412.8(3)	2393.31(18)	2501.0(4)
Z/ρ (g cm^{-3})	2/1.264	2/1.275	2/1.165
T(K)	100.01(11)	99.99(10)	273(2)
μ (mm^{-1})	0.568	0.573	0.544
coll.reflns	6773	6580	8813
indep reflns	6000	5849	7614
FLACK para.	-0.015(18)	0.030(15)	0.023(8)
GOF on F^2	1.036	1.051	1.049
Residuals (e Å^{-3})	0.967, -0.559	0.902, -0.633	0.496,-0.293
R1^b, wR2^b	0.0590/0.1494	0.0553/0.1400	0.0471/0.1242

R1[c], wR2[c]	0.0657/0.1582	0.0627/0.1494	0.0540/0.1280

[a] $\alpha(°) = \gamma(°) = 90$ [b] $I > 2\sigma$ [c] All data

Table 2.2. Selected bond distances (Å) and angles (º) of **1a**.

Ni1-N1	2.121(5)	N1-Ni1-N2	79.1(2)
Ni1-N2	2.073(6)	N2-Ni1-N4	94.9(2)
Ni1-N3	2.103(6)	N4-Ni1-N5	91.4(2)
Ni1-N4	2.091(6)	N5-Ni1-N1	95.8(2)
Ni1-N5	2.161(6)	N1-Ni1-N7	92.9(2)
Ni1-N7	2.073(6)	N7-Ni1-N4	94.5(2)
N1-C9	1.268(9)	N1-Ni1-N4	170.6(2)
N3-C23	1.264(9)	N2-Ni1-N5	168.0(2)
N5-C37	1.284(9)	N3-Ni1-N7	172.8(2)

There are three parallelly displaced π...π type interactions between phenyl rings and either pyridine or imidazole (Figure 2.2b). All three are centroid to centroid distances at <4 Å put them within the range expected for π...π stacking (Table 2.3).[18] As per Sherril and coworkers theoretical calculations, a vertical distance between pyridine...benzene ring stacked in parallelly displaced situation of 3.4 Å (in the present case between 3.3 to 3.4 Å, Table 2.3) and horizontal displacement of ~ 1.5 Å would result in stabilization of ~ 3 kcal/mol in interaction energy per interaction.[19] This is a substantial gain in stabilization Such calculations were not reported for imidazole...phenyl ring interactions. But the similarity with pyridine...phenyl ring distances suggest a similar stabilization might be present in this case too (Table 2.3). Similar interactions are present in $[Ni(S\text{-}L1)_3]^{2+}$.[14] These three are most likely responsible for the stabilization of this fac configuration. This was pointed out by others as well.[14] Overall, structural characterizations showed three parallelly displaced π...π type interactions between phenyl rings and either pyridine or imidazole are strong and have been preserved in all the present and previously reported structures.[14] Complex **1d** is structurally similar to **1a** and **1b**. The only

difference is in chirality. Carbon center has *R*-chirality in **1d** and *S*-chirality in **1a** and **1b**. Comparison of structural parameters like volume, a, b, c lengths (~ 12 Å, 13 Å and 15 Å), monoclinic and space group is $P2_1$ of the three is similar as well. Even Ni-N bond length suggests that **1d** (2.104 Å) is almost equal to **1a** (2.103 Å) and **1b** (2.098 Å) and bond angles are also very similar but not same (Table 2.2, S1 and S3). Switching the chirality of one ligand by substituting *S*-L2 to *R*-L2, would bring two possibilities; (i) loss of phenyl…imidazole interaction or (ii) sterically unfavorable -CH_3 … -C-H interactions (Figure 2.1c). Reactions with *R*-L2 (Section 2.2.9) did not yield any crystals. Thus we are unable to test this using structural characterization. It is more likely that the unfavorable interactions between sterically demanding -CH_3 … -C-H interactions (Figure 2.1c) by switching from *S*-L2 to *R*-L2 is preventing the formation of the complex.

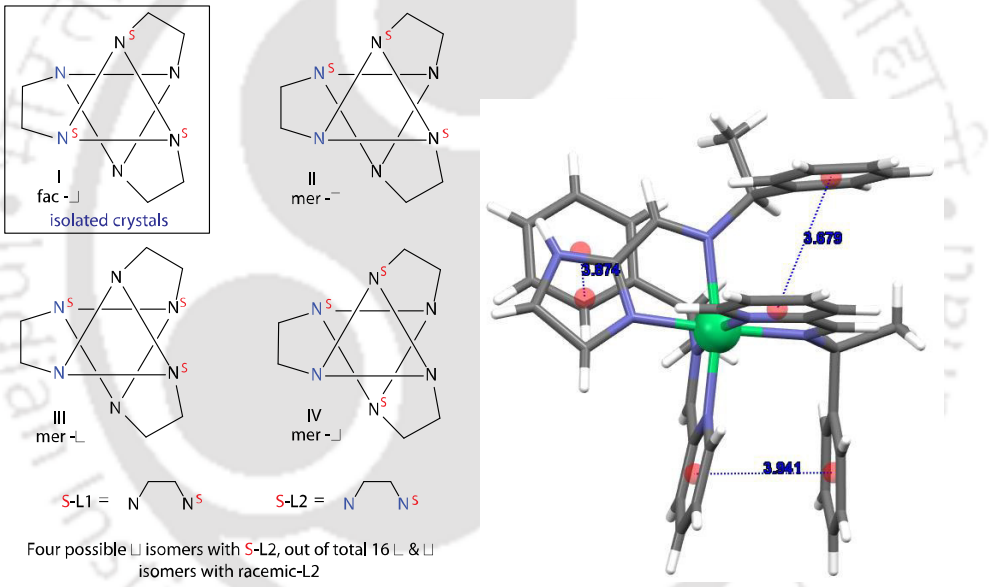

Figure 2.2. (a) Number of possible isomers of Complex **1a** and (b) Intra-molecular interactions in [Ni(*S*-L1)$_2$(*S*-L2)](ClO$_4$)$_2$(**1a**).

Table 2.3. Comparison of distance and displacement between Complex **1a** and [Ni(*S*-L1)$_3$](ClO$_4$)$_2$] complex.

Complex	Centroid to centroid (Å)	Vertical distance (Å)	Displace -ment (Å)	Ref.
[Ni(*S*-L1)$_2$(*S*-L2)](ClO$_4$)$_2$(**1a**)				This work
Imidazole(N2)...Phenyl (C15-C20)	3.941	3.447	1.855	
Pyridine(N4)...Phenyl(C29-C34)	3.679	3.323	1.578	

Imidazole (N7)...Phenyl(C1-C6)	3.874	3.381	1.891	
$[Ni(S\text{-}L1)_3](ClO_4)_2$				[14]
Pyridine(N5)...Phenyl(C23-C28)	4.003	3.383	2.139	
Pyridine(N1)...Phenyl(C37-C42)	3.638	3.314	1.500	
Pyridine(N3)...Phenyl(C9-C14)	3.841	3.424	1.740	

Table 2.4. Non-covalent interactions in Complex **1a**

D-H...A	D-H (Å)	H. . .A(Å)	D. . .A(Å)	DHA(°)
Inter-molecular				
N6-H6..O1	0.86	2.09	2.885(15)	153
C11-H11..O7	0.93	2.55	3.427(12)	157
C12-H12..O8	0.93	2.59	3.398(10)	145
C14-H14..O2	0.93	2.37	3.123(11)	138
C22-H22c..O1	0.96	2.52	3.455(14)	166
C23-H23..O2	0.93	2.54	3.380(9)	150
C26-H26..O5	0.93	2.51	3.330(15)	147
C42-H42c..O4	0.96	2.51	3.468(16)	178
C39-H39..π(C29-C34)	0.93[§]	2.85[§]	3.605[§]	9.79[§]

The acceptable range of D...A for N-H..O, 2.5-3.2 Å; for C-H..O, 3.0-4.0 Å; N-H/C-H... π 2.5–4.5 Å, from ref.[30-33]. [§]Calculated from Mercury.[34]

2.4.3 Other characterizations

X-ray powder diffraction patterns of **1a** and **1b** were recorded and compared (Figure 2.3). Both are identical. This indirectly supports the bulk of the crystals of **1a** being identical with **1b**. FTIR spectra of **1a** and **1b** show similar $\nu_{C=N}$ stretching frequency at ~ 1640 cm^{-1} assigned to. Strong and broad absorption ~ 1100 cm^{-1} confirms the presence of perchlorate anion (Figure 2.4). The electrospray ionization mass spectrum (ESI-MS) of complex **1a** in acetonitrile analyzed in detail (Figure 2.5). The peaks identified by mass value and relative isotopic abundance ratios (Figure 2.5). The peaks observed at 338.63 and 676.27 mass units are assigned for $[Ni(S\text{-}L1)_2(S\text{-}L2)]^{2+}$ (*m*/2, calcd. 338.63) and $\{[Ni(S\text{-}L1)_2(S\text{-}L2)]\text{-}H\}^{+}$ (*m*/1, 676.63) respectively. The spectrum contains some other mass peaks.[19] The mass spectrum for

1b is almost identical to **1a** (Figure 2.5) having similar fragmentation pattern. Elemental analysis of **1a** and **1b** confirm the expected values (Experimental section).

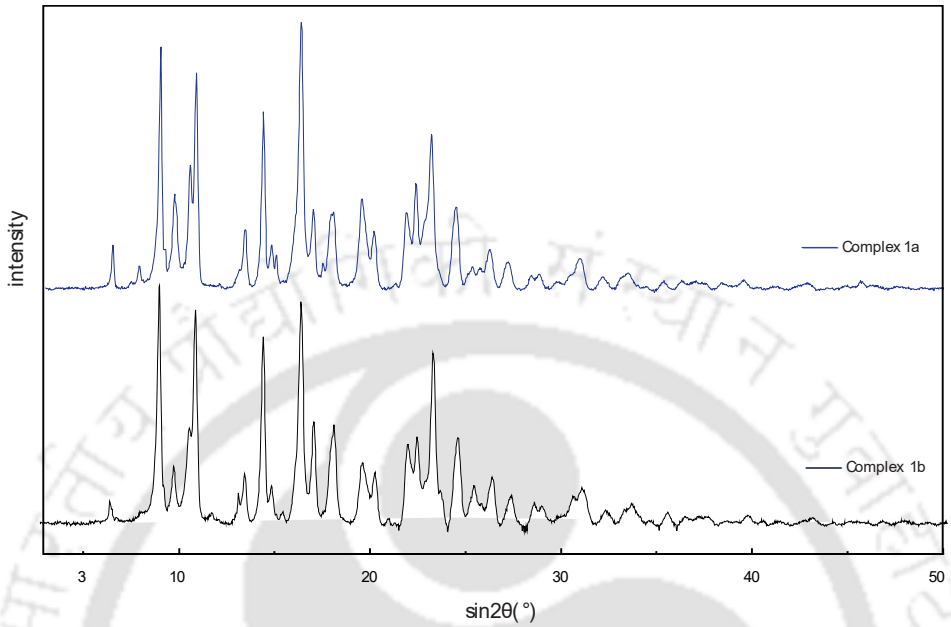

Figure 2.3. Powder X-ray diffraction patterns of **1a** and **1b**.

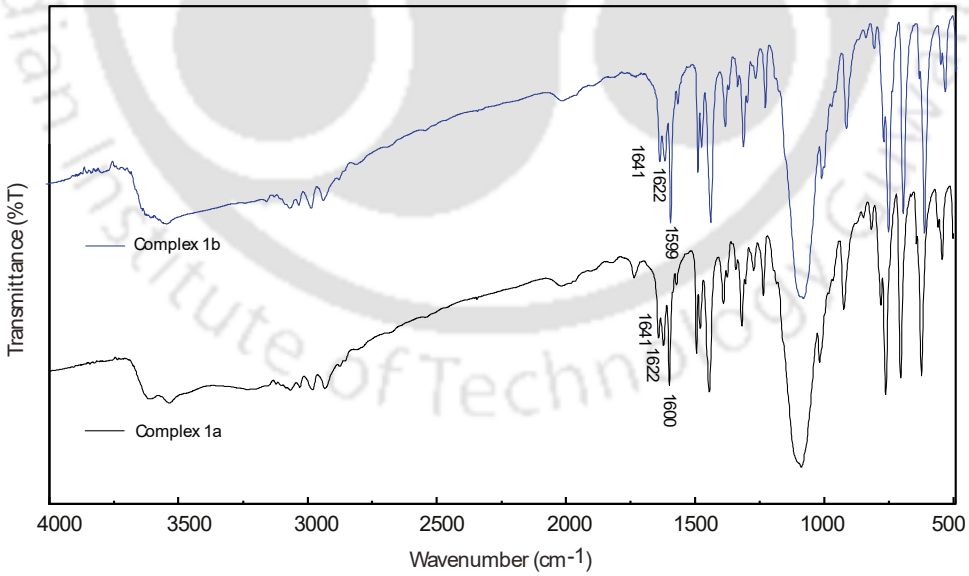

Figure 2.4. FTIR spectrum of **1a** and **1b**.

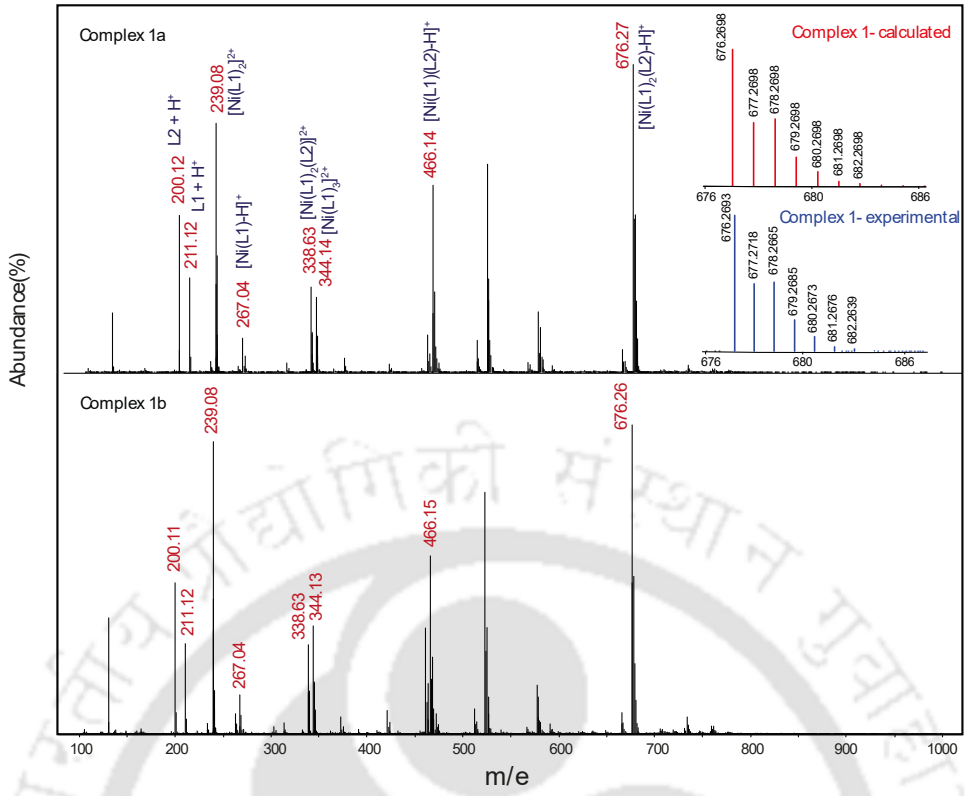

Figure 2.5. ESI-MS spectrum of **1a** along with the molecular ion peak of experimental isotopic pattern and its calculated isotopic pattern in comparison with complex **1b**.

2.4.4 Complexation with R-L2 instead of S-L2 (1c)

We attempted to synthesize, $[Ni(S\text{-}L1)_2(R\text{-}L2)](ClO_4)_2$ using enantiopure *R*-L2. No precipitate or crystalline solid was isolated even after increasing the quantity of precipitant. Eventually, an amorphous solid (**1c**) was scrapped out after removing the solvent under vacuum and washed with the ethyl acetate to remove unreacted ligand as much as possible. FTIR of **1c** (Figure S2) shows is not very different than **1a**, or $[Ni(S\text{-}L1)_3](ClO_4)_2$ as all of these have a very similar composition. It has a broad peak at ~ 3500 cm^{-1} and a sharp peak at ~ 1750 cm^{-1}. The mass spectra of **1c** (Figure S3) is not particularly revealing. This is not surprising given the labile nature of the complexes. The noted differences are; L2 peak is more abundant, $[Ni(L1)_2(L2)\text{-}H]^+$ peak is less abundant and multiple unassigned peaks between 700-800 mass units are now more prominent (Figure S3). From these, the formation of $[Ni(S\text{-}L1)_2(R\text{-}L2)]^{2+}$ is not conclusive. The solid (**1c**) is more likely to be a mixture of species along with $[Ni(S\text{-}L1)_3]^{2+}$.

2.4.5 Electronic transitions and magnetic moment

The electronic spectra of the complexes in acetonitrile show two broad transition centers around 545 nm and 880 nm with ε values between 10-20 M^{-1} cm^{-1} (Experimental Section). The spectra are essentially the same for both **1a** and **1b** (Figure 2.6). The low ε value is indicative of Laporte forbidden ligand-field transitions of octahedral Ni(II). A complex with similar N_6 coordination, $[Ni(imidazole)_6]^{2+}$, shows ligand field transitions at 355, 568 and 970 nm assigned for $^3T_{2g}(P)\leftarrow{}^3A_{2g}$, $^3T_{1g}\leftarrow{}^3A_{2g}$ and $^3T_{2g}\leftarrow{}^3A_{2g}$ transitions expected for an octahedral ^3F ground state.[18] Although, more accurately, these states will further split due to the lowered symmetry of D_3 from perfect octahedron that will further broaden the peaks.[20] In the present case, considering approximately octahedral symmetry, we tentatively assign the absorption maxima at 539 nm and 878 nm as $^3T_{1g}\leftarrow{}^3A_{2g}$ and $^3T_{2g}\leftarrow{}^3A_{2g}$ respectively. We did not observe the $^3T_{2g}(P)\leftarrow{}^3A_{2g}$ transition possibly due to overlap with stronger charge transfer transitions. Despite the broadness, the $^3T_{2g}\leftarrow{}^3A_{2g}$ transition at 878 nm for **1a** can be used to estimate and compare the ligand field strength of the ligand.[20] The reported values of $^3T_{2g}\leftarrow{}^3A_{2g}$ transition for $Ni(H_2O)_6]^{2+}$, $Ni(imidazole)_6]^{2+}$ and $Ni(2,2'\text{-bipyridyl})_3]^{2+}$ are 1176, 970 and 862 nm respectively.[21] Thus the ligand field is much stronger than aquo or imidazole complex, but closer to bipyridyl complexes. This is much higher than our previously reported histidine derived ligand ($^3T_{2g}\leftarrow{}^3A_{2g}$ transition at 1025 nm for $[Ni_2$ (μ-OAc) $(salhis)_2]^{1-}$).[6] The solid-state room temperature magnetic moment was measured to be ~ 2.80 B.M. (Experimental Section), which is close to the spin-only value of 2.83 B.M. for two unpaired electrons. This is lower than the usual range of 2.9-3.5 B.M. for Ni (II) octahedral complexes due to spin-orbit coupling.[22] However, examples of Ni (II) octahedral complexes showing magnetic moments < 2.9 B.M. has been reported.[23]

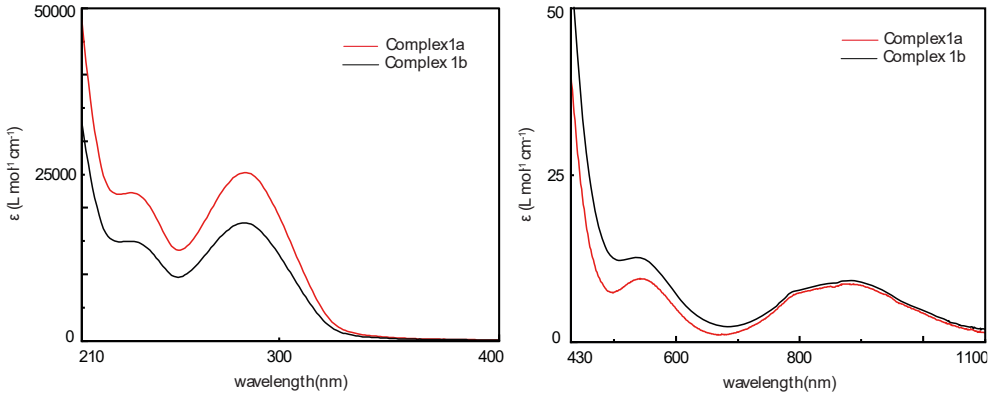

Figure 2.6. UV-visible spectra of **1a** and **1b** in acetonitrile.

2.4.6 Chiral Enhancement and Circular dichroism spectra

The structural characterization showed only *S*-L2 from a racemic mixture is bound in **1a** in the single crystalline state. In the past, we used HPLC, and chiral column to calculate chiral enhancement in bulk.[24] That proved to be difficult for the Schiff base ligands in the chiral column that we have used. To calculate chiral enhancement we used circular dichroism using equation (1) as well as optical rotation on **1a** using **1b** as enantiopure reference compound.[25] The CD spectra of complex **1a** and **1b** at the same concentration (10 mg in 10 mL acetonitrile) were recorded under identical conditions. Ellipticity values at 238 nm and 302 nm of enantiopure **1b** were taken as calculated value and that of **1a** were taken as experimental value. The % *ee*, calculated using equation (1), Enantiomeric excess = (R_{exp} / R_{calcd}) x 100 % ---------- (1)

A series of solution of enantiopure complex **1b** (enantiopure by synthesis) were made in acetonitrile. Concentration range used are from 0.1 g /100 mL to 1 g /100 mL. Plot of concentration vs optical rotation were linear with fitting parameter R^2 = 0.99 (Figure 2.8). Optical rotation of complex **1a** at 0.2 g / 100 mL and 0.4 g / 100 mL in acetonitrile were experimentally determined (R_{exp}). Expected optical rotation (R_{calcd}) for 100% *ee* were calculated from the plot (Figure 2.8) at these concentrations. Enantiomeric excess(*ee*) in complex **1a** were determined using the following formula:

The % *ee* for crystalline **1a** was determined to be 89.9 and 91.6 at 0.2 g / 100 mL and 0.4 g /100 mL from optical rotation experiments. Considering the nature of the experiment and possible error in solution preparation, the value of 89.9 and 91.2 are

very close. The error is at < 2%. The circular dichroism (CD) spectra of **1a** and **1b** in acetonitrile at the same concentration (Figure 2.7a). Both spectra are identical both in terms of peak position and ellipticity values. The similar comparison also showed that the complex **1d**, [Ni(*R*-L1)$_2$(*R*-L2)](ClO$_4$)$_2$, is the mirror image isomer of **1a** and **1b** (Figure 2.7a), (Scheme 2.1). The % *ee* for **1a** from CD spectra using equation (1) was found to be 88 and 96 at 238 nm and 302 nm respectively. The observed enhancement (~ 90% *ee*) is much higher than we observed before for 1-phenylethylamine (40-60% *ee* in crystalline form).[6,7] Enhancement in crystalline form can be a result of multiple factors: (a) solubility difference between the diastereoisomers, (b) non-covalent interactions in crystals and (c) solution equilibrium favoring one diastereoisomer. Direct measurement of solution equilibrium for the paramagnetic metal complex is difficult. We chose to precipitate the amorphous form of **1a** before crystallization and measured the chiral enhancement. The % *ee* for amorphous precipitates of **1a** was determined to be 53.7% and 58.1% at 0.2 g / 100 mL and 0.4 g /100 mL from optical rotation experiments and 56.4 and 68.4 at 238 nm and 302 nm respectively from CD experiments. This is higher than we had observed for 1-phenylethylamine (0 % *ee* in precipitated amorphous form). There is considerable enhancement in bulk due to factors other than crystallization. Circular dichroism is much less intense at the same concentration (10 mg/10 mL) with respect to either of **1c** or [Ni(*S*-L1)$_3$](ClO$_4$)$_2$ (Figure 2.7b). We observed a positive cotton effect ~ 325 nm, which was not present in **1b** but similar to one observed for [Ni(*S*-L1)$_3$](ClO$_4$)$_2$ (Figure 2.7b). This seems to be a mixture of compounds having [Ni(*S*-L1)$_3$](ClO$_4$)$_2$, among other things.

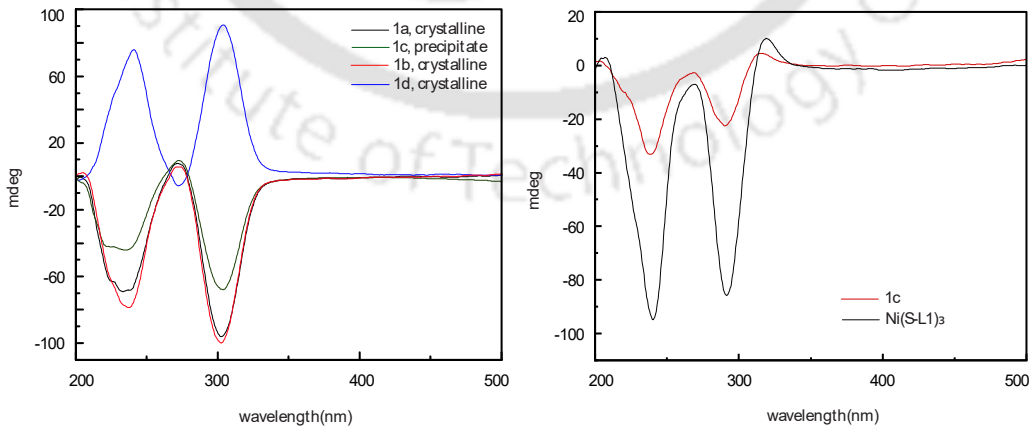

Figure 2.7. (a)Circular dichroism spectra of **1a**, **1b** and **1d** in crystalline form and **1c** in precipitated form in acetonitrile having the same concentration. (b) CD specta of [Ni(*S*-L1)$_3$](ClO$_4$)$_2$ and product from reaction with *R*-L2 (**1c**) in acetonitrile .

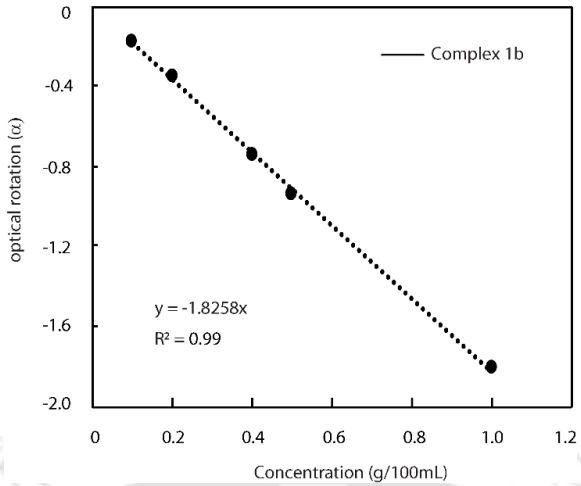

Figure 2.8. Optical rotation vs concentration plot of Complex **1b**.

2.4.7 Cyclic voltammetry of the complexes.

Discussions in the previous sections support the discrimination of *R*-L2 over *S*-L2 in the formation of **1a**. The extent of discrimination is such that the $[Ni(S\text{-}L1)_2(R\text{-}L2)]^{2+}$ was isolated as a solid powder even when only *R*-L2 was used. Earlier, for 1-phenylethylamine with a dinuclear host, we were able to isolate both diastereoisomers.[6,7] Unlike earlier, the discrimination is much higher (earlier 0% *ee* in amorphous state) in the present case (~59 % *ee* in amorphous state). We wanted to test if this difference is could be utilized for electrochemical detection of the enantiomer. Cyclic voltammetry of $[Ni(2,2'\text{-bipyridine})_3]^{2+}$ has been the subject of multiple reports.[26-28] Cyclic voltammogram(CV) of **1a** shows a quasi-reversible oxidation at +1.44 V (ΔE_p = 111 mV) (Figure 2.9 and Table 2.5). By comparison with $[Ni(2,2'\text{-bipyridine})_3]^{2+}$, we assign the oxidation as Ni^{II}/Ni^{III}.[28] The cyclic voltammograms of **1b** and **1c** are at the same concentration (4.2 mg/5 mL) compared (Figure 2.9). Though **1c** is different from **1a** but it is not a mixture but a pure compound (Scheme 2.1). The discrimination of one enantiomer is visible in the CV, but not a clear on-off type.

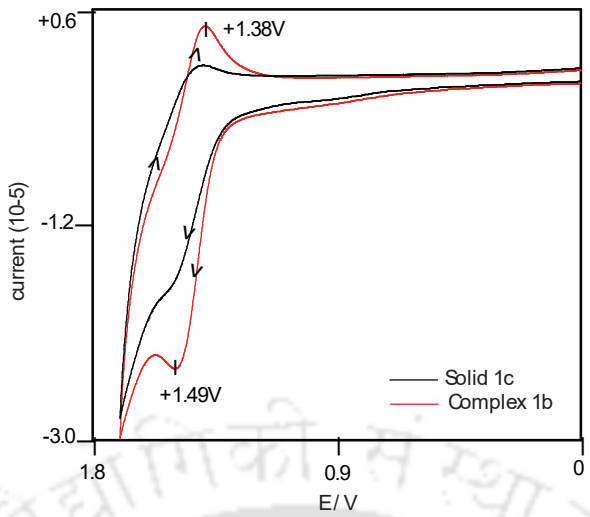

Figure 2.9. Cyclic Voltammogram of complex **1a** and **1c**. Scan rate of 100 mV s^{-1}. Glassy carbon working electrode. $Ag/AgNO_3$ reference electrode.

Table 2.5. Electrochemical data of **1a**, **1b**, **1c** and $[Ni(S\text{-}L1)_3]^{2+}$ (present work) and $[Ni(bpy)_3]^{2+}$ (from Ref. 21).

Complex	Oxidation		$Fe(bpy)_3^{3+}/Fe(bpy)_3^{2+}$	Ferrocene	
	$\Delta E_{1/2}$ (V)	ΔE_p (mV)	$\Delta E_{1/2}$ (V)	$\Delta E_{1/2}$ (V)	ΔE_p (mV)
$Ni(bpy)_3$	+1.45	-	+0.77	-	-
1	+1.44	111	+0.75	+0.09	75
1a	+1.45	102	+0.75	+0.09	75
$Ni(S\text{-}L1)_3$	+1.49	95	+0.75	+0.09	75

Conclusions

Recognition or resolution of 1-phenylethylamine within a coordination complex using non-covalent interactions are difficult. However, there was no enhancement of *S*-1-phenylethylamine in the solid precipitated without crystallization. We used quick precipitation without crystallization as a way to estimate chiral enhancement in solution as NMR methods are difficult to use for paramagnetic complexes.[7] In the present case, we observed ~91 % ee in the crystalline state and ~59% ee in the precipitated form measured using optical rotation as well as CD (Figure 2.7 and 2.8). This is much higher than most of the other reports on recognition using coordination complexes.[9-12] More significantly, the % *ee* in the precipitated form indicates that observed enhancement is not entirely due to crystallization. This indirectly support

solution enhancement. Despite our repeated efforts, we were not been able to isolate the other diastereomer **1c** $[Ni(S\text{-}L1)_2(R\text{-}L2)](ClO_4)_2$ structurally using *R*-L2 instead of racemic form of the ligand. The amorphous solid isolated in this case is found to be a mixture. However, we cannot rule out formation of small quantity of the $[Ni(S\text{-}L1)_2(R\text{-}L2)]^{2+}$ in the solution. The structural characterization identified three relatively strong phenyl….pyridine/imidazole interaction within the complex (Figure 2.1 & 2.2). This feature is preserved in the reported homoleptic complexes of the ligand.[14] Switching of chirality on L2 would mean, either the loss of phenyl…imidazole interaction or having unfavorable methyl…CH interaction (Figure 2.1c). These types of π–stacking are more energetically favored, as pointed out by others.[29] It is possible that 'the energetically favored π–stacking' is behind the observation of high enhancement. The high enhancement and difficulty in isolation of the *R*-L2 containing complex encouraged us to explore the electrochemical signature of **1a** as a means of presence and absence of *S*-L2. The cyclic voltammogram (CV) of **1b** and the solid **1c** are different (Figure 2.9) so are their CD (Figure 2.7), but a clear on-off type situation did not occur presumably due to the presence of homoleptic complex of *S*-L1 in **1c**.

References

1. Mustranta, A. Use of lipases in the resolution of racemic ibuprofen. *Appl. Microbiol. Biotechnol.* **1992**, *38*, 61.

2. Cheng, H.; Rogers, J. D.; Demetriades, J. L.; Holland, S. D.; Seibold, J. R.; Depuy, E. Pharmacokinetics and bioinversion of ibuprofen enantiomers in humans. *Pharm. Res.,* **1994**, *11*, 824.

3. Lloyd, K. G.; Davidson, L.; Hornykiewicz, O.; The neurochemistry of Parkinson's disease: effect of L-dopa therapy. *J. Pharmacol. Exp. Ther*. **1975**, *195*, 453.

4. Caner, H.; Groner, E.; Levy, L.; Agranat, I. Trends in the development of chiral drugs. *Drug Discov. Today*. **2004**, *3*, 105.

5. Cherezov, V.; Rosenbaum, D. M.; Hanson, M. A.; Rasmussen, S. G. F.;Thian, F. S.; Kobilka, T. S.; Choi, H. J.; Kuhn, P.; Weis, W. I.; Kobilka, B. K. High-resolution crystal structure of an engineered human β2-adrenergic G protein--coupled receptor*, Science.* **2007**, *318,* 1258.

6. Sahoo, S. C.; Ray, M. Three Point Chiral Recognition and Resolution of Amino Alcohols Through Well-Defined Interaction Inside a Metallocavity. *Chem. Eur. J.* **2010**, *16*, 5004.

7. Das, C. R.; Sahoo, S. C.; Ray, R. Chiral Recognition and Partial Resolution of 1-Phenylethylamine through Noncovalent Interactions Using Binuclear Ni (II) Complex as Host. *Cryst. Growth Des*. **2014**, *14*, 3958.

8. Das, C. R.; Dutta, T.; Ray, M. Effect of ligand and bridge substitution on chiral recognition of 1-phenylethylammonium cation by an anionic binuclear Ni (II) complex, *Inorganica Chim. Acta.* **2019**, *486*, 367.

9. Chin, J.; Lee, S. S.; Lee, K. J.; S. Park.; S. Kim, D. H. A metal complex that binds α-amino acids with high and predictable stereospecificity. *Nature*. **1999**, *401*, 254.

10. Tashiro, S.; Ogura, Y.; Tsuboyama, S.; Tsuboyama, K.; Shionoya, M. Chiral recognition of α-Amino acids by an optically active (2 s, 5 s, 8 s, 11 s)-2, 5, 8, 11-tetraethyl cyclen Cobalt (III) complex. *Inorg. Chem*. **2010**, *50*, 4.

11. Kurtan, T.; Nesnas, N.; Koehn, F. E.; Li, Y. Q.; Nakanishi, K.; Berova, N. Chiral Recognition by CD-Sensitive Dimeric Zinc Porphyrin Host. 2. Structural Studies of Host-Guest Complexes with Chiral Alcohol and Monoamine Conjugates. *J. Am. Chem. Soc*. **2001**, *123*, 5974.

12. Imai, H.; Munakata, H.; Uemori, Y.; Sakura, N. Chiral recognition of amino acids and dipeptides by a water-soluble zinc porphyrin. *Inorg. Chem*. **2004**, *43*, 1213.

13. Yao, S, Y.; Chen, X, Y.; Ou, Y, L.; Ye, B. H. Chiral Recognition and Dynamic Thermodynamic Resolution of Sulfoxides by Chiral Iridium(III) Complexes. *Inorg. Chem.* **2017**, *56*, 878.

14. (a) Howson, S. E.; Allan, L. E. N.; Chmel, N. P.; Clarkson, G. J.; Deeth, R. J.; Faulkner, A. D.; Simpson, D. H.; P. Scott, P. Origins of stereoselectivity in optically pure phenylethaniminopyridine tris-chelates M (NN′)3n+ (M= Mn, Fe, Co, Ni and Zn). *Dalt. Trans.* **2011**, *40*, 10416. (b) Howson, S. E.; Allan, L. E. N.; Chmel, N. P.; Clarkson, G. J.; Gorkum, R. V.; Scott, P. Self-assembling optically pure Fe(A–B)3 chelates, Chem.

Commun., **2009,** 1727. (c) Howson, S. E.; Scott, P. Comments on "Synthesis and characterisation of enantiopure copper(II) complexes with chiral bidentate ligands", *Dalton Trans*., **2011**, *40*, 4332. (d) Synthesis and isolation of the ligand *S*-L1; Schoumacker, S.; Hamelin, O.; Teti, S.; Pecaut, J.; Fontecave, M. Activation of Oxaziridines by Lewis Acids: Application in Enantioselective Sulfoxidation, *J. Org. Chem.* **2005**, *70*, 301.

15. Kelly, S. L.; Kadish, K. M. Electron-transfer and ligand-addition reactions of (TPP) $CrClO_4$ and (TPP)Cr(NO) in nonaqueous media. *Inorg. Chem*. **1984**, *23*, 679.

16. Farrugia, L. J.; WinGX and ORTEP for Windows: an update. *J. Appl. Crystallogr*. **2012**, *45*, 854.

17. Sheldrick, G. M.; Crystal structure refinement with SHELXL, Acta Crystallogr. Sect. C Struct. Chem. **2015**, *71*, 3.

18. Grimme, S. Do special noncovalent π-π stacking interactions really exist? *Angew. Chemie Int. Ed*. **2008**, *47*, 3430.

19. Dubey, M.; Koner, R. R.; Ray, M. Sodium and potassium ion directed self-assembled multinuclear assembly of divalent nickel or copper and l-leucine derived ligand. *Inorg. Chem*. **2009**, *48*, 9294.

20. A.B.P. Lever, Inorganic electronic spectroscopy, **1968.**

21. England, J.; Bill, E.; Weyhermüller, T.; Neese, F.; Atanasov, M.; Wieghardt, K. Molecular and electronic structures of homoleptic six-coordinate cobalt (I) complexes of 2, 2′: 6′, 2 ″-terpyridine, 2, 2′-bipyridine, and 1, 10-phenanthroline. An experimental and computational study. *Inorg. Chem*. **2015**, *54*, 12002.

22. Earnshaw, A. Introduction to magnetochemistry, Elsevier, **2013**.

23. Figgis, B. N.; Lewis, J. A review of magnetochemistry, *Prog. Inorg. Chem*. **1964**, *6*, 37.

24. Sahoo, S. C.; Dubey, M.; Alam, M. A.; Ray, M. Effect of metal coordination and intra-molecular H-bond on the acidity of phenolic proton in a set of structurally characterized octahedral Ni (II) complexes of l-histidine derivative. *Inorganica Chim. Acta*. **2010**, *363*, 3055.

25. Albrecht, M.; Osetska, O.; Abel, T.; Haberhauer, G.; Ziegler, E. An enantiomerically pure siderophore type ligand for the diastereoselective 1 : 1 complexation of lanthanide(III) ions. *Beilstein J. Org. Chem*. **2009**, *5*, 78.

26. R. Prasad, D.B. Scaife, Electro-oxidation and electro-reduction of some iron (II), cobalt (II) and nickel (II) polypyridyl complexes in acetonitrile, *J. Electroanal. Chem. Interfacial Electrochem*. **1977**, *84*, 386.

27. Katayama, Y.; Toshimitsu, Y.; Miura, T. Electrode kinetics of the redox reaction of tris (2, 2′-bipyridine) nickel complexes in an ionic liquid. *Electrochim. Acta.* **2014**, *131*, 36.

28. Henne, B. J.; Bartak, D. E. Metal-vapor synthesis and electrochemistry of bis (bipyridyl) nickel (0). *Inorg. Chem*. **1984**, *23*, 369.

29. Hohenstein, E. G.; Sherrill, C. D. Effects of heteroatoms on aromatic π-π interactions: benzene- pyridine and pyridine dimer. *J. Phys. Chem. A.* **2009**, *113*, 878.

30. Nishio, M.; Hirota, M.; Umezawa, Y.; Evidence, Nature and Consequences, **1998**.

31. Desiraju, G. R.; Steiner, T. The Weak Hydrogen Bond, **1999**.

32. Desiraju, G. R. Hydrogen bridges in crystal engineering: interactions without borders, Acc. Chem. Res. **2002**, *35*, 565.

33. Nishio, M. CH/π-Hydrogen Bonds in Crystals. *ChemInform*. **2004**, 35, no--no.

34. Macrae, C. F.; Edgington, P. R.; McCabe, P.; Pidcock, E.; Shields, G. P.; Taylor, R.; Towler, M.; Streek, J. V. D. Mercury: visualization and analysis of crystal structures. *J. Appl. Crystallogr*. **2006**, *39*, 453.

Chapter III

Chiral resolution of 1-phenylethylamine in Schiff base form using kinetically inert Fe (II) complexes

Introduction

In principle, mixing two different ligand and metal salt can generate multiple two homoleptic and multiple heteroleptic complex in solution. The isolation of one heteroleptic complex depends on the relative stability and solubility of that complex compared to others. It seldom led to mixture. Earlier we isolated $[Ni(S\text{-}L1)_2(S\text{-}L2)](ClO_4)_2$ from MeCN / ethylacetate without encountering problem (chapter II). Octahedral Ni(II) complexes are kinetically labile and all possible product in solution was in equilibrium. The product with less solubility could crystalize out exclusively shifting the equilibrium in its favor. In contrast, $[Fe(S\text{-}L1)_3]^{2+}$ is a low-spin, kinetically inert complex.[1] Thus, species distribution in solution is expected to be very different and isolation of one will depends on number of factors including the spin-state of the complexes. There are examples of chiral resolution using metals like Zn(II), Co(III), Cu(II), Ni(II) but not using Fe(II) low-spin complex.[2-5] After exploring chiral resolution of 1-phenylethylamine in labile Ni (II) complexes (previous chapter) we used kinetically inert Fe (II) complex (this chapter) instead. In order to do so we have synthesized $[Fe(S\text{-}L1)_2(S\text{-}L2)](ClO_4)_2$ from three different reaction pathways (reaction I, II and III) (Scheme 3) and checked its effect on chiral resolution (reaction I), magnetic and electronic properties how different they behave as compared to a kinetically labile Ni(II)-complex.

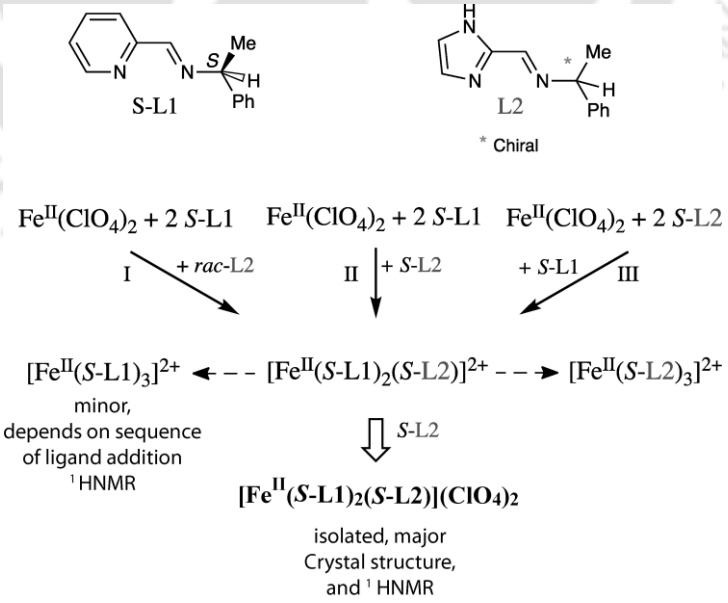

Scheme 3.1. Reactions I – III varying the sequence of ligand addition along with possible products.

3. Experimental Section

3.1 Materials and Methods

Same material and methods of analyses were used as in the previous chapter. $Fe(ClO_4)_2.7H_2O$ used here has been purchased from Aldrich Chemical Co.

3.2 Syntheses

The syntheses and characterization of the ligands *S*-L1, *S*-L2, *R*-L1, and *R*-L2 are given in the previous chapter. These ligands are used here to make Iron(II) complexes and used for all the experiments.

3.2.1 [Fe(*S*-L1)$_2$(*S*-L2)](ClO$_4$)$_2$ (reaction I)[2a]

The ligand *S*-L1(0.150 g, 0.71 mmol, 2 eq.) was dissolved in 3 mL of acetonitrile and stirred initially at room temperature. To the stirred solution, $Fe(ClO_4)_2{\cdot}7H_2O$(0.131 g, 0.36 mmol, 1 eq.) in 4 mL of acetonitrile was added dropwise, which turned it to a dark purple solution followed by the addition of racemic-L2(0.142 g, 0.71 mmol, 2 eq.) in 5 mL acetonitrile and stirred for 4 h. The solvent was layered with ethyl acetate, covered properly, and kept in the refrigerator for crystallization. Dark purple crystals appeared after 3-4 days. The compound was found to be diamagnetic. The complex is soluble in both methanol and acetonitrile. Yield (64%). FTIR (KBr, cm^{-1}): $\upsilon_{(C=N)stretch}$ 1613(s). μ_{eff} (powder, 298K): 0.77.

3.2.1 [Fe(*S*-L1)$_2$(*S*-L2)](ClO$_4$)$_2$ (reaction II)[2b]

The ligand *S*-L1(0.150 g, 0.71 mmol, 2 eq.) was dissolved in 3 mL of acetonitrile and stirred initially at room temperature. To the stirred solution, $Fe(ClO_4)_2{\cdot}7H_2O$(0.131 g, 0.36 mmol, 1 eq.) in 4 mL of acetonitrile was added dropwise, which turned it to a dark purple solution followed by the addition of *S*-L2(0.71 g, 0.36 mmol, 1 eq.) in 3 mL acetonitrile and stirred for 4 h. The solvent was layered with ethyl acetate, covered properly, and kept in the refrigerator for crystallization. Dark purple crystals appeared after 3-4 days. The compound was found to be diamagnetic. The complex is soluble in both methanol and acetonitrile. Yield (67%). FTIR (KBr, cm^{-1}): $\upsilon_{(C=N)stretch}$ 1615(s). μ_{eff} (powder, 298K): 1.04

3.2.2 [(*S*-L2)$_2$Fe(*S*-L1)](ClO$_4$)$_2$ (reaction III)[2c]

The ligand *S*-L2(0.150 g, 0.75 mmol, 2 eq.) was dissolved in 10 mL of acetonitrile and stirred initially at room temperature. To the stirred solution, $Fe(ClO_4)_2 \cdot 7H_2O$(0.138 g, 0.37 mmol, 1 eq.) in 10 mL of acetonitrile was added dropwise, which turned it to a dark red solution followed by the addition of *S*-L1(0.079 g, 0.37 mmol, 1 eq.) in 5 mL acetonitrile which turned the solution to dark purple and stirred for 4 h. The solvent was reduced and layered with ethyl acetate, covered properly, and kept in the refrigerator for crystallization. Dark purple crystals appeared after 2 days. The compound was found to be diamagnetic. The complex is soluble in both methanol and acetonitrile. Yield (67%). Anal. Calcd. for $[Fe(C_{14}H_{14}N_2)_2(C_{12}H_{13}N_3)] \cdot 2(ClO_4) \cdot 1.25CH_3OH \cdot 0.5CH_3CN$: C, 54.25; H, 5.10; N, 10.99; found C, 54.58; H, 5.37; N, 10.78. FTIR (KBr, cm^{-1}): $\upsilon_{(C=N)stretch}$ 1615(s). μ_{eff} (powder, 298K): 0.8

3.3 X-ray Data Collection, Structure Solvation and Refinement

All the crystals show desolvation to a different degree. Thus, the crystals were covered with grease (Vaseline) and mounted on glass fiber for data collection. All geometric and intensity data for the crystals of **2a** and **2b** were collected at a low temperature using a 'CrysAlisPro 1.171.40.23a (Rigaku Oxford Diffraction, 2018)' diffractometer equipped with a fine focus 1.75 kW sealed tube Mo-Kα (λ = 0.71073 Å) X-ray source. The SMART software was used for data acquisition and the 'CrysAlisPro 1.171.40.23a (Rigaku OD, 2018)' software for data extraction and reduction. Absorption corrections were done using spherical harmonics, implemented in SCALE3 ABSPACK scaling algorithm. The final refinements were performed on WinGX environment.[6] Almost all non-hydrogen atoms in the complexes were refined anisotropically. In **2a** and **2b**, 'SQUEEZE' was performed in order to remove the disordered solvent molecules.[7] All of the hydrogen atoms were added in the refinement stage. The molecular weight from structure and bulk may not match as the dry powdered form of crystals was used for elemental analysis and other studies.

3.4 Results and Discussion

3.4.1 Syntheses

The mixed ligand complexes were synthesized by two different sequential addition of the ligands as shown in (Scheme 3.1). For reaction I and II we kept the sequence of ligands the same and only changed the stoichiometric ratio. The enantiopure *S*-L1 was reacted with Iron (II) salt first before the addition of *racemic*-L2 (reaction I) or *S*-L2 (reaction II). For **2a**, the ratio of Fe: *S*-L1: *racemic*-L2 used was 1:2:2. The use of *racemic*-L2 at double the quantity than required for $[Ni(S\text{-}L1)_2(L2)]^{2+}$ was to maximize yield in case only one of the enantiomers of L2 binds. Complex **2b** using enantiopure S-L2 was used as a reference compound. A second synthetic pathway shown in reaction III (Complex **2c**) was used where the sequence of addition of the ligands were reversed along with the stoichiometric ratio. For **2c**, the ratio of *S*-L2: Fe: *S*-L1 used was 2:1:1 (Scheme 3). All the complexes (**2a-c**) was characterized by FTIR, ESI-MS and 1HNMR spectra.

3.4.2 Molecular structures of the complex 2b

The molecular structure of the unit is viewed along the C_3 axis along with key bond length and angles. The crystal selected for single crystal X-ray diffraction had the chiral space group $P2_1$. The asymmetric unit contains one complex molecule, two perchlorate anions and one acetonitrile molecule. The geometry around Fe(II) slightly deviated from the perfect octahedron. This is evident from the deviation of angles from the ideal value of 90º for in-plane angles and 180º for axial angles (Table 3.2) with Fe-N bond lengths with Pyridine-N is 1.959 and 1.973 Å, one with imidazole-N is 1.980 Å. The average Fe-N bond length in a kinetically inert Fe complex is lesser than than the average Ni-N bond length in the similar kinetically labile Ni complex (Table S7). This means that all the Fe-N bonds are equal but in Ni-complex the axial Ni-N bonds are longer than the equatorial one. A shorter distance between Fe-N-H...O (2.813 Å) than its corresponding Ni-analogue (2.885 Å) (Table S8) shows that it has a stronger H-bonding with the perchlorate anion. The complex **2b** is a facial (fac) isomer with all three imines are on a triangular face. The pyridines and imidazole are in the opposite triangular face. The complex is an Δ isomer. This is one out of 16 possible isomers. In all the reported single crystal X-ray structures of $[M(S\text{-}L1)_3]^{2+}$, where M is either nickel (II) or iron (II), have this preference.[8] All the chiral centers at

C5, C19, and C33 have the S-conformation. Each heterocyclic ring is π-stacked forming a parallel-displaced configuration [P1a(-) or P1b] type with the phenyl ring from the neighbouring ligand.[9] The displacement between the imidazole...phenyl moiety 3.120(Å) is less compared to the displacement between the pyridine…phenyl moieties [3.644(Å) and 3.794(Å)]. This means the imidazole…phenyl ring is comparatively more strained, possibly due to the NH-group of the imidazole participates in H-bonding with an oxygen atom of perchlorate molecule N(2)-H(2)…O(5) by shifting towards it (Table 3.3). This H-bond also reduces the disorderedness of one perchlorate anion compared to the other. and this is also accompanied by a few short contacts with perchlorate anions as well as other complex in the lattice. This π-stacks contribute to a particular chirality of the third ligand (L2) having S conformation as with R conformer, no crystals were obtained. Overall, structural characterizations showed three parallelly displaced π...π type interactions between phenyl rings and either pyridine or imidazole are strong and have been preserved in all the present and previously reported.[10] The structural comparison of Complex **2a** is similar to Complex **2b** (Table S5 and S6).

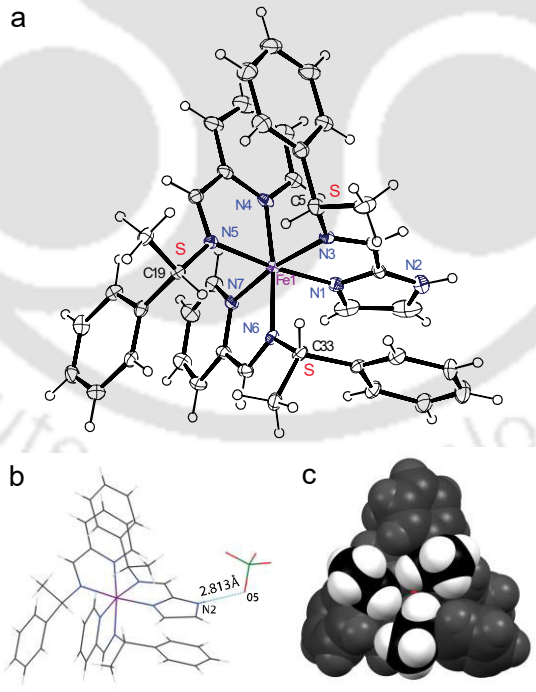

Figure 3.1. (a) ORTEP diagram of the cationic part of Complex **2b**. Thermal ellipsoids set to 50% probability level. **(b)** Model highlighting the H-bonding between **2b** and the surrounding perchlorate anion. **(c)** Space filling model of **2b**, highlighting the orientation of the methyl group within the complex.

Table 3.1. Crystallographic data and refinement parameters of complexes.

	2a	**2b**
Empirical formula	C42 H44 N8 Fe1 O8 Cl2	C42 H44 N8 Fe1 O8 Cl2
fw	915.60	915.60
crystal system	Monoclinic	Monoclinic
space group	$P12_11$	$P12_11$
a, A°	12.1942(7)	12.1925(7)
b, A°	13.2349(4)	13.1896(5)
c, A°	15.3764(8)	15.3653(8)
$\beta(°)^a$	107.612(6)	107.415(5)
V, $Å^3$	2365.3(2)	2357.7(2)
Z/ρ (g cm^{-3})	2/1.286	2/1.290
T(K)	293(2)	293(2)
μ (mm^{-1})	0.488	0.490
coll.reflns	7281	6968
indep reflns	6494	6253
FLACK para.	-0.014(18)	0.04(2)
GOF on F^2	1.029	1.038
Residuals (e $Å^{-3}$)	0.921, -0.486	1.025, -0.460
$R1^b$, $wR2^b$	0.0502/0.1285	0.0573/0.1457
$R1^c$, $wR2^c$	0.0573/0.1359	0.0634/0.1522

[a] $\alpha(°) = \gamma(°) = 90$ [b] $I > 2\sigma$ [c] All data

Table 3.2. Selected bond length (Å) and angles (º) for the complex **2b**.

Fe1-N1	1.960(4)	N6-Fe1-N7	81.42(17)
Fe1-N3	2.003(4)	N5-Fe1-N7	91.62(17)
Fe1-N4	1.965(4)	N4-Fe1-N7	93.56(17)
Fe1-N5	1.962(4)	N1-Fe1-N7	90.88(18)
Fe1-N6	1.978(4)	N1-Fe1-N3	81.00(18)
Fe1-N7	1.960(4)	N5-Fe1-N4	81.29(17)
N3-C4	1.288(7)	N4-Fe1-N6	173.11(17)
N5-C18	1.289(6)	C4-N3-C5	119.3(5)
N6-C32	1.285(7)	C1-N1-Fe1	137.3(5)

Table 3.3. Non covalent interactions in complex **2b**.

D-H...A	D-H (Å)	H. . .A(Å)	D. . .A(Å)	DHA(°)
Inter-molecular				
N2-H2A..O1	0.86	1.97	2.825(11)	174
C18-H18..O4	0.93	2.56	3.390(7)	148
C27-H27..N4	0.93	2.56	3.051(7)	114
C27-H27..O4	0.93	2.40	3.154(7)	139
C29-H29..O8	0.93	2.57	3.346(8)	142
C32-H32..O8	0.93	2.57	3.425(6)	152
C2-H2…π(C6-C11)	0.93	2.79	3.479	131

The acceptable range of D...A for N-H..O, 2.5-3.2 Å; for C-H..O, 3.0-4.0 Å; N-H/C-H... π 2.5–4.5 Å, from ref. [11-14] §Calculated from Mercury.

3.4.3 FTIR spectra and ESI-MS of Complex 2b

FTIR spectra of **2b** shows $\nu_{C=N}$ stretch assigned to ~ 1613. Strong and broad absorption ~ 1100 cm^{-1} confirms the presence of perchlorate anion (Figure 3.2). Complex **2a** and **2c** showed similar stretching frequencies around the same values (Figure S4 and S5) The ESI-MS spectrum of **2b** (Figure 3.3) showed the presence of

the protonated molecule, at m/z 674.28 (z = 1) corresponding to $[Fe(L1)_2(L2)\text{-}H]^+$. The other abundant ions corresponding to the formation of bis complex of $[Fe(L1)(L2)\text{-}H]^+$ (z = 1). The spectrum also showed a prominent peak at m/z 238.09 (z = 2) of $[Fe(L1)_2]^{2+}$. Both of the bis complexes formed as a result in the loss of one ligand (either L1 or L2) from the parent complex. This complex also showed the presence of the homoleptic tris complex $[Fe(L1)_3]^{2+}$ at 343.14 (z = 2) There were trace amounts of the ligand L1 at m/z = 211.12 and free amine at m/z = 122.09 respectively in the spectrum. The spectrum of **2a** (Figure S6) is mostly similar to that of **2b** in terms of both speciation and fragmentation pattern.

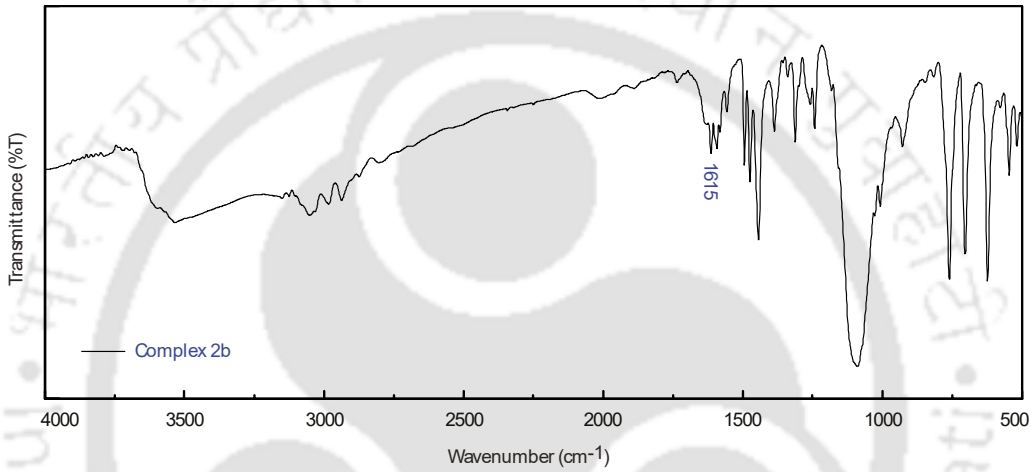

Figure 3.2. FTIR spectrum of Complex **2b**.

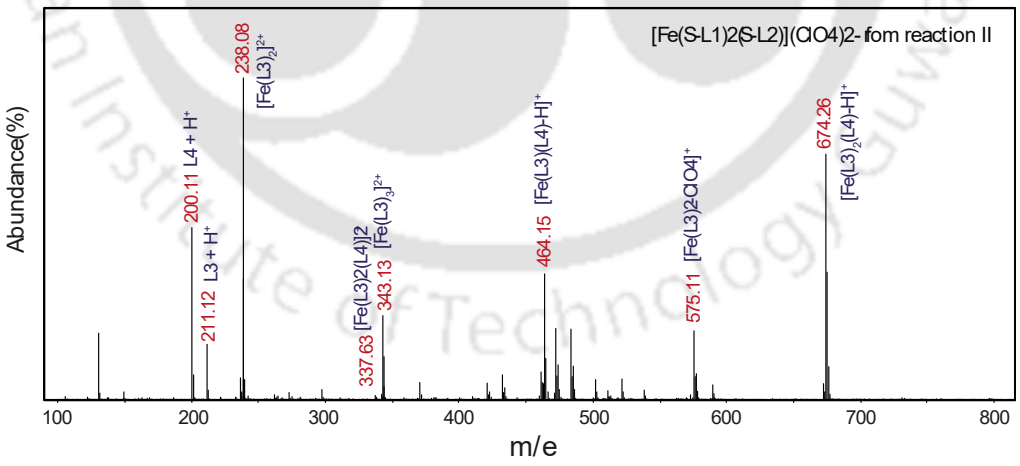

Figure 3.3. ESI-MS spectrum diffraction pattern of in positive ion mode.

3.4.4 NMR spectra of [Fe(*S*-L1)$_2$(*S*-L2)] in comparison with [Fe(*S*-L1)$_3$]$^{2+}$

The ^{1}HNMR of the mixed ligand shows the presence of the homoleptic complex [Fe(*S*-L1)$_3$](ClO$_4$)$_2$ (Figure 3.4). This happens because of the sythesis sequence when *S*-L1 is added initially along with the Fe(ClO$_4$)$_2$ the homoleptic complex is formed and due to the inert nature of the complex, minute amount stays in the solution along with the mixed ligand complex which is detected in many solution spectra. The ratio of *S*-L1 in homoleptic : mixed ligand complex is 3:2 which is seen in the picture (Figure 3.4, reaction II). Imine-H and chiral-H peak of *S*-L2 have been identified while the rest of the peaks are mixed with the other in the multiplet region δ(6.8-7.6) ppm. The plot of reaction III shows a decrease of the Imine-H peak of the homoleptic complex from as compared to reaction II. This is due to the formation of the hompletic in solution here is less on changing the sequence of the addition of the ligands. We have minimised it's formation but we have not been able to eliminate it completely. NMR we can conclude that [Fe(*S*-L1)$_3$](ClO$_4$)$_2$ is present in the solution at room temperature.

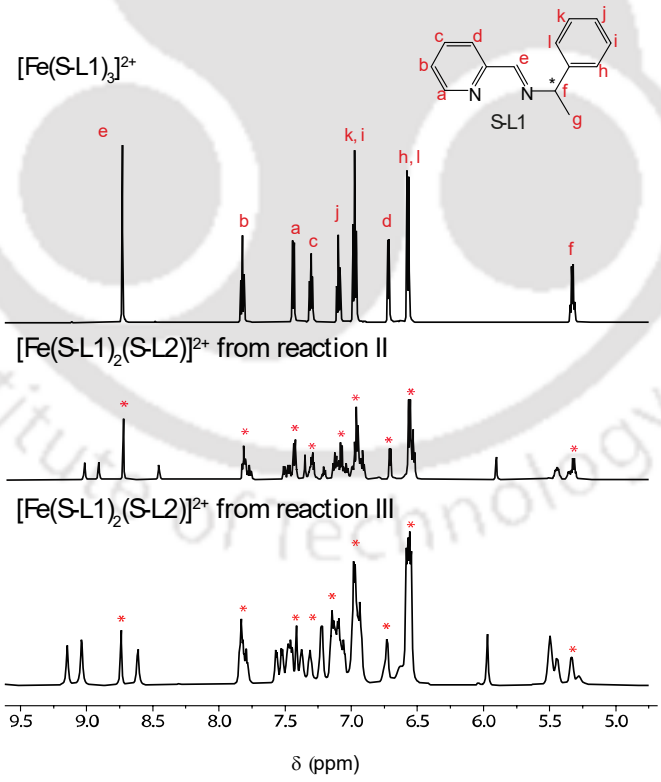

Figure 3.4. ^{1}H NMR spectra of homoleptic [Fe(*S*-L1)$_3$]$^{2+}$ complex and isolated products from reactions II and III of Scheme I in CD$_3$CN. The '*' marked peaks have contribution from homoleptic complex present in heteroleptic complex.

^{13}C NMR of homoleptic complex $[Fe(S\text{-}L1)_3]^{2+}$ and mixed ligand complex $[Fe(S\text{-}L1)_2(S\text{-}L2)]^{2+}$ was done in acetonitrile at room temperature (Figure S29 and S30). The ^{13}C NMR spectra of the mixed ligand complex shows the presence of the homoleptic complex along with as shown by 1H-NMR spectra. However the ^{13}C NMR spectra did not give us any extra information.

3.5 Electronic spectra of 2b.

The electronic spectra of the complex in acetonitrile show strong bands between 200-300 nm corresponding to ligand centered $\pi-\pi^*$ transitions. The complex have strong MLCT bands between 300-700 nm (Figure 3) at 519 nm ($\varepsilon = 4378\ M^{-1}\ cm^{-1}$) and 567 nm ($\varepsilon = 5566\ M^{-1}\ cm^{-1}$) with high 'ε' values. The high intense 'ε' values is indicative of the low-spin nature of the complex at room temperature. The slight structural deviation from a perfect octahedron gives rise to an additional third MLCT band at 358 nm (2645 $M^{-1}\ cm^{-1}$).[8] Complex **2a** and **2c** having the same coordination environment show similar charge transitions at room temperature as shown in Figure 3.5.

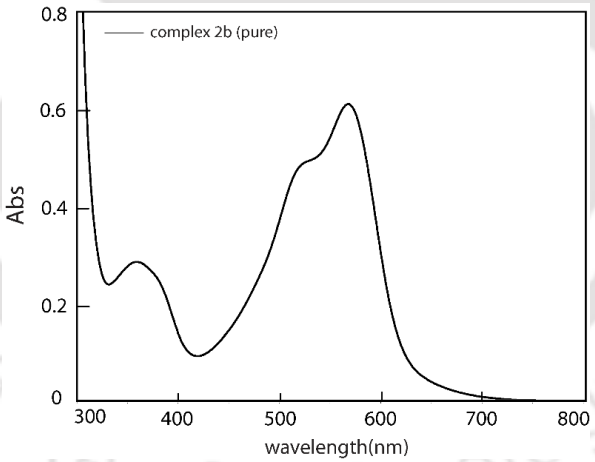

Figure 3.5. UV-visble spectrum of $[Fe(S\text{-}L1)_2(S\text{-}L2)](ClO_4)_2$ highlighting the charge transfer region (300-800 nm).

3.6 Electrochemical properties of Complexes 2b and 2c.

Comparing the cyclic voltammogram of the complexes, it is observed that $[Fe(S\text{-}L1)_2(S\text{-}L2)](ClO_4)_2$ show a clear reversible oxidation peak at ($E_{1/2}$ = + 1.00 V) and one small shoulder. The small shoulder peak matched exactly with the $[Fe(S\text{-}L1)_3](ClO_4)_2$ plot having a single oxidation peak at ($E_{1/2}$ = + 1.12 V) (Figure 3.6a). However in

reaction II, we saw a similar voltammogram but the shoulder here was a bare minimum (Figure 3.6b). The formation of the homoleptic complex is also detected here but it is less. The amount of *S*-L1 given in reaction III is half equivalent than that in reaction II which could be the reason that the formation of $[Fe(S\text{-}L1)_3]^{2+}$ is much less as observed in cyclic voltammetry. Along with ^{1}HNMR and ESI-MS spectra, we could also electrochemically detect the presence of $[Fe(S\text{-}L1)_3](ClO_4)_2$ in solution equilibrium with $[Fe(S\text{-}L1)_2(S\text{-}L2)](ClO_4)_2$ at room temperature.

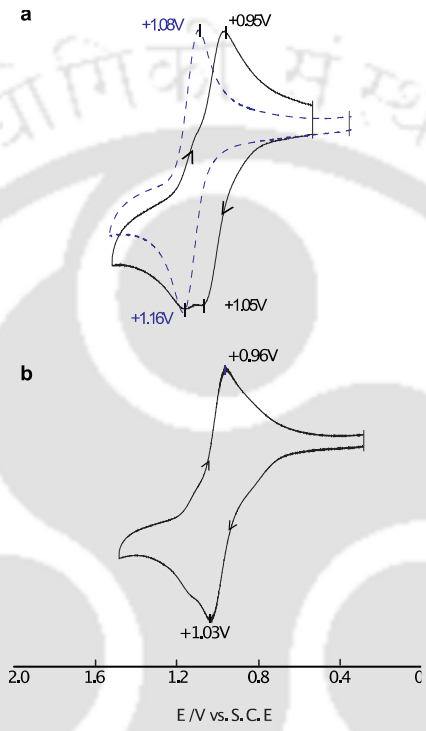

Figure 3.6. The Fe^{II}/Fe^{III} redox couple in cyclic voltammetry of isolated products of (a) reaction II and (b) reaction III of Scheme I in MeCN. The redox couple of $[Fe(S\text{-}L1)_3]^{2+}$, blue dashed plot in (a), is overlapped to show its presence.

3.7 Enantiomeric excess in kinetically inert a complex

CD spectra of the complex **2a** and **2b** bands are at comparable wavelengths and relative intensities to the corresponding peaks assigned to MLCT transitions in the UV-visible spectrum. From ^{1}HNMR and Cyclic voltammetric (Figure 3.5) studies we observed the homoleptic $[Fe(S\text{-}L1)_3]^{2+}$ complex in solution equilibrium with the heteroleptic complex $[Fe(S\text{-}L1)_2(S\text{-}L2)]^{2+}$ as it was expected to be (Figure 3.4 and 3.6). But still we wanted to test the % enhancement in inert complexes. Chiral enhancement in the crystalline and the precipitated form have benn calculated by circular dichroism studies using similar method like Ni (II) complexes in the previous

chapter. From the spectra the observed enhancement in isolated bulk crystals in Fe-complex was found to be (~ 66% *ee*) and the enhancement in isolated bulk amorphous form was found to be (~ 54% *ee*). When we compared the % *ee* with a kinetically labile Ni(II) complex, we found a substantial decrease from what we had observed before in Ni-complex.

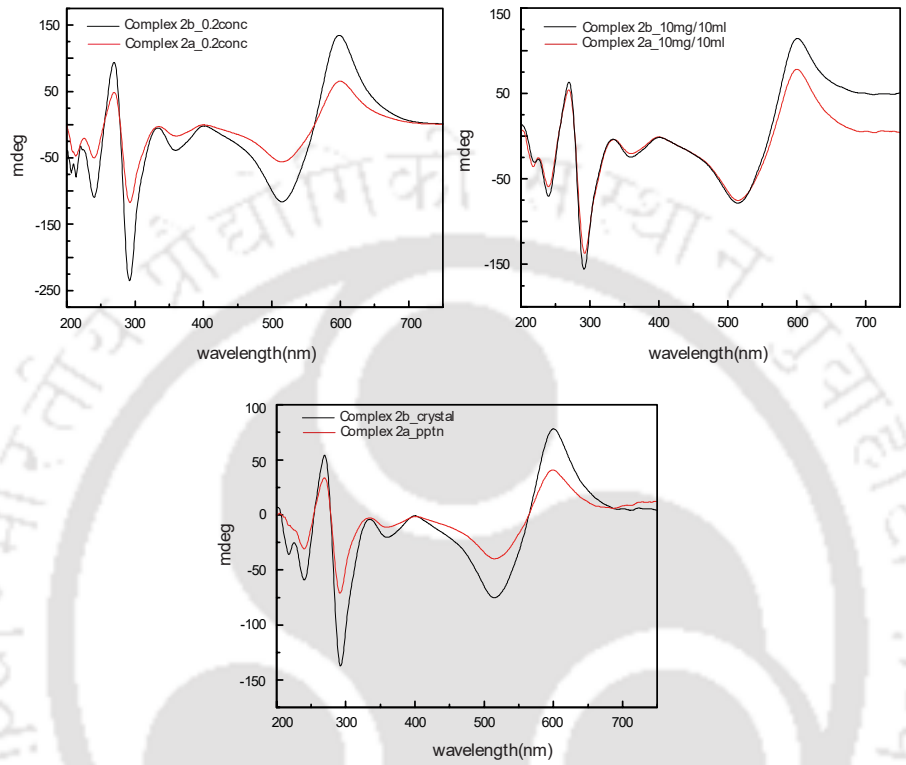

Figure 3.7. Concentration dependant Circular Dichroism spectra of Complexes **2a** and **2b** complexes comparing the racemic and pure form in acetonitrile.

Conclusions

We attempted the synthesis of $[Fe(S\text{-}L1)_2(S\text{-}L2)]^{2+}$ by three different methods (Scheme I). The two reactions (reaction II and III) we used enatiomerically pure ligand reversing the sequence of addition. The third one (reaction I) is identical with reaction II except that the racemic version of the L2 was used in double quantity to induce chiral recognition. Enantiomeric enhancement from CD spectra was observed in isolated bulk crystals in Fe-complex was found to be (~ 66% *ee*) and in isolated bulk amorphous form was found to be (~ 54% *ee*) (Figure 2) in comparison with Ni(II) complex it was found to be (~ 90% *ee*) in crystallized form and (~ 59%) amorphous form. Digging deep we found out the reason for decreased enhancement was the presence of $[Fe(S\text{-}L1)_3]^{2+}$ which is present as an impurity along with Fe-

mixed ligand complex. This was evident from ES-MS, NMR and cyclic voltammetric experiments. However from reaction III we were able to isolate the Fe-mixed ligand complex which had the impurity but much less in quantity. This happens either due to the addition of the *S*-L2 ligand first which drives the reaction towards the mixed ligand complex than the homoleptic one or the amount of *S*-L1 ratio of reaction II : reaction III is 2:1 which lead to lesser formation of the homoleptic complex. From NMR we could see the imine-H from the homoleptic complex is decreased in reaction III (Figure 4). Even cyclic voltammogram showed minute presence of the homoleptic complex (Figure 7). The crystal structure and chiral enhancement from CD shows that chiral recognition does take place same way as in Ni(II) complexes. However, the low-spin kinetically inert nature of $[Fe(S\text{-}L1)_3]^{2+}$ and $[Fe(S\text{-}L1)_2(S\text{-}L2)]^{2+}$ leads to complication by unintentional formation of $[Fe(S\text{-}L1)_3]^{2+}$. It could be minimised by changing the ligand addition sequence but could never be avoided completely. For resolution through formation of mixed ligand complex, kinetically inert complexes is not the viable option.

References

1. Yao, S, Y.; Chen, X, Y.; Ou, Y, L.; Ye, B. H. Chiral Recognition and Dynamic Thermodynamic Resolution of Sulfoxides by Chiral Iridium(III) Complexes. *Inorg. Chem.* **2017**, *56*, 878.

2. Chin, J.; Lee, S.S.; Lee, K.J.; Park, S.; Kim, D.H. A metal complex that binds α-amino acids with high and predictable stereospecificity, *Nature*. **1999**, *401*, 254.

3. Murphy, D. M.; Caretti, I.; Carter, E.; Fallis, I. A.; G€obel, M. C.; Landon, J.; Doorslaer, S. V.; Willock, D. J. Visualizing Diastereomeric Interactions of Chiral Amine-Chiral Copper Salen Adducts by EPR Spectroscopy and DFT. *Inorg. Chem*. **2011**, *50*, 6944.

4. Imai, H.; Munakata, H.; Uemori, Y.; Sakura, N. Chiral Recognition of Amino Acids and Dipeptides by a Water-Soluble Zinc Porphyrin. *Inorg. Chem*., **2004**, *43*, 1211.

5. Tashiro, S.; Ogura, Y.; Tsuboyama, S.; Tsuboyama, K.; Shionoya, M. Chiral recognition of α-Amino acids by an optically active (2 s, 5 s, 8 s, 11 s)-2, 5, 8, 11-tetraethyl cyclen Cobalt (III) complex, *Inorg. Chem.* **2010**, *50*, 4.

6. Farrugia, L. J.; WinGX and ORTEP for Windows: an update. *J. Appl. Crystallogr*. **2012**, *45*, 854.

7. Sheldrick, G. M.; Crystal structure refinement with SHELXL, *Acta Crystallogr. Sect. C Struct. Chem*. **2015**, *71*, 3.
8. Howson, S. E.; Allan, L. E. N.; Chmel, N. P.; Clarkson, G. J.; Deeth, R. J.; Faulkner, A. D.; Simpson, D. H.; P. Scott, P. Origins of stereoselectivity in optically pure phenylethaniminopyridine tris-chelates M (NN′)3n+ (M= Mn, Fe, Co, Ni and Zn). *Dalt. Trans*. **2011**, *40*, 10416.
9. Hohenstein, E. G.; Sherrill, C. D. Effects of heteroatoms on aromatic π-π interactions: benzene- pyridine and pyridine dimer. *J. Phys. Chem. A*. **2009**, *113*, 878.
10. Bhattacharya, S.; Ray, M. Chiral resolution of 1-phenylethylamine in Schiff base form within a mixed ligand complex of Ni(II). *Inorganica Chim. Acta*. **2020**, *502*, 119338.
11. Desiraju, G. R.; Steiner, T. The Weak Hydrogen Bond. **1999**.
12. Desiraju, G. R. Hydrogen bridges in crystal engineering: interactions without borders, *Acc. Chem. Res*. **2002**, *35*, 565.
13. Nishio, M. CH/π-Hydrogen Bonds in Crystals. *ChemInform*. **2004**, *35*, no--no.
14. Macrae, C. F.; Edgington, P. R.; McCabe, P.; Pidcock, E.; Shields, G. P.; Taylor, R.; Towler, M.; Streek, J. V. D. Mercury: visualization and analysis of crystal structures. *J. Appl. Crystallogr.* **2006**, *39*, 453.

Chapter IV

Effect of pyridine and imidazole group on spin-state and electrochemical properties within chiral bidentate Fe(II) complexes

Introduction

In the previous chapter we have seen how chiral resolution is affected due to change in spin-state of the metal. Due to low-spin, the mixed ligand [Fe(*S*-L1)$_2$(*S*-L2)](ClO$_4$)$_2$ complex we could see the presence of the homoleptic complex [Fe(*S*-L1)$_3$]$^{2+}$ (here Complex **1**) as an impurity which is observed from ^{1}HNMR and cyclic voltammetric analysis. Spin-state of Fe(II) is capable of flipping between high-spin to low-spin with a significant difference in lability. Hence, reactivity has garnered attention due to the frequent occurrence of spin-crossover phenomena and observation of thermochromism in these due to spin-crossover behaviors in the solid-state.[1] Studies are mostly restricted to solid-state magnetism, and Mössbauer spectroscopic experiment as most of the spin-crossover behavior occurs at low temperature.[1] Imidazole forms the main structure of some well-known components of human organisms, that is, the amino acid histidine, Vit-B12, purines, histamine, and biotin. Imidazole-containing drugs have a broad scope in remedying various dispositions in clinical medicine.[2] The effect of replacing pyridine with imidazole on redox and the spin-state properties discussed in the thesis is relevant to biomimetic chemistry. On the other hand, pyridine donor is typical in ligands related to biomimetic chemistry.[3]

In the present work, we chose three different octahedral Fe(II) complexes (Scheme 1) using bidentate Schiff bases. All have three imines (N donor) and either three pyridines or 2-imidazole or 4-imidazole donors (Scheme 4.1) and studied the difference between imidazole and pyridine functionality and their effect on the electrochemical behavior and spin states. We studied their solution magnetic moment and cyclic voltammetry. Here we report on changing pyridine donor to imidazole donor, there is a change in redox potential is associated with an accompanying spin-state change. The difference between pyridine and imidazole analog is quite noticeable. Further, **2** (Figure 4.9) shows two redox couple for low-spin and high-spin forms.

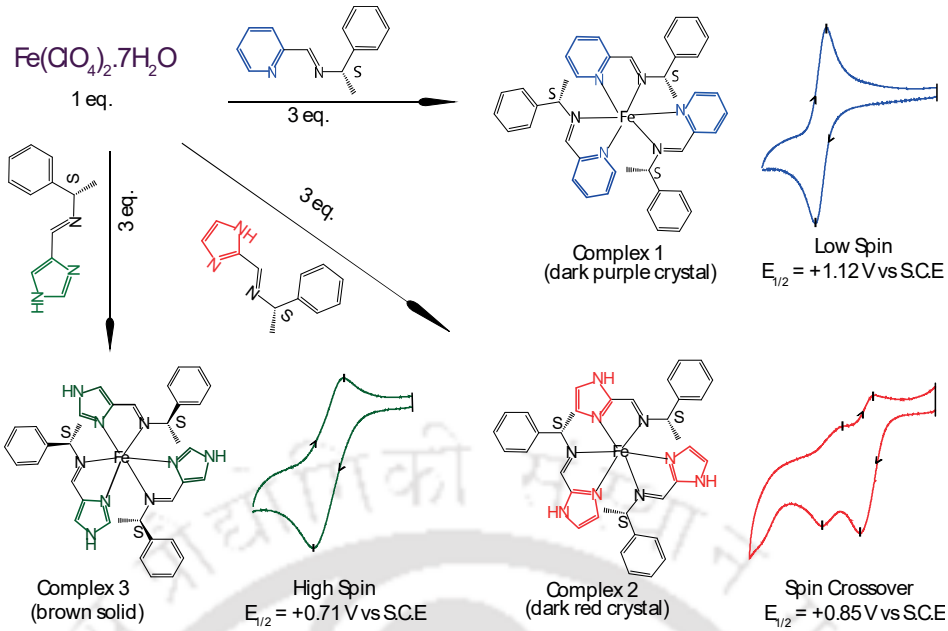

Scheme 4.1. Schematic representation of the reaction pathway of the $[FeL_3]^{2+}$ mononuclear complexes.[L = *S*-L1, *S*-L2 and *S*-L3]

4.1. Experimental Section

4.1.1. Materials and Methods.

Materials and methods used in this chapter are same as in the last chapter unless specifically mentioned. Variable temperature ^{1}HNMR spectra of **2** were recorded using ECZR Series 600 MHz NMR SPECTROMETER at SAIF (IIT Mumbai). Variable temperature UV-visible spectra of **1-3** were recorded using Agilent Technologies Cary 8454 UV−visible spectrophotometer. Elemental analysis measurements were done using EuroEA300 Elemental Analyzer, Euro Vector, Italy, with a solid sampler from IIT Guwahati Biotech Park.

4.1.2. Room temperature solid-state magnetic measurements. Magnetic susceptibility of powdered crystals was measured using a Sherwood Scientific magnetic balance MSB-1.[4a] Each measurement used 40-50 mg of sample.

4.1.3. Variable temperature solid-state magnetic susceptibility. Variable temperature magnetic susceptibility data were collected by using a Quantum Design MPMS3 SQUID magnetometer at a fixed field strength of 0.5 T. About 20 mg sample of **2** was taken for the measurement and recorded over a temperature range of 4 to 350

K, and for **3** almost 6 mg was taken and recorded over a temperature range of 4 to 300 K.

4.1.4. Room temperature solution magnetic measurements. Solution magnetic moments measured following Evans method [4b] using concentric NMR tube by Wilmad and CD_3CN and benzene as an internal reference. About 8-9 mg sample was dissolved in 1 mL of CD_3CN containing <1% benzene. We use both benzene and TMS here as reference compounds. The same solvent mixture without the sample was used as a reference in the outer part of the concentric tube The solution of Complex **2** was prepared immediately after mixing, 400 µl of the mixed solution was put into the 5 mm NMR tube. This technique is based on the frequency shift of an NMR signal of a co-dissolved compound, benzene, by the magnetic field due to an accompanying paramagnetic species. The calculation used the reported procedure for NMR with superconducting magnets.[4c – 4e] Magnetic moments reported used molecular formula from analytical results, and diamagnetic corrections were performed. [4f – 4h] 5mm NMR tube with capillary insert. A 1% benzene in CD_3CN solution was used as the reference. A coaxial double NMR tube is used, and the inner capillary tube contains the C_6H_6/CD_3CN mixture (1:99). The solution containing the paramagnetic solution is to be measured, and a 1 % benzene is situated in the outer tube. The paramagnetic metal species produces a relative frequency shift in the benzene signal.[5]

4.1.5. Temperature-dependent solution visible spectra. Variable temperature UV−visible spectra were recorded on Agilent Cary 8454 UV−visible spectrophotometer using Chemstation software. Each measurement required a concentration of 0.01 mM solution in acetonitrile using a 1 cm path length cuvette. The wavelength region was between 300-800 nm. The temperature range was recorded from room temperature 293 K to 233 K, decreasing (10-20) K interval.

4.1.6. Measurement of redox potentials. Cyclic Voltammetric measurements were performed using CH instruments Electrochemical Workstation. Three electrodes set up consist of an $Ag/AgNO_3$ reference electrode, glassy carbon working electrode, and a platinum rod of 1.0 mm diameter used as an auxiliary electrode. $Ag/AgNO_3$ reference electrode filling solution had 0.01 M $AgNO_3$ in acetonitrile with 0.15 M TBAP as supporting electrolyte. This type of reference electrode tends to shift potential with time due to solvent evaporation. Hence all potentials were calibrated

with respect to both ferrocene and $[Fe(2,2'\text{-bipyridine})_3](ClO_4)_2$ every day of the measurements. The redox potential for ferrocene and $[Fe(2,2'\text{-bipyridine})_3](ClO_4)_2$ in acetonitrile were taken to be 0.41 V and 1.06 V vs S.C.E respectively.[6a-6b] All potentials reported relative to S.C.E (saturated calomel electrode). Measurements were carried out using approximately 1 mM solution of the complexes in dry acetonitrile solvent under inert N_2 atmosphere and a scan rate of 100 mV s^{-1}. 0.15 M TBAP was used as a supporting electrolyte. Using this setup, the ΔEp of ferrocene and $[Fe(2,2'\text{-bipyridine})_3](ClO_4)_2$ were found to be 60 and 74 mV respectively.[6c] The redox potential of the complexes ($E_{½}$ = 0.5x(E_{pa} +E_{pc}), where E_{pa} is anodic, and E_{pc} are cathodic peak potential respectively) and peak to peak separation (ΔE_p, the separation between E_{pa} and E_{pc}). Every measurement was followed by a measure of redox couple of $[Fe(bpy)_3](ClO_4)_2$ used as a reference of potential and ΔE_p check. The ΔE_p value for $[Fe(bpy)_3](ClO_4)_2$ with our setup was observed between 71-76 mV, which is slightly higher than the ideal ~60mV expected for 1e reversible redox process.[7a] Using our setup, ferrocene did show an ideal separation of 60mV.[6a]

4.2. Syntheses and characterization

Synthesis of *S*-L1 and *S*-L2 have been given in Chapter II.(Section 2.1)

4.2.1 *S*-L3

(S,E)-1-(1H-imidazol-4-yl)-N-(1-phenylethyl)methanimine. (S)-1-phenylethylamine (0.500 g, 4.12 mmol, 1 eq.) was stirred in 10 mL methanol. A solution of imidaloze-4-aldehyde (0.396 g, 4.12 mmol, 1 eq.) in 10 mL methanol was added dropwise to the first solution. The initial colorless solution turned yellowish upon warming in a water bath for 30 mins. The mixture was stirred for 3 h at room temperature. Solvent was evaporated to obtain a yellow oil. It was washed with 10ml of n-hexane followed by 10ml of diethyl ether. The oil was dried in a desiccator for 2-3 days to obtain the yellow solid. Yield 565 mg, 68%. FTIR (KBr, cm^{-1}) $\upsilon(C{=}N)_{str}$ 1643(s), $\upsilon(Ar\text{-}C\text{-}C)_{str}$ 1496(s) and 1452(s), $\upsilon(Ar\text{-}C\text{-}H)_{bending}$ 739(s) and 695(s). ^1H NMR (600 MHz, $CDCl_3$, ppm): 8.32 (Imine-H, s, 1H), 7.45 (Im-H, s, 1H,), 7.38 (Im-H, s, 1H), 7.30 (Ph-H, m), 4.55 (Chiral-H, q, 1H, J = 6.6 Hz), 1.60 (Methyl-H, d, 3H, J = 6.6 Hz). ESI-MS ($[M + H]^+$): calcd 200.1187; found 200.1198.

4.2.2 $[Fe(S\text{-}L1)_3](ClO_4)_2$ (1)

The ligand *S*-L1(0.150 g, 0.71 mmol, 3 eq.) was dissolved in 4 mL of acetonitrile and stirred initially at room temperature. To the stirred solution, $Fe(ClO_4)_2{\cdot}7H_2O$(0.087 g, 0.24 mmol, 1 eq.) in 4 mL of acetonitrile was added dropwise, which turned it to dark purple clear solution stirred for 4 h. The solvent was layered with ethyl acetate, covered properly, and kept in the refrigerator for crystallization. Dark purple crystals appeared after 2-3 days. The crystals were filtered, washed with 5 mL of ethyl acetate and 5 mL of diethyl ether. The complex is soluble in both methanol and acetonitrile. Yield (64%). Anal. Calcd. for $[Fe(C_{14}H_{14}N_2)_3]{\cdot}2(ClO_4)$: C, 57.00; H, 4.78; N, 9.50; found C, 56.81; H, 5.02; N, 9.08. FTIR (KBr, cm^{-1}): $\upsilon(C{=}N)_{str}$ 1615(s), $\upsilon(Ar\text{-}C\text{-}C)_{str}$ 1496(s) and 1445(s), $\upsilon(Cl\text{-}O)_{str}$ 1091(s), $\upsilon(Ar\text{-}C\text{-}H)_{bending}$ 759(s) and 704(s).

4.2.3 $[Fe(S\text{-}L2)_3](ClO_4)_2$ (2)

The ligand *S*-L2(0.150 g, 0.75 mmol, 3 eq.) was dissolved in 4 mL of acetonitrile and stirred initially at room temperature. To the stirred solution, $Fe(ClO_4)_2{\cdot}7H_2O$(0.092 g, 0.25 mmol, 1 eq.) in 4 mL of acetonitrile was added dropwise, which turned it to a deep red clear solution and stirred for 4 h. The solvent was layered with an equal amount of ethyl acetate and diethyl ether, covered properly, and kept in the refrigerator for crystallization. Dark red crystals appeared after 2-3 days. The crystals were filtered, washed first with 5 mL of ethyl acetate followed by 5 mL diethyl ether. It was dried overnight in the desiccator. The complex is soluble in both methanol and acetonitrile. Yield ~ 0.176 g (67%). Anal. Calcd. for $[Fe(C_{12}H_{13}N_3)_3].2(ClO_4)\ {\cdot}3H_2O{\cdot}\ CH_3CN{\cdot}CH_3COOCH_2CH_3$: C, 48.71; H, 5.45; N, 13.52; found C, 48.84; H, 6.03; N, 13.84. FTIR (KBr, cm^{-1}): $\upsilon(C{=}N)_{str}$ 1709(s), $\upsilon(Ar\text{-}C\text{-}C)_{str}$ 1494(s) and 1443(s), $\upsilon(Cl\text{-}O)_{str}$ 1074(s), $\upsilon(Ar\text{-}C\text{-}H)_{bending}$ 757(s) and 699(s).

4.2.4 $[Fe(S\text{-}L3)_3](ClO_4)_2$ (3)

The ligand *S*-L3(0.150 g, 0.75 mmol, 3 eq.) was dissolved in 4 mL of acetonitrile and stirred initially at room temperature. To the stirred solution, $Fe(ClO_4)_2{\cdot}7H_2O$(0.092 g, 0.25 mmol, 1 eq.) in 4 mL of acetonitrile was added

dropwise, which turned it to a reddish yellow clear solution and stirred for 4 h. The solvent was layered with an equal amount of ethyl acetate and diethyl ether, covered properly, and kept in the refrigerator for crystallization. Light brown precipitate appeared after 2-3 days. The was filtered, washed with 5 mL of ethyl acetate followed by 5 mL of diethyl ether. The complex is soluble in both methanol and acetonitrile. Yield ~ 0.180 g. Anal. Calcd. for $[Fe(C_{14}H_{14}N_2)_2(C_{12}H_{13}N_3)]\cdot 2(ClO_4)\cdot 4H_2O\cdot 2CH_3CN$: C, 47.96; H, 5.35; N, 15.69; found C, 47.77; H, 5.39; N, 15.79. FTIR (KBr, cm^{-1}): $\upsilon(C=N)_{str}$ 1635(s), $\upsilon(Ar\text{-}C\text{-}C)_{str}$ 1496(s) and 1450(s), $\upsilon(Cl\text{-}O)_{str}$ 1067 (s) $\upsilon(Ar\text{-}C\text{-}H)_{bending}$ 756(s) and 700(s).

4.3. X-ray data collection, structure solution and refinement

All the crystals show desolvation to a different degree. Thus, the crystals were covered with grease (Vaseline) and mounted on glass fiber for data collection. All geometric and intensity data for the crystals of **2** were collected at room temperature using a Bruker SMART APEX CCD diffractometer equipped with a fine focus 1.75 kW sealed tube Mo-Kα (λ = 0.71073 Å) X-ray source. The SMART software was used for data acquisition and the 'Bruker SAINT' software for data refinement and reduction. Absorption corrections were done using SADABS. After the initial solution and refinement with SHELXL, the final refinements were performed on WinGX environment. Almost all non-hydrogen atoms in the complexes were refined anisotropically. 'SQUEEZE' was performed in order to remove the disordered solvent molecules. All of the hydrogen atoms were added in the refinement stage. The molecular weight from structure and bulk may not match as the dry powdered form of crystals was used for elemental analysis and other studies.

4.4 Results and Discussion

4.4.1. Syntheses

The Schiff base ligands were synthesized by condensing the chiral amine and the aldehyde in methanol. The *S*-L1 was isolated as a yellow oil while S-L2 and S-L3 Schiff bases containing 2-imidazole and 4-imidazole were white and yellow powder. The FTIR spectra showed a strong vibration near 1650 cm^{-1} assigned as C=N stretch of the imine formed. The ligands were characterized by proton NMR and Mass spectrometry (Experimental section). Complexes **1-3** were prepared in ligand:metal in

3:1 ratio in acetonitrile.

4.4.2 Crystal structure of Complex 2.

Complex **2** was crystallized in a chiral space group P1 with one molecule of the cationic complex and two perchlorate anions in the asymmetric unit. The final structural parameters are in Table S9, and the selected bond and lengths are in Table S10. The ORTEP diagram of the complex cation showed an octahedral Fe(II) complex (Figure 4.1). The geometry around the central metal atom slightly deviates from a perfect octahedron. This is evident from the deviation of angles from the ideal value of 90º for in-plane angles and 180º for axial angles (Table S10). All the Fe-N (imidazole) bond lengths are slightly shorter than Fe-N (imine), showing a stronger interaction between the iron and the imidazolate rings.[6b]

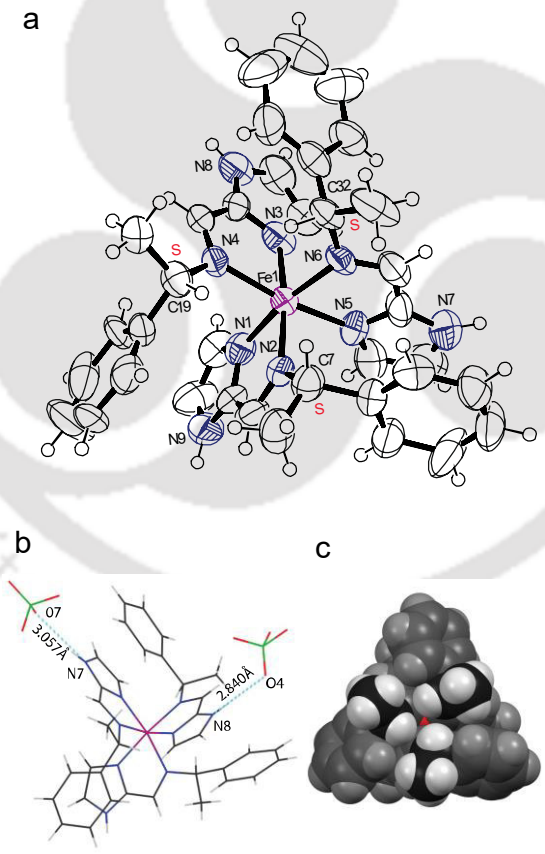

Figure 4.1. (a) ORTEP diagram of the cationic part of Complex **2**. Thermal ellipsoids set to 50% probability level. (b) A chemical diagram of the same. (c) Model highlighting the H-bonding between the complex and the surrounding perchlorate anions.

Complex **2** having an average Fe-N (imidazole) bond length of 1.99 Å and an average Fe-N (imine) bond length of 2.03 Å, which is similar to the complex $[Fe^{II}(L^{9})_3]^{2+}$ having an N-methylimidazole ring instead of an unsubstituted imidazole (**2**).[8a] The average bond lengths of **5** and **6** having imidazole moiety are slightly shorter (~ 0.3-0.5 Å) compared to **2**.[8b] This is because the bond lengths were measured at 100 K, where they behave as low spin complexes. The average Fe-N bond length for high spin d^6 complexes is said to be > 2.1 Å.[8c] The average Fe-N bond length value of **2** falls between that of high spin and low spin bond lengths (LS < 2.01 < HS). The crystal also contains H-bonded interactions between two imidazole NH (N7 and N8) and two of the perchlorate oxygen (O4 and O7) having 3.057 Å and 2.840 Å (Figure 1c). Two O-atoms (O6 and O8) of the same perchlorate anion weakly interacts with $C_{imidazole}$ (C24 and C36) of two adjacent imidazole rings ~3.26 Å (Table S11).

4.4.3. Solid-state magnetic behavior.

Room temperature magnetic moment of the complexes **1-3** have been measured at room temperature (298K) (Table 4.1). Complex **1** having pyridine donor showed a value of μ_{eff} = 1.04 B.M. This indicates that it is essentially low-spin Fe(II) in the solid-state. This is comparable to value ~1 reported for Fe(II) low-spin complex $[Fe(bpy)_3](ClO_4)_2$.[4g, 9] Magnetic moments of Complex **2** having 2-imidazole group showed a value of μ_{eff} = 2.54 B.M and Complex **3** showed a value of μ_{eff} = 5.06 B.M. This means **2** has an intermediate spin and **3** is high-spin in nature. This is against the expected range of spin-only 4.90 to 5.45 B. M. with an orbital contribution for high-spin Fe(II). Lower magnetic moments of **2** and **3** indicate either a low-spin or magnetic coupling exists in the solid-state.

Temperature dependant magnetic studies were done on both **2** and **3** in the temperature range of 4-350 K at a fixed field of 0.5 T. The experimental data were corrected for underlying diamagnetism, calculated using Pascal's constants.[4f-4h] The susceptibility data on a crystalline sample **2** showed a sharp decrease in $\chi_M T$ value from 2.4 to 0.8 as the temperature decreases from (350-250) K. It decreased gradually from thereon to a final value of around 0.2 at 4 K. (Figure 4.2a) This result indicates that the complex undergoes a significant conversion to low spin within the temperature range of (350-250)K. Then as we move further down, the amount of low spin species is dominant over the high spin species. The measurement of a powdered

sample of **3** shows a gradual decrease in $\chi_M T$ value from 3.0-1.8 with a fall in temperature from 300 to 3K (Figure 4.2b). According to Curie-Wiess law, the plot of **3** is linear throughout the temperature range ($\theta = 0°$) (Figure S10), which shows that in bulk, it is paramagnetic. The magnetic moment for a high spin d^6 complex is expected to fall within the range of 5.0–5.2 μB.[10] Compared to **2**, Howson reported a similar complex, having shown the same trend in susceptibility behavior on varying the temperature. The observation of paramagnetic behavior in the imidazole system results from the combined effects of the reduced π donation and π acceptor ability of the ligand.[11-14] Therefore, we observe that **2** (d^6 system) shows a spin-crossover within the given temperature range, whereas **3** is d^6-high spin throughout the given temperature range.

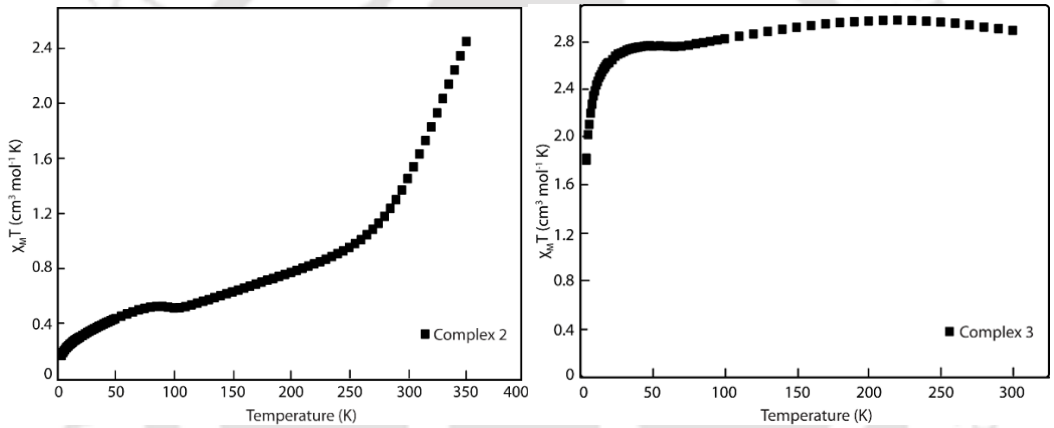

Figure 4.2. Plot of $\chi_M T$ *vs*. T in the range (4–350) K for (a) Complex **2** and (b) Complex **3**.

Table 4.1. Solid-state magnetic moment of the Complexes **1-3** at 298K.

Complex	Donor group	μ_{eff} (solid) (R.T)	Spin-state	Spin-crossover
1	Pyridine	1.04	Low-spin	No
2	2-imidazole	2.54	Intermediate spin	Yes
3	4-imidazole	5.06	High-Spin	No

4.4.4. Solution state magnetic behavior.

We have measured the room temperature solution magnetic moment of the complexes **1-3** have been measured at room temperature (293 K) (Table 4.2) using the

Evan's method.[15a, 15b]. Complex **1** having pyridine donor showed a value of μ_{eff} = 1.60 B.M. This indicates that it is essentially low-spin Fe(II) in solution. Magnetic moments of Complex **2** having 2-imidazole group showed a value of μ_{eff} = 4.80 B.M and Complex **3** having 4-imidazole group showed a value of μ_{eff} = 5.40 B.M. This means **2** and **3** are predominantly high-spin in solution. Temperature dependant magnetic susceptibility of Compound **2** in solution has decreased gradually with the lowering of temperature (300-230) K (Figure 4.3). Since we have limitations when using solvent (in this case, CD_3CN having a freezing point ~ -228K), we could not go further to show the full crossover range as shown in the solid phase. The value of $\chi_M T$ is decreased from 3.2 cm^3 mol^{-1} K at 300K to ~1.5 cm^3 mol^{-1} K at 233K. Similarly, we have performed ^{1}HNMR of the same compound over the same temperature range (Figure 4.4). At room temperature, it is paramagnetic, having broad or no peaks. As we lower the temperature, we could see sharp peaks appearing, accounting for forming the low spin species in the solution. Both ^{1}HNMR and Evan's method showed the expected crossover behavior of **2** within the given temperature range. In conclusion, we could say that complex **2** exhibits a spin-crossover property both in the solid and the solution phase. Both ^{1}HNMR and Evan's method showed the expected crossover behavior of **2** within the given temperature range. In conclusion, we could say that out of the three complexes, **2** exhibits a spin-crossover property both in the solid-state and solution.

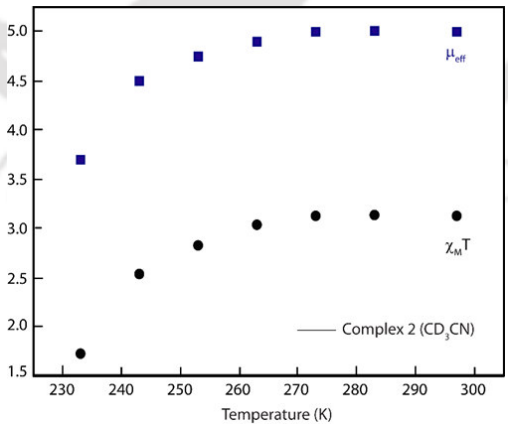

Figure 4.3. Combined plot of χMT vs. T and μ_{eff} vs. T of Complex **2** within the temperature range (230-300)K in CD_3CN.

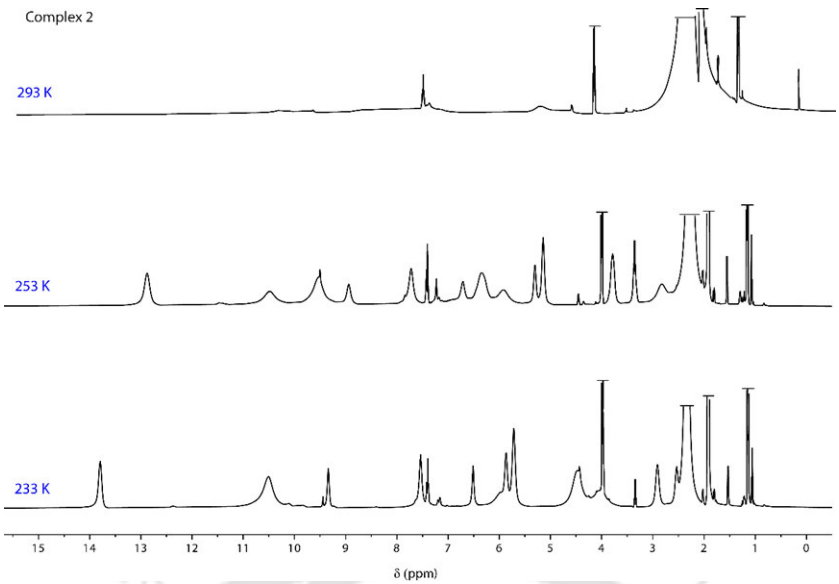

Figure 4.4. Variable temperature ^{1}HNMR of Complex **2** at 293K, 253K, and 233K in CD_3CN.

Table 4.2. Solution magnetic moment of the Complexes **1-3** at 293K.

Complex	Donor group	μ_{eff} (CD_3CN) (R.T)	Spin-state	Spin-crossover
1	Pyridine	1.60	Low-spin	No
2	2-imidazole	4.80	High-spin	Yes
3	4-imidazole	5.40	High-Spin	No

4.4.5. FTIR and ESI-MS spectra of the Complexes 1-3.

FTIR spectra shows strong and broad absorption ~ 1100 cm^{-1} confirms the presence of perchlorate anion (Figure S7-S9). The ESI-MS spectrum of **1** (Figure S11) showed the presence of the protonated molecule, at m/z 343.15 (z = 2) corresponding to $[Fe(L1)_3]^{2+}$, and a less abundant ion corresponding to the ClO_4^{2-} adduct of $[Fe(L1)_3(ClO_4^{2-})]^{+}$ (z = 1). The spectrum also showed a prominent peak at m/z 238.08 (z = 2) corresponding to the bis complex $[Fe(L1)_2]^{2+}$ which resulted as a result in the loss of one ligand from the parent complex. The spectrum also showed trace amounts of the ligand L1 at m/z = 211.12 and free amine at m/z = 122.09. The ESI-MS spectrum of **2** (Figure S12) which is labile in nature has more fragmentation than **1** even at low fragmentor voltage. The most prominent fragmentor ion was shown at m/z = 781.06 (z = 1) having the composition $[Fe(L2)_3$-H]

$^{+}(CH_3CN)(CH_3COOCH_2CH_3)$ (z = 1). The other lesser abundant fragments were at m/z = 553.10 of $[Fe(L2)_2(ClO_4^{2-})]^{+}$ (z = 1) and m/z = 453.14 of $[Fe(L2)_2\text{-}H]^{+}$ (z = 1) respectively. This corresponded to their bis complexes after the loss of one ligand. The spectrum also showed the presence of trace amounts of the ligand L1 at m/z = 211.12 and free amine at m/z = 122.09. The mass of complex **3** was not stable even under the effect of very low fragmentary voltages as the spectrum showed a single sharp peak of the ligand at m/z = 200.10 of $[L3+H]^{+}$. (Figure S13)

4.4.6. UV-visible studies of 1-3.

Fe(II) complexes generally show a metal to ligand charge transfer (MLCT) band between 500-600 nm in the low-spin state, with a high molar extinction coefficient.[16] The ligand field transitions, $^1T_1 \leftarrow {}^1A_1$ and $^1T_2 \leftarrow {}^1A_1$ for low-spin Fe(II), are usually obscured by MLCT in complexes with Schiff base ligands.[15a] On the other hand, the high-spin octahedral Fe(II) complex shows one very weak d-d transition $^5Eg \leftarrow {}^5T_{2g}$ in the 700-900 nm region.[16a] Table 4.3 summarizes the electronic transitions observed (300-1100 nm) in the same solvent as magnetic moments and cyclic voltammetry. Complex **1** showed the expected MLCT transitions between 500-600nm with high ε values (~ 10,000 M^{-1} cm^{-1}) having pyridine in its coordination environment (Figure 4.5). The intense charge transfer bands and the absence of weak *d-d* transition confirm the low spin nature in the solution. For low spin $[Fe(bpy)_3](ClO_4)_2$, λ_{max} at 519 nm (ε, 14,400 M^{-1} cm^{-1}) was assigned to be an MLCT band under the same conditions.[16] In contrast, the imidazole containing **2** and **3** shows a weaker charge transfer band (ε, ~1000 M^{-1} cm^{-1}) between 400-500nm and *d-d* transition between 780 -900 nm (ε, 7-30 M^{-1} cm^{-1}). Charge transfer bands of high-spin Fe(II) are usually less intense, unlike low spin Fe(II). Less intense charge transfer and *d-d* transition show the presence of high spin species in the solution. The CT bands in **2** and **3** are blue-shifted, which is again another noticeable difference from **1**.

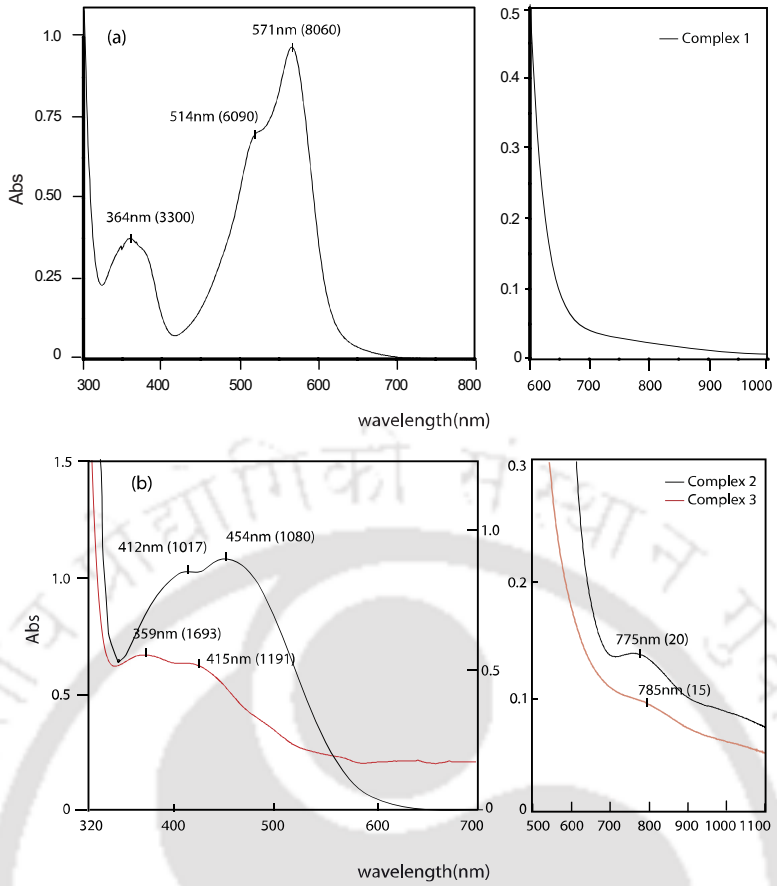

Figure 4.5. UV-visible spectra in acetonitrile of (a) Complex **1** and (b) Complex **2** and **3** combined.

Table 4.3. UV-visible spectra of the Complexes **1**-**3** in acetonitrile at 298K.

Complex	Spin-state	*d-d transition* nm(M^{-1} cm^{-1})	CT-band
1	Low-spin	no	364(3300), 515(6090), 571(8060)
2	High-spin	775(20)	412(1020), 454(1080)
3	High-Spin	785(15)	359(1700), 416(1200)

The charge transfer region of all the complexes was measured to -40°C. Complex **1,** as mentioned above obtained at room temperature, exhibited an intense band at 515nm (ε = 6092, M^{-1} cm^{-1}), 566nm (ε = 8607 M^{-1} cm^{-1}) corresponding to MLCT bands at room temperature, which remained unchanged on lowering the temperature (Figure 4.6a). This proves the presence of low spin species throughout the temperature range. **2** has shown the most enhancement in the MLCT region on

decreasing the temperature, having its intensity more than doubled at -40°C as well as a redshift of from 454nm to 493nm (Figure 4.6b). This supports the increase in the presence of the low spin species as compared to the high spin species at lower temperatures. **3,** on the other hand, showed the minimum change in intensity over the temperature range (Figure 4.6c). This accounts for the high spin species in the solution exclusively.[17]

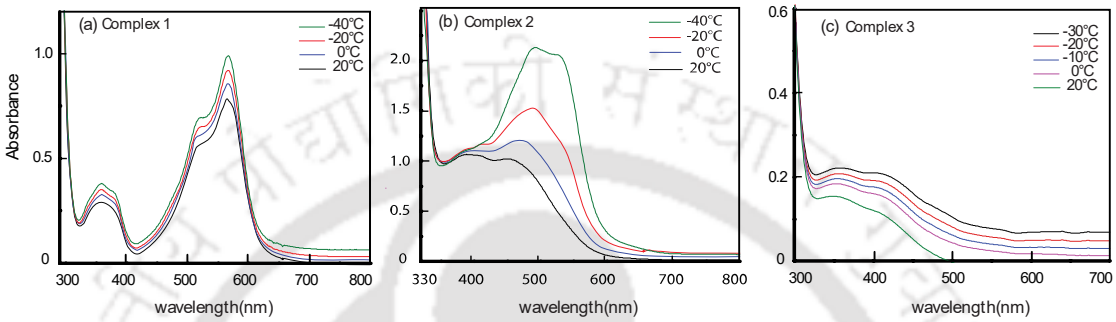

Figure 4.6. Variable temperature plot of UV-visible spectra of the Complexes **1-3** in acetonitrile with the temperature (233-293) K.

In conclusion, we have spectrophotometrically detected that **1** remained low spin, and **3** remained high spin in solution, showing minimal intensity enhancements on lowering the temperature. **2** on the other hand, showed not only a very high increase in CT intensity but also a shift of wavelength by about 40nm showing the presence of low spin more than the high spin species which was initially present at room temperature.

4.4.7 Electrochemical properties of 1-3.

We have measured the cyclic voltammetry of the complexes **1-3** using an identical setup (Experimental Section) summarized in Table 4.4. Complex **1** showed a reversible oxidation peak at + 1.12V and ΔE_p of 78 mV (Figure 4.7a). The plot shows that it is both chemically and electrochemically reversible. Complex **3** having a single oxidation peak at +0.71 V (Figure 4.7b) and a ΔE_p of 190 mV. This shows that it is chemically reversible but electrochemically irreversible. Complex **2** showed two closely spaced redox couple of unequal height (Figure 4.7c) having an oxidation peak of +0.85 V and +1.11 V and ΔE_p value of >100 mV. It is also chemically reversible but electrochemically irreversible. From DPV plot, **2** shows two redox couple in MeCN assigned to low-spin and high-spin forms in 20% and 80%, respectively at

room temperature (Figure 4.7c).The reversible nature of the complexes is also demonstrated by recording the potential at different scan rates (Figure S11). Thus, the CV experiment shows that **1** containing pyridine oxidizes at a higher potential with a considerable difference of ~270 mV from **2** and 410 mV from **3** having the imidazole group. It is also concluded from the ΔE_p values that **2** and **3** are both chemically reversible, whereas **1** is both chemically and electrochemically reversible. Solution magnetic data and electronic spectra have already established that pyridine containing complex is low spin and imidazole containing complex is high spin in solution. Hence, we could also detect the change in pyridine *vs*. imidazole functionality electrochemically as well.

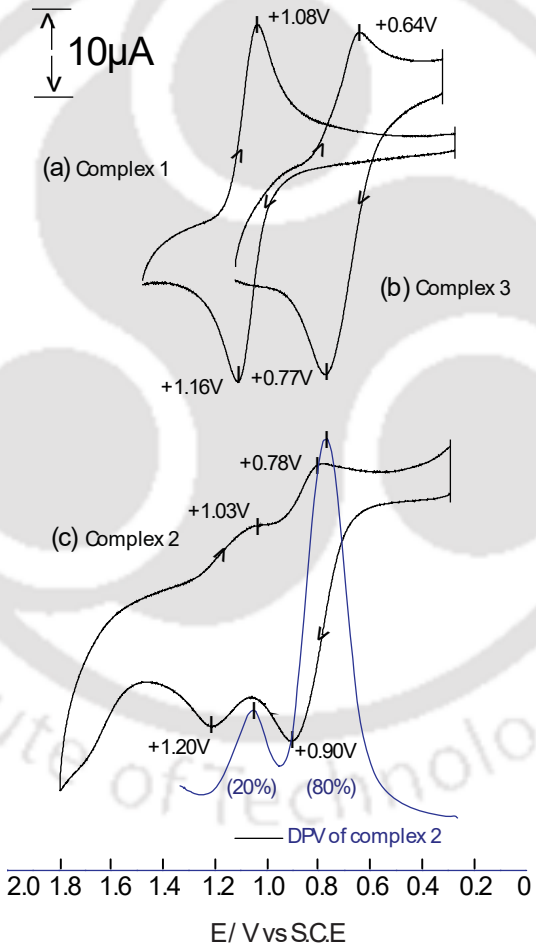

Figure 4.9. Cyclic Voltammetry diagram plot of Complexes **1**-**3**. Variable scan rate (500,200,100,50 and 10) mV/s diagram of the same in acetonitrile.

Table 4.4. Redox potential of the Complexes **1-3** in acetonitrile at 298K.

Complex	Spin-state	$E_{1/2}$, V	ΔE_p, mV
1	Low-spin	1.12	78
2	High-spin	1.11, 0.85	190, 119
3	High-Spin	0.49	190

Conclusions

Three mononuclear chiral Schiff base Fe(II) complexes containing pyridine and imidazole heterocyclic rings have been utilized in this chapter. The change in the coordination environment around the metal atom has resulted in a significant difference in their spin states and electrochemical properties. Magnetic Susceptibility results showed pyridine containing complex **1** was found to be low-spin in the solid-state (μ_{eff} = 1.04) as well as the solution state (μ_{eff} = 1.60). Complex **3,** having a 4-imidazole group, was found to be exclusively high spin both in solid (μ_{eff} = 5.06) and solution(μ_{eff} = 5.40). Complex **2**, having the 2-imidazole group, showed a noticeable difference in the magnetic moment between the solid (μ_{eff} = 2.54) and solution state (μ_{eff} = 4.8). Variable temperature magnetic study in solid and in solution revealed the spin crossover property of **2**, but **3** remains high spin throughout the given temperature range (4- 350) K. UV-visible studies have shown intense MLCT bands in **1** as seen in low spin complexes but less intense MLCT bands in **2** and **3** and the forbidden (*d-d*) transition corresponding to the high spin state in solution. With a decrease in the temperature in **2**, an increase in the MLCT band intensity was observed, with a blue shift of ~ 40nm. No such change was seen in complexes **1** and **3**. The change in the spin state of **1-3** has been detected electrochemically as well. Complex **1** showed a reversible oxidation peak at + 1.12 V. **3** showed a redox couple at +0.71 V *vs*. S.C.E. **2** showed two redox peaks, one at +0.85V corresponding to the high spin and one at +1.11 V corresponding to the low spin species. ΔE_P value suggests that **2** and **3** are chemically reversible but electrochemically irreversible. **1**, on the other hand, is both chemically and electrochemically reversible.

References

1. (a) Konig, E.; Ritter, G.; Kulshreshtha, S. K. The nature of spin-state transitions in solid complexes of iron(II) and the interpretation of some associated phenomena. Chem. Rev. 1985, 85, 219. (b) Scheidt, W. R.; Reed, C. A. Spin-state/stereochemical relationships in iron porphyrins: implications for the hemoproteins. Chem. Rev. 1981, 81, 543. (c) Harding, D. J.; Harding, P.; Phonsri, W. Spin crossover in iron(III) complexes. Coord. Chem. Rev. 2016, 313, 38. (d) Gütlich, P.; Gaspar, A. B.; Garcia, Y. Spin state switching in iron coordination compounds. Beilstein J. Org. Chem. 2013, 9, 342.
2. A. Kleeman, J. Engel, B. Kutscher, and D. Reichert, Pharmaceutical Substances: Syntheses, Patents, Applications of the Most Relevant APIs, Thieme Medical, New York, NY, USA, 3rd edition, 1999.
3. (a) Holm, R. H.; Kennepohl, P.; Solomon, E. I. Structural and Functional Aspects of Metal Sites in Biology. Chem. Rev. 1996, 96, 2239. (b) Costas, M.; Mehn, M. P.; Jensen, M. P.; Que, L. Dioxygen Activation at Mononuclear Nonheme Iron Active Sites: Enzymes, Models, and Intermediates. Chem. Rev. 2004, 104, 939. (c) Jasniewski, A. J.; Que, L. Dioxygen Activation by Nonheme Diiron Enzymes: Diverse Dioxygen Adducts, High-Valent Intermediates, and Related Model Complexes. Chem. Rev. 2018, 118, 2554.
4. (a) Evans, D. F. New Type of Magnetic Balance. *J Phys E Sci Instrum* **1974,** *7*, 247. (b) Evans, D. F. The determination of the paramagnetic susceptibility of substances in solution by nuclear magnetic resonance. *J. Chem. Soc.* **1959**, 2003. (c) Schubert, E. M. Utilizing the Evans method with a superconducting NMR spectrometer in the undergraduate laboratory. *J. Chem. Ed.* **1992,** *69*, 62 (d) Piguet, C. Paramagnetic Susceptibility by NMR: The "Solvent Correction" Removed for Large Paramagnetic Molecules. *J. Chem. Ed.* **1997,** *74,* 815. (e) Ostfeld, D.; Cohen, I. A. A cautionary note on the use of the Evans method for magnetic moments. *J. Chem. Ed.* **1972,** *49*,

829. (f) Earnshaw, A. Introduction to Magnetochemistry; Academic: London and New York, 1968, 113. (g) Figgis, B. N.; Lewis, J. The Magnetic Properties of Transition Metal Complexes In *Progress* in Inorganic Chemistry; Wiley: 1964, 37. (h) O'Connor, C. J. In *Progress* in Inorganic Chemistry; Wiley: 1982, 203.

5. Evans, R.; Henbest, K. B.; Hayward, M. A.; Britton, M. M.; Maedac, K.; Timmel, C. R. SQUID magnetometry as a tool for following a clock reaction in solution. *Dalton Trans*., **2009**, 2467.

6. (a) Kelly, S. L.; Kadish, K. M. Electron-transfer and ligand-addition reactions of (TPP) CrClO4 and (TPP) Cr (NO) in nonaqueous media. *Inorg. Chem.* **1984,** *23*, 679. (b) Weiner, M. A.; Basu, A. Et_3P^+- and nitro-substituted pyridines and bipyridines. Their behavior as ligands in iron(II), cobalt(II), and ruthenium(II) complexes. *Inorg. Chem.* **1980,** *19*, 2797. (c) Ray, M.; Mukerjee, S.; Mukherjee, R. Manganese (III) Complexes of 1,2-Bis(2-Pyridinecarboxamido)benzene - Synthesis, Spectra, and Electrochemistry. *Dalton Trans.* **1990,** *12*, 3635.

7. (a) Weiner, M. A.; Basu, A. Et3P+- and Nitro-Substituted Pyridines and Bipyridines. Their Behavior as Ligands in Iron(II), Cobalt(II), and Ruthenium(II) Complexes. *Inorg*. *Chem*. **1980**, *19*, 2797. (b) Decurtins, S.; Felix, F.; Ferguson, J.; Guedel, H. U.; Ludi, A. The electronic spectrum of tris(2,2'-bipyridine)iron(2+) and tris (2,2'-bipyridine)osmium(2+). *J. Am. Chem. Soc*. **1980**, *102*, 4102. (c) Williams, R. J. P. The absorption spectra of some complex ions of analytical importance. *J Chem. Soc*. **1955**, 137.

8. (a) Howson, S. E.; Allan, L. E. N.; Chmel, N. P.; Clarkson, G. J.; Deeth, R. J.; Faulkner, A. D.; Simpson, D. H.; Scott, P. Origins of stereoselectivity in optically pure phenylethaniminopyridine tris-chelates M $(NN')_3^{n+}$ (M= Mn, Fe, Co, Ni and Zn). *Dalton Trans.* **2011,** *40*, 10416. (b) Brewer, C.; Brewer, G.; Luckett, C.; Marbury, G. S.; Viragh, C.; Beatty, A. M.; Scheidt, W. R. Proton Control of Oxidation and Spin State in a Series of Iron Tripodal Imidazole Complexes. (c)

Orpen, A. G.; Brammer, L.; Allen, F. H.; Kennard, O.; Watson, D. G.; Taylor, R. Supplement. Tables of bond lengths determined by X-ray and neutron diffraction. Part 2. Organometallic compounds and co-ordination complexes of the d- and f-block metals. Dalton Trans., **1989**, S1.

9. Sugden, S. Magnetochemistry. J. Chem. Soc., **1943**, 328.
10. F. A. Cotton and G. Wilkinson, Advanced Inorganic Chemistry, John Wiley & Sons, Inc., New York, **1988**.
11. Cowan, J. A. Inorganic Biochemistry: An Introduction, Wiley-VCH, New York, **1997**.
12. Gutlich, P.; Garcia, Y.; Goodwin, H. A. *Chem. Soc. Rev*., **2000**, *29*, 419–427.
13. Dosser, R. J.; Eilbeck, W. J.; Underhill, A. E.; Edwards, P. R.; Johnson, C. E.; *J. Chem. Soc. A*, **1969**, 810.
14. Childs, B. J.; Craig, D. C.; Scudder, M. L.; Goodwin, H. A. *Inorg. Chim. Acta*, **1998**, *274*, 32.
15. (a) Evans, D. F. Proc. Chem. Soc., **1958**, 115; (b) Loliger, J.; Wilkins, R. G. *J. Chem. Educ*., **1972**, *49*, 646.
16. (a) Lever, A. B. P. Inorganic Electronic Spectroscopy; Elsevier: New York, **1968**. (b) Nelson, S. M. Comprehensive Coordination Chemistry. The Synthesis, Reactions, Properties and Applications of Coordination Compounds; Pergamon: United Kingdom, **1987**, 1419.
17. Thorarinsdottir, A. E.; Gaudette, A. I.; Harris, T. D. Spin-crossover and high-spin iron(ii) complexes as chemical shift 19F magnetic resonance thermometers. *Chem. Sci.* **2017**, *8*, 2448.

Chapter V

Investigation the effect of pyridine and imidazole on solution magnetic and electrochemical properties within achiral Fe(II) complexes

Introduction

Previously we have observed the change in spin-state with varying donor group (pyridine, 2-imidazole and 4-imidazole). We drew a simple connection between magnetic and electrochemical property with the change in donor group of the Complexes **1**-**3**. We did not want to restrict our study to these three compounds. So in order to validate the findings in the previous chapter we continue the same study with some other Fe(II) complexes. In this chapter we report a few more Fe (II) complexes having similar donor groups but with different amine (Scheme 5.1). All the complexes have been synthesized, characterized, and their solution magnetic moment, uv-visible spectroscopy and cyclic voltammetry has been studied in detail. We noticed that the changing pyridine with differently substituted imidazole effect both redox potential and spin-state change. The changes are consistent among the different sets of complexes.

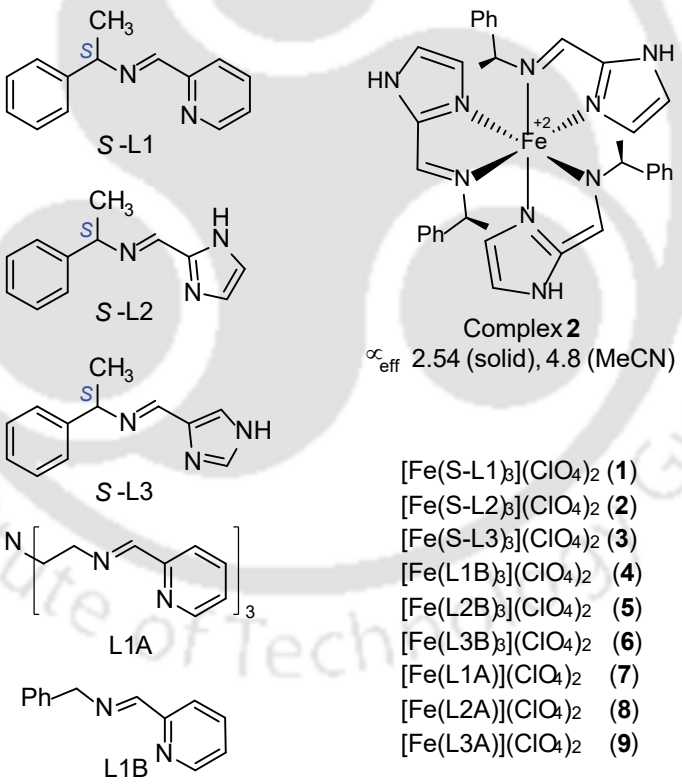

Scheme 5.1. List of ligands and their respective Fe(II) complexes (**4**-**9**) in this chapter.

5.1 Experimental Section

5.1.1 Materials and Methods.

Materials and methods used in this chapter are same as in Chapter IV unless specifically mentioned. Tris(2-aminoethyl)amine and Benzylamine was purchased from Merck.

Solid-state and solution magnetic susceptibility measurements, UV-visible studies and electrochemical studies have been performed using the same setup as discussed in the previous chapter.

5.1.2 Syntheses and characterization

5.1.3 Complex 4, 7, 8 and 9.

These were synthesized following the reported procedure. Synthesis of **7** reported by Struch and coworkers.[1c] Complex **8** and **9** have been reported by Brewer and coworkrs.[1b] Complex **7** has been reported by Howson and coworkers.[1a] Howson and coworkers reported **1** in a single pot reaction without isolation of ligand.[1a]

5.1.4 L1B.

Benzylamine (0.500 g, 4.66 mmol, 1 eq.) was stirred in 10 mL methanol. A solution of Pyridine-2-carboxaldehyde (0.500 g, 4.66 mmol) in 10 mL of methanol was added dropwise to the first solution. It was stirred at room temperature for 10 minutes and then air refluxed at 55 °C on the water bath for 2 h. It was then stirred for 1 h at room temperature, forming a deep yellow solution. The solvent was then removed in a rotatory evaporator, and the yellow oil was taken in 15 mL ethyl acetate, dried over anhydrous sodium sulphate for 15 mins. Ethyl acetate was removed to get a deep yellow oil. Yield 780 mg, 85%. FTIR (KBr, cm^{-1}) $\upsilon(C{=}N)_{str}$ 1653(s), υ(Ar-C-C)$_{str}$ 1503(s) and 1448(s), υ(Ar-C-H)$_{bending}$ 732(s) and 697(s). ^{1}H NMR (500 MHz, $CDCl_3$, ppm): 8.50 (Imine, s, 1 H), 8.65 (Py-H^a, d, 1 H, J = 5 Hz), 8.07 (Py-H^d, d, 1 H, J = 7.5 Hz), 7.74 (Py-H^c, t, 1 H, J = 3.5 Hz), 7.33 (Py-H^b/Py-H$^{f\text{-}j}$, m, 6H), 4.67 (H^k, s, 2 H). ESI-MS ([M + H]$^+$): calcd 197.1073; found 197.1053.

5.1.5 L2B.

(E)-N-benzyl-1-(1H-imidazol-2-yl)methanimine. Benzylamine (0.500 g, 4.67 mmol, 1 eq.) was stirred in 10 mL methanol. A solution of imidazole-2-aldehyde (0.448 g, 4.67 mmol, 1 eq.) in 10 mL methanol was added dropwise to the first solution. The initial colourless solution turned light yellow upon warming in a water bath for 30 mins. The mixture was stirred for 3 h at room temperature. The solvent was evaporated to obtain a white solid. Solid was washed with 10 mL of n-hexane followed by 10 mL of undistilled diethyl ether. The solid was dried overnight in a desiccator to obtain the product as off-white solid Yield ~ 0.605 g, 70 %. FTIR (KBr, cm^{-1}): $\upsilon(C=N)_{stretch}$ 1647 (s). ^1H NMR (600 MHz, $CDCl_3$, ppm): 8.37 (Imine-H, s, 1 H), 7.32 (Ph-H, m, 5 H), 7.19 (Im-H, s, 1 H,), 6.82 (Im-H, s, 1 H), 4.97 (methylene-H, s, 2 H). ESI-MS ($[M + H]^+$): calcd 186.1025; found 186.1093.

5.1.6 L3B.

Benzylamine (0.500 g, 4.66 mmol, 1 eq.) was stirred in 10 mL methanol. A solution of imidazole-4-aldehyde (0.448 g, 4.66 mmol) in 10 mL of methanol was added dropwise to the first solution. It was stirred at room temperature for 10 minutes and then air refluxed at 50 °C on the water bath for 1 h. It was then stirred for 3 h at room temperature forming a white turbid solution. The solvent was then removed in a rotatory evaporator and the white solid was washed first with n-hexane (2 X 3 mL) followed by diethyl ether (2 X 3 mL). It was dried overnight and kept in the desiccator. Yield 820 mg, 83%. FTIR (KBr, cm^{-1}) $\upsilon(C=N)_{str}$ 1653(s), $\upsilon(Ar\text{-}C\text{-}C)_{str}$ 1503(s) and 1448(s), $\upsilon(Ar\text{-}C\text{-}H)_{bending}$ 732(s) and 697(s). ^1H NMR (600 MHz, CD_3OD, ppm): 8.51 (Imine-H, s, 1H), 7.79 (Im-H, s, 1H,), 7.58 (Im-H, s, 1H), 7.33 (Ph-H, m), 4.75 (methylene-H, s, 2H). ESI-MS ($[M + H]^+$): calcd 186.1026; found 186.1035.

5.1.7 $[Fe(L1B)_3](ClO_4)_2$ (4)

The ligand L1-B (0.150 g, 0.76 mmol, 3 eq) was stirred in 5 mL acetonitrile at room temperature. To the stirred solution, $Fe(ClO_4)_2 \cdot 7H_2O$(0.093 g, 0.25 mmol, 1 eq.) in 5 mL of acetonitrile was added dropwise, which turned it into a dark purple solution and was stirred for 4 h. The reaction mixture was layered with an equal amount of ethyl acetate, covered properly, and kept in the refrigerator. Solid product was obtained after a day. It was filtered and the solid was washed first with 5 mL of ethyl acetate followed by 5 mL of diethyl ether. It was dried overnight in the desiccator. The complex is soluble in acetonitrile. Yield ~ 0.145 g. FTIR (KBr, cm^{-}

^{1}): υ(C=N)$_{str}$ 1616(s), υ(Ar-C-C)$_{str}$ 1496(s) and 1449(s), υ(Cl-O)$_{str}$ 1086 (s) υ(Ar-C-H)$_{bending}$ 747(s) and 701(s).

5.1.8 [Fe(L2B)$_3$](ClO$_4$)$_2$ (5)

The ligand L2B (0.150 g, 0.80 mmol, 3 eq.) was dissolved in 5 mL of acetonitrile and stirred initially at room temperature. To the stirred solution, Fe(ClO$_4$)$_2$·7H$_2$O(0.099 g, 0.27 mmol, 1 eq.) in 5 mL of acetonitrile was added dropwise, which turned it into a dark red solution and the solution was stirred for 4 h. It was stirred for 3hrs and then solvent was removed to get a hygroscopic sticky solid. It was initially dried in vacuum using pump for 30mins. 5-6ml of ether was added to it and kept overnight in the refrigerator. Next day ether was decanted and the solid was dried and collected. It was recrystallized from the solid in acetonitrile: ether mixture 1:3 kept in refrigerator for 4-5 days. Crystals were aggregated onto each other. Yield = 130mg using 160gm solid. The complex is soluble in acetonitrile. Yield ~ 0.160 g. FTIR (KBr, cm^{-1}): υ(C=N)str 1624(s), υ(Ar-C-C)str 1497(s) and 1442(s), υ(Cl-O)str 1099 (s) υ(Ar-C-H)bending 749(s) and 702(s).

5.1.9 [Fe(L3B)$_3$](ClO$_4$)$_2$ (6)

The ligand L3B(0.150 g, 0.80 mmol, 3 eq.) was dissolved in 5 mL of acetonitrile and stirred initially at room temperature. To the stirred solution, Fe(ClO$_4$)2·7H$_2$O(0.099 g, 0.27 mmol, 1 eq.) in 5 mL of acetonitrile was added dropwise, which turned it into a clear red solution and the solution was stirred for 4 h. The reaction mixture was layered with an equal amount of ethyl acetate, covered properly, and kept in the refrigerator for crystallization. Red crystalline solid appeared after 1-2 days. The solvent was decanted carefully and the solid was washed first with 5 mL of ethyl acetate followed by 5 mL of diethyl ether. It was dried overnight in the desiccator. The complex is soluble in acetonitrile. Yield ~ 0.170 g %). Anal. Calcd. for [Fe(C$_{11}$H$_{11}$N$_3$)$_3$].2(ClO$_4$) ·H$_2$O·3CH$_3$CN·CH$_3$COOCH$_2$CH$_3$: C, 49.69; H, 5.04; N, 16.18; found C, 49.38; H, 5.34; N, 16.36. FTIR (KBr, cm^{-1}): υ(C=N)str 1610(s), υ(Ar-C-C)str 1499(s) and 1450(s), υ(Cl-O)str 1081(s) υ(Ar-C-H)bending 737(s) and 705(s).

5.1.10 [Fe(L1A)$_3$](ClO$_4$)$_2$ (7)

The ligand L1A(0.150 g, 0.36 mmol, 1 eq.) was dissolved in 5 mL of acetonitrile and stirred initially at room temperature. To the stirred solution, Fe(ClO4)2·7H2O(0.135 g, 0.36 mmol, 1 eq.) in 5 mL of acetonitrile was added dropwise, which turned it into a clear red solution and the solution was stirred for 4 h. The reaction mixture was layered with an equal amount of ethyl acetate, covered properly, and kept in the refrigerator for crystallization. Dark purple crystals appeared after 2 days. The solvent was decanted carefully and the solid was washed first with 5 mL of ethyl acetate followed by 5 mL of diethyl ether. It was dried overnight in the desiccator. The complex is soluble in acetonitrile. Yield ~ 68 %. FTIR (KBr, cm^{-1}): υ(C=N)str 1609(s). ESI-MS ($[M + H]^+$): calcd 568.81; found 568.92.

5.1.11 $[Fe(L2A)_3](ClO_4)_2$ (8)

The ligand L2A(0.150 g, 0.39 mmol, 1 eq.) was dissolved in 5 mL of methanol and stirred initially at room temperature. To the stirred solution, $Fe(ClO_4)_2·7H_2O$(0.145 g, 0.39 mmol, 1 eq.) in 5 mL of acetonitrile was added dropwise, which turned it into a clear red solution and the solution was stirred for 4 h. The reaction mixture was filtered, and kept for slow evaporation at room temperature for crystallization. Dark red crystals appeared after 1-2 days. The solvent was decanted carefully and the solid was washed first with 5 mL of ethyl acetate followed by 5 mL of diethyl ether. It was dried overnight in the desiccator. The complex is soluble in acetonitrile. Yield ~ 73 %. FTIR (KBr, cm^{-1}): υ(C=N)str 1629(s). ESI-MS ($[M + H]^+$): calcd 535.74; found 535.11.

5.1.12 $[Fe(L3A)_3](ClO_4)_2$ (9)

The ligand L3A(0.150 g, 0.39 mmol, 1 eq.) was dissolved in 5 mL of methanol and stirred initially at room temperature. To the stirred solution, $Fe(ClO_4)_2·7H_2O$(0.145 g, 0.39 mmol, 1 eq.) in 5 mL of acetonitrile was added dropwise, which turned it into a clear red solution and the solution was stirred for 4 h. The reaction mixture was filtered, and kept for slow evaporation at room temperature for crystallization. Light orange crystals appeared after 2 days. The solvent was decanted carefully and the solid was washed first with 5 mL of ethyl acetate followed by 5 mL of diethyl ether. It was dried overnight in the desiccator. The complex is soluble in acetonitrile. Yield ~

69 %. FTIR (KBr, cm^{-1}): υ(C=N)str 162(s). ESI-MS ($[M + H]^+$): calcd 535.74; found 535.10.

5.2 Results and Discussion

5.2.1 Syntheses

The Schiff base ligands were synthesized by condensing the amine and the aldehyde in methanol. L2B and L3B was isolated as a white powder. The FTIR spectra showed a strong vibration near 1650 cm^{-1} assigned as C=N stretch of the imine formed. The ligand was characterized by proton NMR and Mass spectrometry (Experimental section). L1A, L2A and L3A were not isolated. They were used for the one-pot syntheses of the Complexes **7-9**. Complexes **8** and **9** were synthesized in methanol and Complexes **4-7** has been synthesized from acetonitrile. Complexes **4** and **7** has a distinctive purple colour. The imidazole containing complexes are dark but lacks the purple tinge All of the complexes used for this study was crystalline in nature. The FTIR spectra of all showed imine stretch between 1600-1700 cm^{-1} and large broad perchlorate stretch ~1100 cm^{-1} (Experimental section). Complexes **4-9** been characterized by mass spectra (Figure S15-S19) and and **4** and **7** has additional ^{1}HNMR spectra as well (Figure S21-S22).

5.2.2 Solid-state magnetic behavior of 4-9.

We reported magnetic moments of **4-9** at room temperature. Complexes **4**, **6** and **7** was found to be ~1 B.M. which indicate that these complexes are essentially low-spin Fe(II) in the solid-state (Table 5.1). This is comparable to value ~1 reported for Fe(II) low-spin complex $[Fe(bpy)_3](ClO_4)_2]$.[7] Complex **7** with a different counter ion, and **4** have been assigned as low-spin by other reports as well.[1a, 1c] Magnetic susceptibility for the rest of the complexes is at least an order of magnitude higher (Table 5.1). Magnetic moments vary between 2.54 to 5.06 B.M. as against the expected range of spin-only 4.90 to 5.45 B. M. with an orbital contribution for high-spin Fe(II). Lower magnetic moments of **5**, **8**, and **9** indicate either a low-spin component is present or magnetic coupling exists in the solid-state. Using Mossbauer spectroscopy on solid samples, Brewer and coworkers established that **8** is a mixture of both high-spin and low-spin species at room temperature, but **9** contain only high-spin species.[1b] With BF_4^- counter ion, Mossbauer spectrum of crystalline solid of **9** at 298K contains a small quantity of low-spin component but no low-spin component in

the anhydrous sample as shown by Sunatsuki and coworkers.[2a] Multiple reports point out that in the solid-state of the complexes, with imidazole donor, the ratio of low-spin and high-spin Fe(II) depends on a number of factors such as different counter ion as well as amount or type of solvent of crystallization.[2]

5.2.3 Solution magnetic behavior of 4-9.

The solution magnetic moments for **4** and the reference complex $[Fe(bpy)_3](ClO_4)_2$ are zero indicates that only low-spin Fe(II) species in solution (Table 5.1). The low magnetic moment (<1.7 B. M.) of **7** suggests the low-spin component being the dominant species in solution. The magnetic moment values of **5**, **6**, **8** and **9** are found to be predominantly high-spin at room temperature (Table 5.1). Temperature dependant magnetic susceptibility studies of **5** and **6** (Figure 5.1) showed the decrease of susceptibility value as we lower the temperature from 300 to 230 K. At low temperture we could also see an increase in absorbance value which is characteristic to Fe(II) low-spin species in solution. This shows the crossover nature of the complexes within the given temperature range.

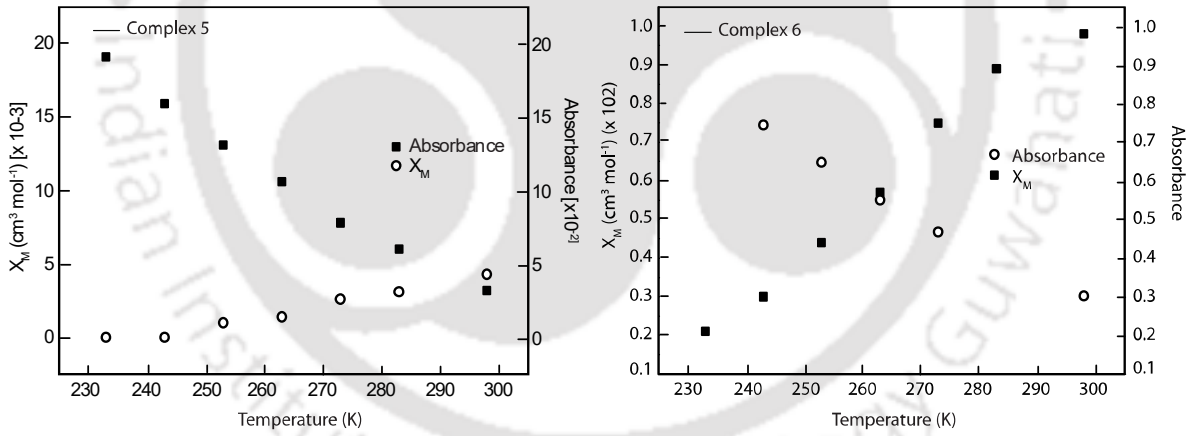

Figure 5.1. X_M *vs.* T and Abs. *vs.* T plot of Complex **5** and **6** within the temperature range (230-300) K in CD_3CN.

5.2.4 Variable temperature ^{1}HNMR of Complex 6.

Variable temperature ^{1}HNMR was also recorded in the same temperature range (Figure 5.2). The complex was high spin at room temperature (300K), and it had no peak initially. As we lower the temperature, the proportion of low spin species became more dominant, which is evident from the formation of the peaks. Since there are quite a bit of high spin species still in the solution, that is why the peaks we see

here are not sharp, and no splitting is observed. We could probably observe more of the the low spin species if we go further below 230 K, but with acetonitrile as a solvent, it is not possible.

We conclude complex **4** and **7** as low-spin species in solution. Both of them have three pyridine moiety as the donor. Complexes **5**, **6, 8** and **9** have more high-spin species in solution. These complexes contain three of either 2- or 4- substituted imidazole moiety as the donor. Complex **6** is notable for the significant shift in the magnetic moment from solid to solution.

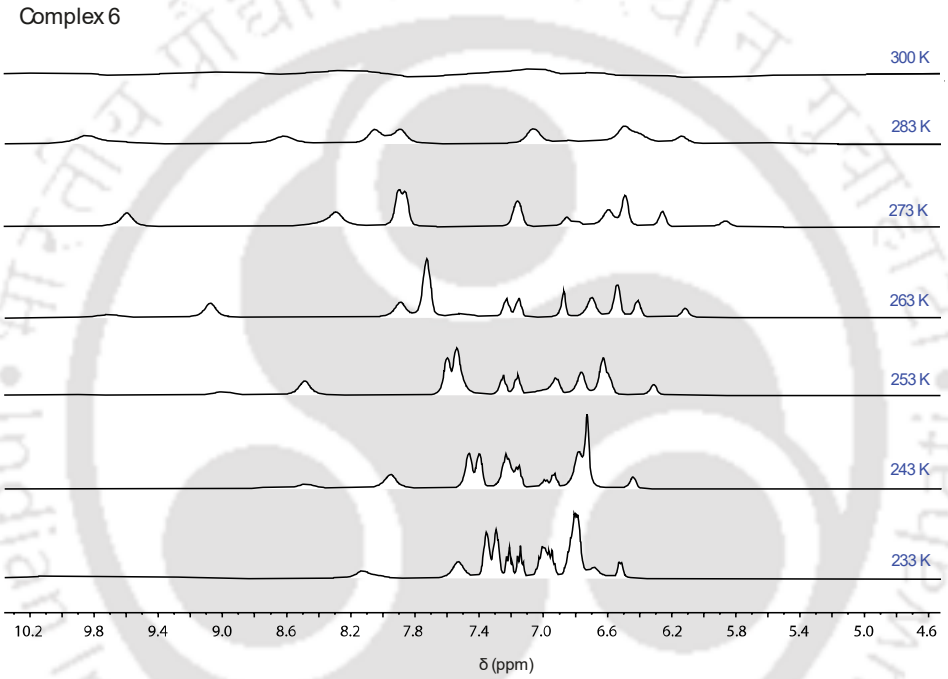

Figure 5.2. Variable temperature ^{1}HNMR spectrum of Complex **6** within the temperature range (230-300) K in CD_3CN.

5.2.5 UV-visible spectra of the complexes 4-9.

Complexes **4** and **7** showed the expected MLCT transitions between 500-600nm with **ε** values (~ 10,000 M^{-1} cm^{-1}), supporting their similarity in coordination environment. This and the lack of weak *d-d* transition confirm their low-spin nature in acetonitrile.[3] On the other hand, the imidazole containing **5**, **6** and **8** and **9** shows a weaker charge transfer band (**ε**, 1000 - 2000 M^{-1} cm^{-1}) between 400-500nm as well as *d-d* transition between 780 -900 nm (**ε**, 7-30 M^{-1} cm^{-1}) (Figure 5.3). MLCT bands of high-spin Fe(II) are usually less intense than their low-spin counterpart.[2d] Presence of

less intense charge transfer and *d-d* transition indicate the presence of mainly high-spin species in solution. However, the presence of a minor quantity of low-spin species cannot be ruled out. The other notable trend is that the charge transfer (CT) band in imidazole donor-containing complexes are significantly blue-shifted compared to their pyridine analogues.

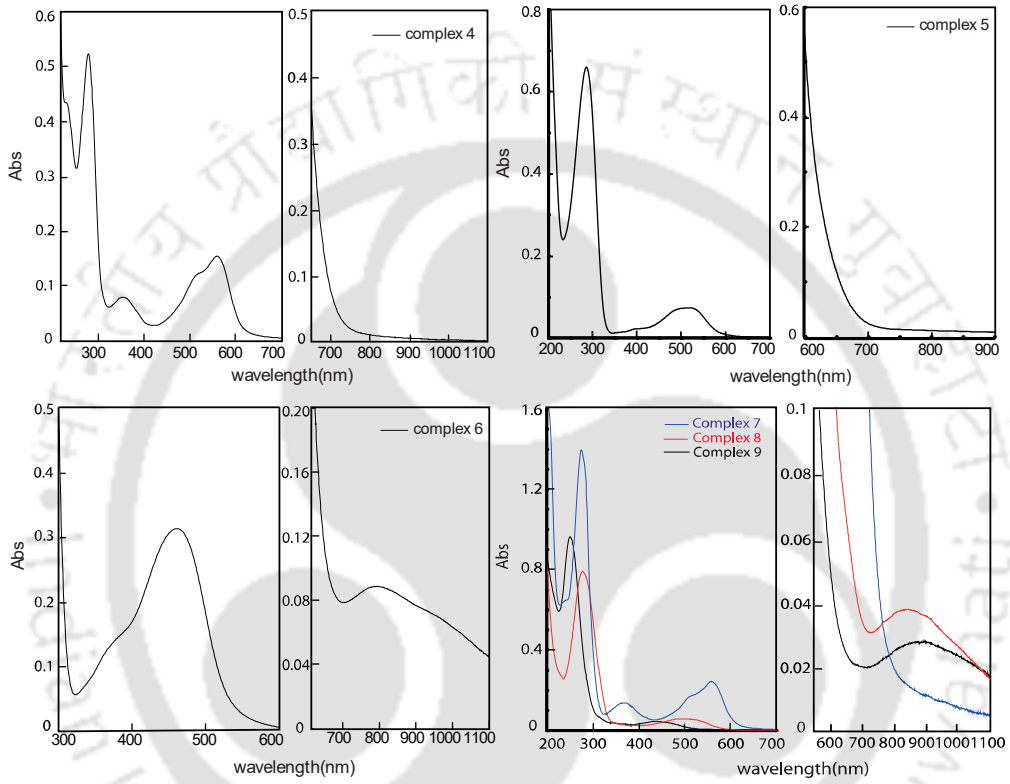

Figure 5.3. UV-visible spectra of Complexes **4-9** in acetonitrile.

The CT band of some of the complexes was recorded up to -40 ºC (Figure 5.4) The intensity enhancement is very high, absorbance is more than doubled in **5**, **6, 8** and **9** (Figure 5.4). All of these had solution magnetic moment < 5 B.M. supporting the presence of low-spin component at room temperature (Table 5.1). On decreasing the temperature, we observe the increase in CT band intensity corresponding to the increase in low-spin species.

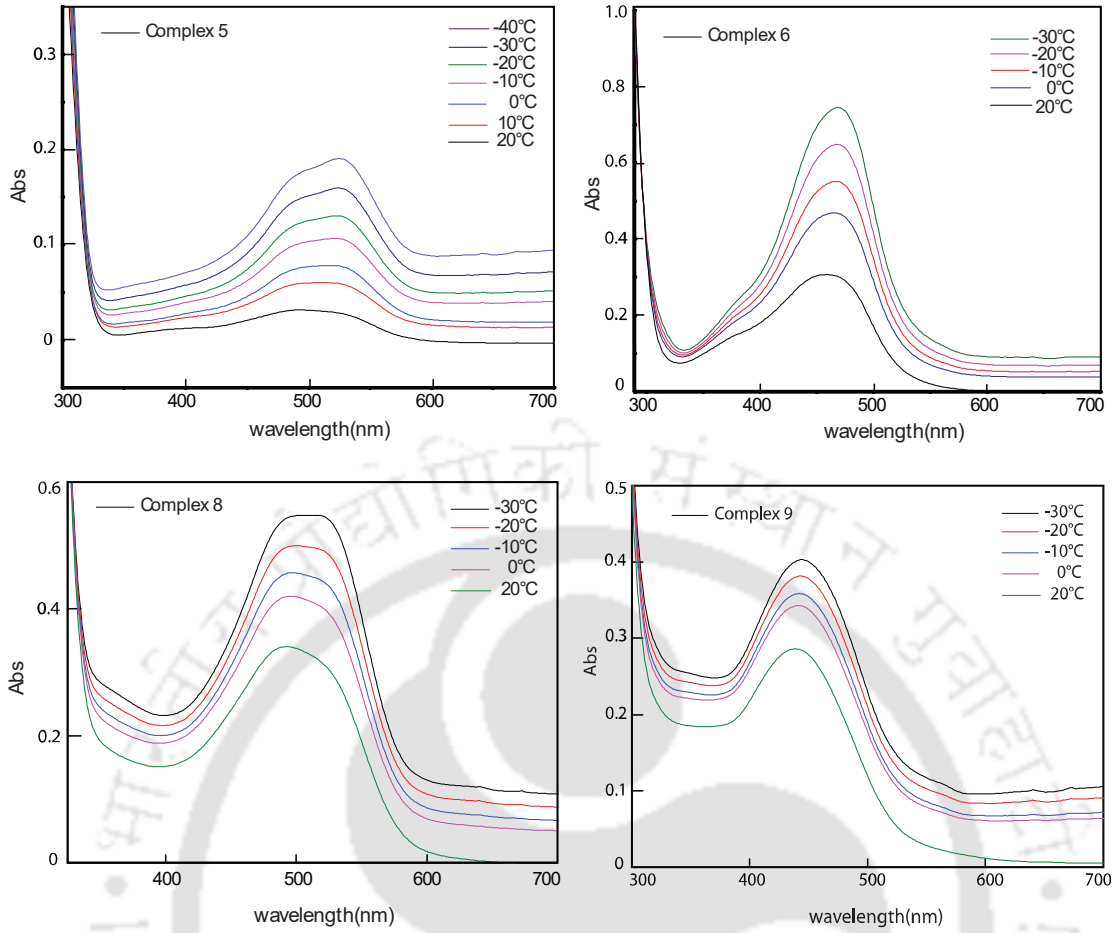

Figure 5.4. Variable temperature plot of UV-visible spectra of the Complexes **5**, **6**, **8** and **9**. in acetonitrile with the temperature (243-293) K.

5.2.6 Electrochemical behavior of the complexes 4-9.

The redox potential of **4**, each having three imine and three pyridine donor, are highest and lies within a very narrow range of ~ 1.14 V vs SCE (Figure S23). This is similar to reported redox potential of a Fe(II) complex with four pyridine donor and 2 imine donor at 1.08 V vs. SCE.[4] Complex **7** despite having donors similar to **1** and **4**, oxidizes at + 0.92 V vs SCE (Figure S26). The ligand L1A (Scheme 5.1) in **7** have an apical nitrogen which does not bind in solid state[1c,5] but interaction in solution can not be ruled out. The shift could be the result of this. The redox potentials of imidazole containing complexes (**3**, **5**, **6** & **8**), all of which are essentially high-spin at room temperature, are far lower than their low-spin analogues (Figure S24, S25, S27 and S28, Table 5.1). Oxidation in low-spin octahedral iron(II) removes electron from fully filled t_{2g} level which is non-bonding type. On the other hand, oxidation of high-spin d^6

octahedral removes electron from anti-bonding e_g orbitals and without penalty of breaking the fully filled shell. Hence the large shift is likely to be a combined effect of change in donor as well as spin-state. We plotted the potentials on a scale (Figure 5.6). High-spin and low-spin complexes are in two widely different region. Differences within 2-imidazole and 4-imidazole analogue, both of which are high-spin at room temperature, are lower at ~140mV.

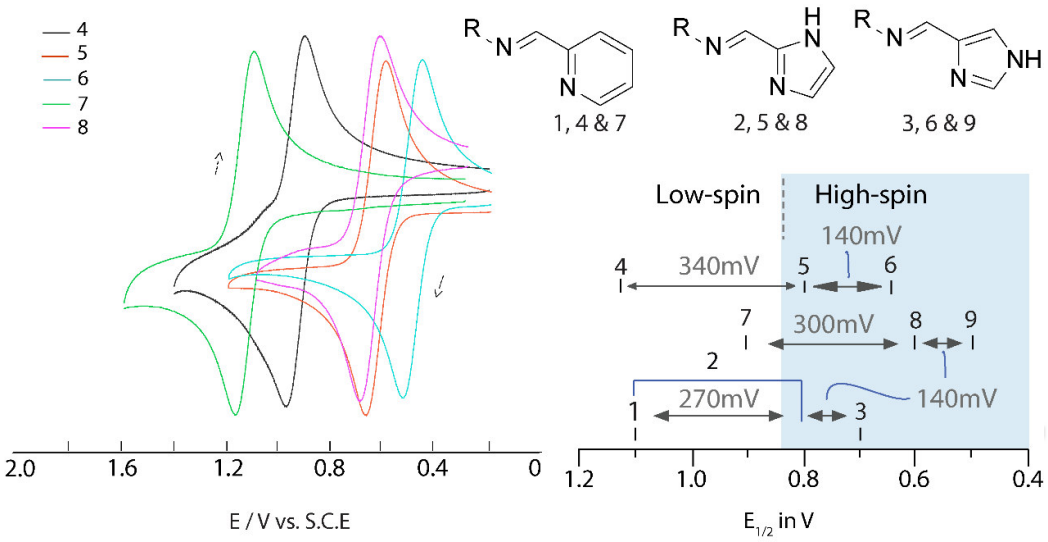

Figure 5.5. To illustrate the effect of donor atoms on redox potential ($E_{½}$) of the complexes plotted on a scale. Complexes **1**, **4** & **7** contains pyridine donor, **2**, **5** and **8** has 2-imidazole donor, and **3**, **6** & **9** has 4-imidazole donor. Complexes in the shaded region are essentially low-spin in solution. Complex **2** showed both high-spin and low-spin redox couple.

5.2.7 Comparative behavior between Complex 1-9.

We now compare all the complexes **1-9** we discussed over the two chapters (Chapter IV and V). Complexes **1**, **4** and **7** have pyridine group and complexes **5**, **6**, **8** and **9** have imidazole group. Magnetic susceptibility studies showed pyridine containing complexes **1**,**4** and **7** was found to be low spin and imidazole containing **5**, **6**, **8** and **9** was found to be high spin at room temperature in solution. Temperature dependant susceptibility data showed Complex **2**, **5** and **6** having 2 and 4-imidazole group been found to show cross-over property in solution. **6** showed sharp decrease in χ_M and increase in absorbance with the decrease in temperature as compared to the

others. Electronic spectra showed intense CT bands (ε, ~10,000M^{-1}) between 450-600 nm for low spin complexes (1, 4 and 7) and less intense CT bands (ε, ~1000-2000 M^{-1}) between 400-500 nm and the presence of the forbidden *d-d* transition (ε, ~ 10-30 M^{-1}) between 700-900 nm (5, 6, 8 and 9). On lowering the temperature we observed an increase in CT band due to an increase in the low spin species in equilibrium with high spin species. For **5** and **6** there was no shift in wavelength with the increase in intensity but complex The enhancement in **2** is unique in that it is the only one showing both enhancement in intensity as well as a shift of 454 nm to 493 nm at a lower temperature. Temperature-dependent electronic spectral study on similar complexes did not show such shift.[2d, 6] Cyclic voltammetric experiments showed considerable difference as we move from pyridine to 2-imidazole and 4-imidazole, which is showing similar trend as we saw on moving from **1** to **3**. Solution magnetic moment and electronic spectra established that pyridine containing 1, 4 & 7 are low-spin and 4-imidazole containing 3, 6 & 8 are essentially high-spin in solution. Complex 1 oxidizes at +1.12V, while **3** oxidizes at 410mV lower potential of +0.71 V. Similar differences of 440mV observed between the other set of complexes **4**-**6** as well as between **7**-**9**. We conclude that (i) complexes having the pyridine unit are essentially low-spin both solid and solution pyridine, (ii) complexes with imidazole tend to have more high-spin component at room temperature but not only high-spin except in **3**, and (iii) unlike **5**, **6**, **8** and **9** the low-spin form of **2** is different than its high-spin form. It could be due to a structural rearrangement or conformational change. A comparison of magnetic moments, redox potential and UV-visible spectral data of the complexes at room temperature have been summarized in Table 5.1.

Table 5.1. Magnetic moments, redox potential and UV-visible spectral data of the complexes at room temperature (298K).[a]

Complex	μ_{eff}, B.M. (Solid)	μ_{eff}, B.M. MeCN	Fe^{III}/Fe^{II} couple in MeCN		Electronic spectra in MeCN, nm (ε, $M^{-1}cm^{-1}$)	
			$E_{½}$, V	ΔE_p, mV	*d-d* transition	CT band
1	1.04	1.60	1.12	78	n.o.[e]	364(3300), 515 (6090), 566(8060)
2	2.54	4.80	1.11	190	775(20)	412(1020), 454(1080)
			0.85	119		
			0.49[g]	190[g]		
3	5.06	5.40	0.71	132	785(15)	359 (1700), 416 (1200)
4	1.02	0	1.14	69	n.o.[e]	354 (4500), 512sh, 558(10560)
5	2.00	3.21	0.80	80	n.o.[e]	390 (1764), 512(6200)
6[c]	1.20	4.64	0.66	75	793(7)	368sh, 460(2570)
			0.53[g]	110[g]		
7	1.05	1.25	0.92[b]	69	n.o.[e]	366(7070), 509sh, 557(12350)
8	4.15[d]	4.56	0.62[b]	75	842(27)	493(2080), 533sh
9	4.54[d]	4.55	0.48[b]	75	885(20)	440(1920)
$[Fe(bpy)_3](ClO_4)_2$[f]	0.66[g]	0.0	1.06[f]	74	n.o.[e]	348(9980), 391sh, 483sh, 519(14400)

[a] Details of measurements are in Experimental section. Room temperature solution magnetic susceptibilities were measured using a 600MHz NMR spectrometer. $E_{½}$ values are vs SCE, recorded at a scan rate of $100mVs^{-1}$ using a glassy carbon working electrode in acetonitrile. UV-visible spectra were recorded between 300-1100 nm in acetonitrile [b] Redox potentials of **7** in MeCN and **8**-**9** in Methanol were reported before.[1b,1c] [c] A similar complex using *N*-benzyl-1-(2-methyl-1*H*-imidazol-4-yl)methanimine ligand having different counter ions showed spin crossover in solid

state.[2b, 2c] [d] Reported to show spin-crossover in solid.[1b] [e] n.o. = not observed. [f] The ligand bpy is 2, 2'- bipyridine.[3a] [g] Reported value ~1.[7] [g]redox potential in DMF

Conclusions

We studied two new set of similar complexes **4-9** (Scheme 5.1) using a combination of cyclic voltammetry, magnetic property and UV-visible spectroscopy in acetonitrile. Despite similarity in coordination geometry and donor atoms, the redox potential varied widely (Table 5.1) which could be attributed to the specific donor type and the spin state (pyridine vs 2-imidazole or 4-imidazole) (Figure 5.5). The shift in redox potential between pyridine and 4-imidazole analogue is very high at > 400 mV due to the accompanying spin-state change. Without the accompanying spin-state change, a modest but significant difference of ~140 mV also existed between 2-imidazole and 4-imidazole analogue. While the larger differences due to spin-state change is expected, the difference between 2-imidazole and 4-imidazole analogue means that choosing one imidazole derivative over other in the ligand design could further tune the Fe(II) redox potential. The finding revealed that the magnetic properties of the imidazole analogues in solution can be quite different to that in solid state (Table 5.1). Solution magnetic moment of all five imidazole analogue are essentially high-spin, at least major species, at room temperature (Table 5.1). This is in contrast to the reported solid state values of some of these complexes.[1] Temperature dependent solution magnetic susceptibilities showed that, except for complex **3**, imidazole complexes indeed has a tendency to convert to low-spin at lower temperature. The only exception out of all the complexes used in this study is complex **3**, which is high-spin in solid state as well as in solution.

References

1. (a) Howson, S. E.; Allan, L. E. N.; Chmel, N. P.; Clarkson, G. J.; Deeth, R. J.; Faulkner, A. D.; Simpson, D. H.; Scott, P. Origins of stereoselectivity in optically pure phenylethaniminopyridine tris-chelates M (NN′) 3 n+ (M= Mn, Fe, Co, Ni and Zn). *Dalton Trans*. **2011**, *40*, 10416. (b) Brewer, C.; Brewer, G.; Luckett, C.; Marbury, G. S.; Viragh, C.; Beatty, A. M.; Scheidt, W. R. Proton Control of Oxidation and Spin State in a Series of Iron Tripodal Imidazole Complexes. *Inorg. Chem.* **2004,** *43*, 2402. (c) Struch, N.; Topić, F.; Schnakenburg, G.; Rissanen, K.; Lützen, A. Electron-Deficient Pyridylimines: Versatile

Building Blocks for Functional Metallosupramolecular Chemistry. *Inorg. Chem*. **2018**, *57*, 241.

2. (a) Sunatsuki, Y.; Ohta, H.; Kojima, M.; Ikuta, Y.; Goto, Y.; Matsumoto, N.; Iijima, S.; Akashi, H.; Kaizaki, S.; Dahan, F.; Tuchagues, J.-P. Supramolecular Spin-Crossover Iron Complexes Based on Imidazole−Imidazolate Hydrogen Bonds. *Inorg. Chem.* **2004**, *43*, 4154. (b) Hagiwara, H.; Yamauchi, S.; Matsumoto, N.; Sunatsuki, Y. Synthesis, structures, and magnetic properties of iron(II) complexes, [FeII(HLMe)2](ClO4)2 and its ethanol adduct [FeII(HLMe)2] (ClO4)2·EtOH (HLMe= 2-methylimidazol-4-yl-methylidene amino-2-ethylpyridine): Their structural distortion and spin states. *Polyhedron* **2012**, *48*, 110 (c) Furusho, D.; Nishi, K.; Hashibe, T.; Fujinami, T.; Hagiwara, H.; Matsumoto, N.; Halcrow, M. A.; Iijima, S.; Sunatsuki, Y.; Kojima, M. Assembly Structures and Spin Crossover Properties of Facial and Meridional Isomers of Tris[benzyl(2-methylimidazol-4-ylmethylidene)amine]iron(II) Chloride Hexafluorophosphate. *Chem. Lett.* **2010**, *40*, 72. (d) Chang, H. R.; McCusker, J. K.; Toftlund, H.; Wilson, S. R.; Trautwein, A. X.; Winkler, H.; Hendrickson, D. N. [Tetrakis(2-pyridylmethyl)ethylenediamine]iron(II) perchlorate, the first rapidly interconverting ferrous spin-crossover complex. *J. Am. Chem. Soc* **1990**, *112*, 6814.

3. (a) Weiner, M. A.; Basu, A. Et3P+- and Nitro-Substituted Pyridines and Bipyridines. Their Behavior as Ligands in Iron(II), Cobalt(II), and Ruthenium(II) Complexes. *Inorg. Chem*. **1980**, *19*, 2797. (b) Decurtins, S.; Felix, F.; Ferguson, J.; Guedel, H. U.; Ludi, A. The electronic spectrum of tris(2,2'-bipyridine)iron(2+) and tris (2,2'-bipyridine)osmium(2+). *J. Am. Chem. Soc*. **1980**, *102*, 4102. (c) Williams, R. J. P. The absorption spectra of some complex ions of analytical importance. *J Chem. Soc*. **1955**, 137.

4. Ramesh, K. and Mukherjee, R. N. A low-spin iron(II) diimine complex of a Schiff base ligand: Charge transfer transition and electrochemistry. *Indian J. Chem. Sec. A,* **1991**, *30*, 1057.

5. Brewer, G., et al. Synthesis and characterization of tripodal iron(II) complexes prepared from 2-pyridinecarboxaldehyde and 1-methyl-2-imidazolecarboxaldehyde: stabilization of iron(II) cations with N_6 donor sets. *Inorg. Chim. Acta* **2004**, *357*, 2390.

6. Thorarinsdottir, A. E.; Gaudette, A. I.; Harris, T. D. Spin-crossover and high-spin iron(ii) complexes as chemical shift 19F magnetic resonance thermometers. *Chem. Sci*. **2017**, *8*, 2448.

7. Figgis, B. N.; Lewis, J. The Magnetic Properties of Transition Metal Complexes In *Progress* in Inorganic Chemistry; Wiley: **1964**, 37.

Supplementary Tables and Figures

Table S1. Selected bond length (Å) and angles (º) for the complex [Ni(*S*-L1)$_2$(*S*-L2)](ClO$_4$)$_2$(**1b**).

Ni1-N1	2.096(5)	N1-Ni1-N2	78.9(2)
Ni1-N2	2.086(5)	N2-Ni1-N4	95.0(2)
Ni1-N3	2.114(5)	N4-Ni1-N5	168.1(2)
Ni1-N4	2.072(6)	N5-Ni1-N1	98.2(2)
Ni1-N5	2.152(6)	N1-Ni1-N7	173.1(2)
Ni1-N7	2.072(6)	N7-Ni1-N4	90.6(2)
N1-C9	1.263(8)	N1-Ni1-N4	91.8(2)
N3-C23	1.264(8)	N2-Ni1-N5	91.3(2)
N5-C37	1.272(9)	N3-Ni1-N7	92.5(2)

Table S2. Non-covalent interactions in complex [Ni(*S*-L1)$_2$(*S*-L2)](ClO$_4$)$_2$(**1b**).

D-H...A	D-H(Å)	H. . .A(Å)	D. . .A(Å)	DHA(°)
Inter-molecular				
N6-H6..O2	0.86	2.06	2.857(15)	154
C8-H8c..O2	0.96	2.51	3.449(13)	167
C9-H9..O3	0.93	2.54	3.382(9)	152
C12-H12..O5	0.93	2.51	3.334(15)	147
C25-H25..O6	0.93	2.52	3.391(11)	157
C28-H28..O3	0.93	2.36	3.108(10)	137
C41-H41a..O8	0.96	2.60	3.555(19)	174
C41-H41b..O1	0.96	2.51	3.468(16)	176
C39-H39..π(C29-C34)	0.93[§]	2.83[§]	3.572[§]	137.9[§]
Intra-molecular				
π(C1-C6)-Ph..π(N4)–Py	-	-	3.945[§]	-
π(C29-C34)-Ph..π(N2)–Py	-	-	3.682[§]	-
π(C15-C20)-Ph..π(N7)–Im	-	-	3.865[§]	-

The acceptable range of D...A for N-H..O, 2.5-3.2 Å; for C-H..O, 3.0-4.0 Å; N-H/C-H... π 2.5–4.5 Å, from ref.[30-33]. [§]Calculated from Mercury.[34]

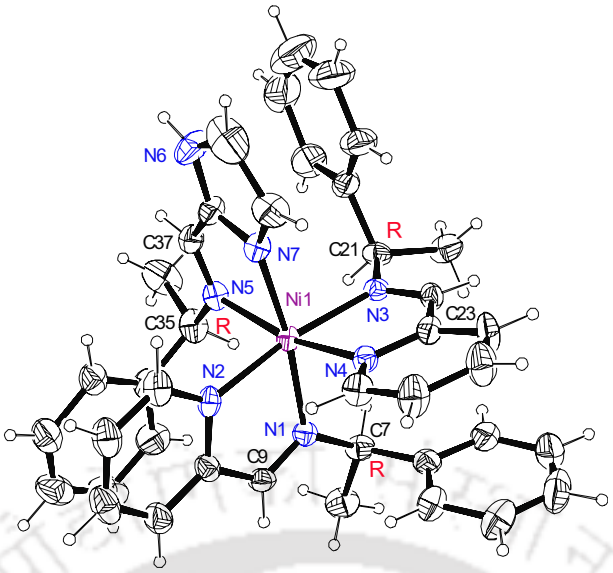

Figure S1. The ORTEP diagram of the cationic part of Complex [Ni(*R*-L1)$_2$(*R*-L2)](ClO$_4$)$_2$(**1d**). Thermal ellipsoid are set to 50% probability level.

Table S3. Selected bond length (Å) and angles (º) for the complex [Ni(*R*-L1)$_2$(*R*-L2)](ClO$_4$)$_2$(**1d**).

Ni1-N1	2.109(5)	N1-Ni1-N2	78.5(2)
Ni1-N2	2.090(5)	N2-Ni1-N4	95.04(19)
Ni1-N3	2.124(5)	N4-Ni1-N5	167.9(2)
Ni1-N4	2.077(5)	N5-Ni1-N1	98.4(2)
Ni1-N5	2.155(5)	N1-Ni1-N7	172.0(2)
Ni1-N7	2.069(5)	N7-Ni1-N4	90.31(19)
N1-C9	1.253(8)	N1-Ni1-N4	92.99(19)
N3-C23	1.266(8)	N2-Ni1-N5	91.27(19)
N5-C37	1.255(9)	N3-Ni1-N7	92.75(19)

Table S4. Non-covalent interactions in Complex [Ni(*R*-L1)$_2$(*R*-L2)](ClO$_4$)$_2$(**1d**).

D-H...A	D-H(Å)	H. . .A(Å)	D. . .A(Å)	DHA(°)
Inter-molecular				
N6-H6..O2	0.86	2.21	3.000(2)	153
C8-H8c..O2	0.96	2.59	3.522(13)	163
C12-H12..O8	0.93	2.57	3.409(19)	150
C28-H28..O4	0.93	2.43	3.209(9)	142
C39-H39..π(C29-C34)	0.93[§]	2.98[§]	3.754[§]	141.57[§]
Intra-molecular				
π(C1-C6)-Ph..π(N4)–Py	-	-	3.969[§]	-
π(C29-C34)-Ph..π(N2)–Py	-	-	3.761[§]	-
π(C15-C20)-Ph..π(N7)–Im	-	-	3.897[§]	-

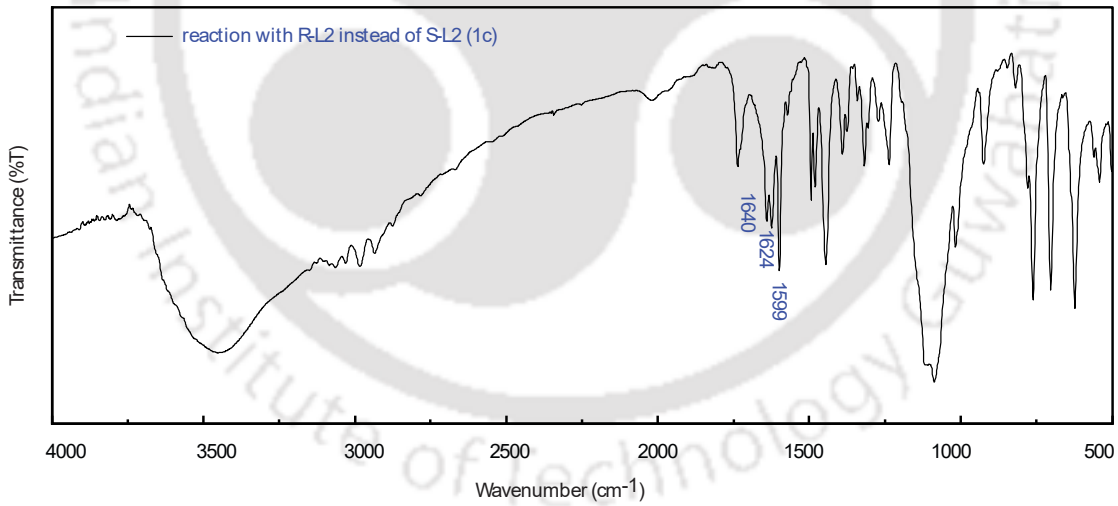

Figure S2. FT-IR spectra of reaction using *R*-L2 instead of *S*-L2 (**1c**).

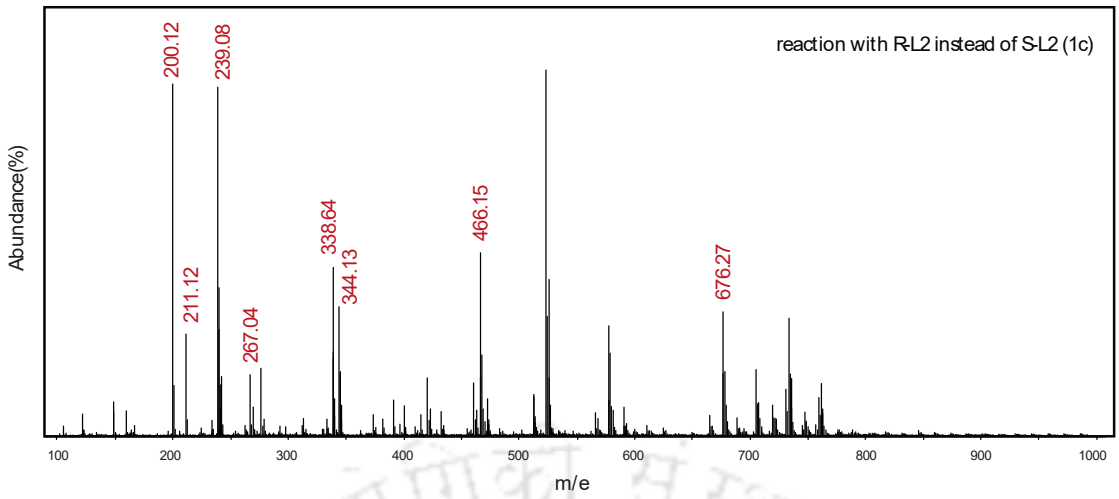

Figure S3. Mass spectra of reaction using *R*-L2 instead of *S*-L2 (**1c**).

Table S5. Selected bond distances (Å) and angles (°) of **2a**.

Fe1-N1	1.980(4)	N6-Fe1-N7	81.40(14)
Fe1-N3	2.017(3)	N5-Fe1-N7	92.09(14)
Fe1-N4	1.973(4)	N4-Fe1-N7	93.47(14)
Fe1-N5	1.966(3)	N1-Fe1-N7	90.71(15)
Fe1-N6	1.985(4)	N1-Fe1-N3	80.60(14)
Fe1-N7	1.959(3)	N5-Fe1-N4	81.11(15)
N3-C4	1.278(6)	N4-Fe1-N6	173.34(15)
N5-C18	1.282(5)	C4-N3-C5	119.7(4)
N6-C32	1.281(5)	C1-N1-Fe1	137.5(4)

Table S6. Non-covalent interactions in Complex **2a.**

D-H...A	D-H (Å)	H. . .A(Å)	D. . .A(Å)	DHA(°)
Inter-molecular				
N2-H2..O5	0.86	1.96	2.813(9)	173
C18-H18..O7	0.93	2.57	3.407(6)	150
C27-H27..N4	0.93	2.55	3.052(6)	114
C27-H27..O7	0.93	2.42	3.167(6)	138
C32-H32..O2	0.93	2.57	3.415(6)	152
C42-H42c..O3	0.96	2.52	3.476(9)	173
C2-H2..π(C6-C11)	0.93[§]	2.69[§]	3.565[§]	157[§]

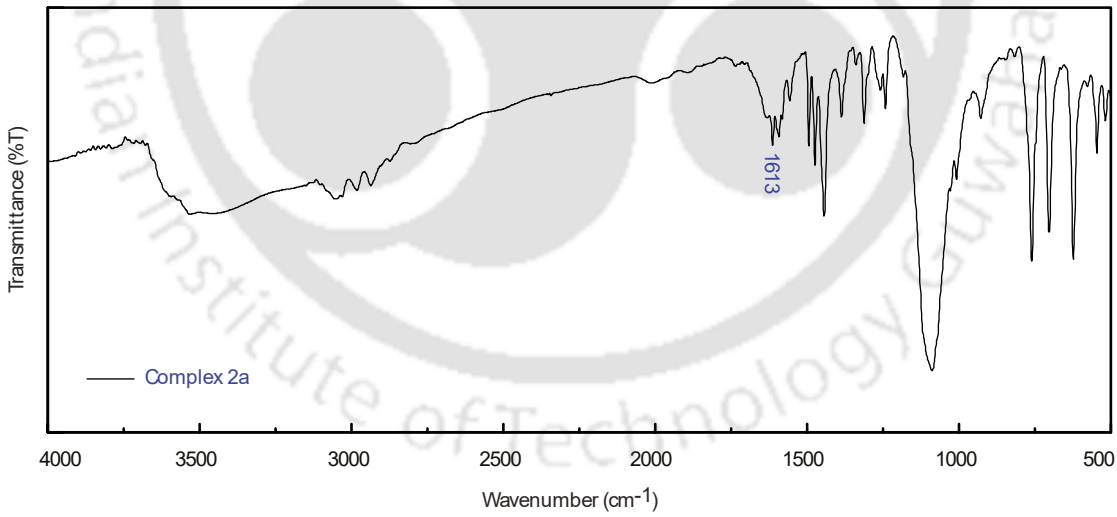

Figure S4. FTIR spectra of Complex **2a**.

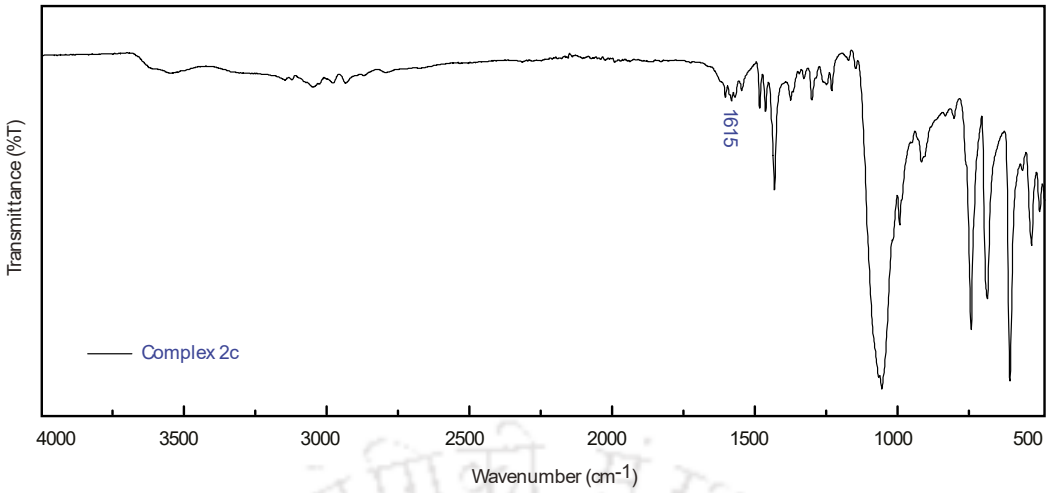

Figure S5. FTIR spectra of Complex **2c**.

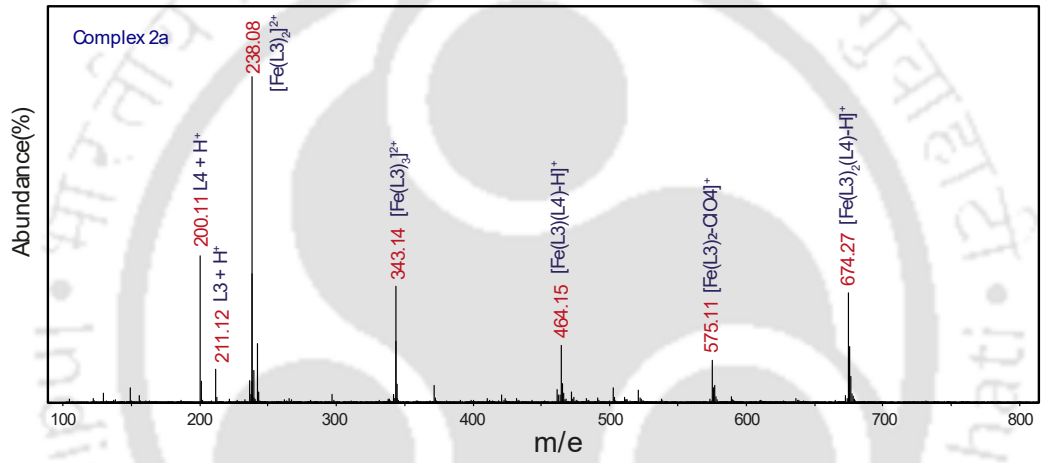

Figure S6. ESI-MS spectra of Complex **2a**.

Table S7. Comparison of average M-N bond lengths.

Average Bond Length (Å)	$[Fe(S\text{-}L1)_2(S\text{-}L2)]^{2+}$	$[Ni(S\text{-}L1)_2(S\text{-}L2)]^{2+}$
$M\text{-}N_{imine}$	1.99	2.13
$M\text{-}N_{ring}$	1.97	2.08

Table S8. Comparison of imidazole N-H bonding with perchlorate oxygen.

	D-H...A	D-H (Å)	H. . .A(Å)	D. . .A(Å)	DHA(°)
	Inter-molecular				
Fe-complex	N2-H2..O5	0.86	1.96	2.813(9)	173
Ni-complex	N6-H6..O5	0.86	2.09	2.885(15)	153

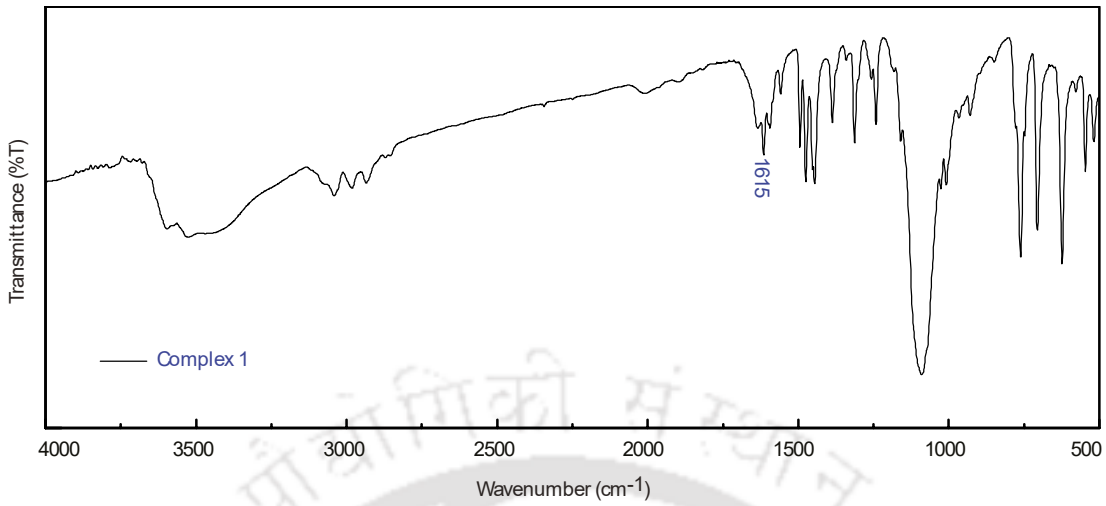

Figure S7. FTIR spectrum of Complex **1**.

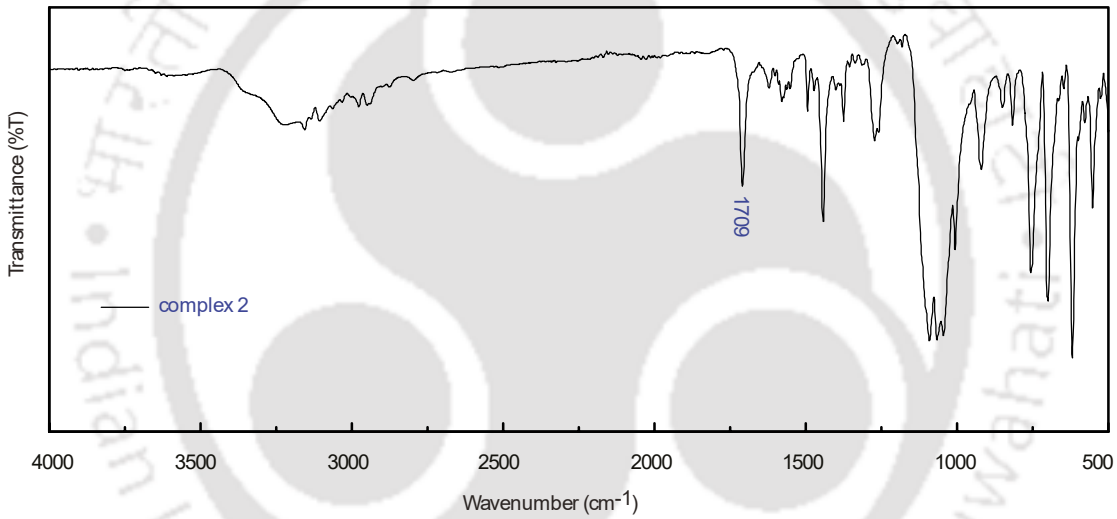

Figure S8. FTIR spectrum of Complex **2**.

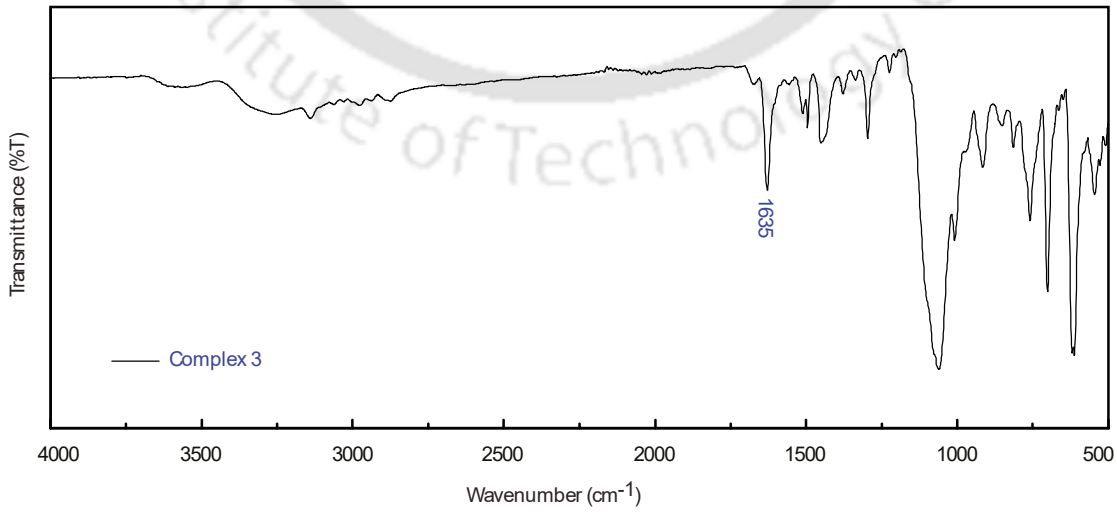

Figure S9. FTIR spectrum of Complex **3**.

Table S9. Crystallographic data and refinement parameters of **2**.

	2
Empirical formula	C36 H39 Cl2 N9 Fe1 O10
fw	852.51
crystal system	Triclinic
space group	*P1*
a, Å	10.0293(12)
b, Å	11.5716(14)
c, Å	12.0919(14)
α(°)	98.026(5)
b(°)	113.717(4)
γ(°)	111.183(4)
V, Å^3	1129.3(2)
Z/ρ (g cm^{-3})	1/1.254
T(K)	293(2)
μ (mm^{-1})	0.507
coll.reflns	7951
indep reflns	5096
FLACK para.	0.001(18)
GOF on F^2	1.022
Residuals (e Å^{-3})	0.363, -0.367
R1[b], wR2[b]	0.0859/0.1969
R1[c], wR2[c]	0.1180/0.2176

Table S10. Selected bond distances (Å) and angles (º) of **2**.

Fe1-N1	2.025(11)	N1-Fe1-N2	80.0(5)
Fe1-N2	2.037(10)	N3-Fe1-N4	80.1(4)
Fe1-N3	1.981(11)	N1-Fe1-N4	171.2(5)
Fe1-N4	2.022(10)	N3-Fe1-N1	92.3(4)
Fe1-N5	1.998(11)	N1-Fe1-N5	92.9(5)
Fe1-N6	2.018(9)	N3 Fe1 N6	170.8(5)
N2-C7	1.497(14)	N4-Fe1-N2	97.5(4)

Table S11. Non-covalent interactions in Complex **2**.

D-H...A	D-H (Å)	H. . .A(Å)	D. . .A(Å)	DHA(°)
Inter-molecular				
N7-H7A..O7	0.86	2.37	3.057(4)	137
N8-H8..O4	0.86	1.99	2.840(4)	157
N9-H9A..O107	0.86	1.98	2.838(4)	175
C24-H24..O8	0.93	2.57	3.261(4)	131
C36-H36..O6	0.86	2.46	3.266(4)	145

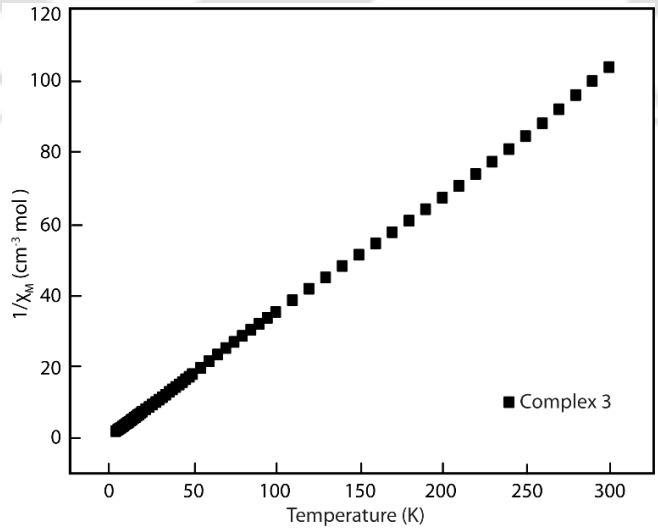

Figure S10. 1/χM vs. T shows the linearity of Complex **3**.

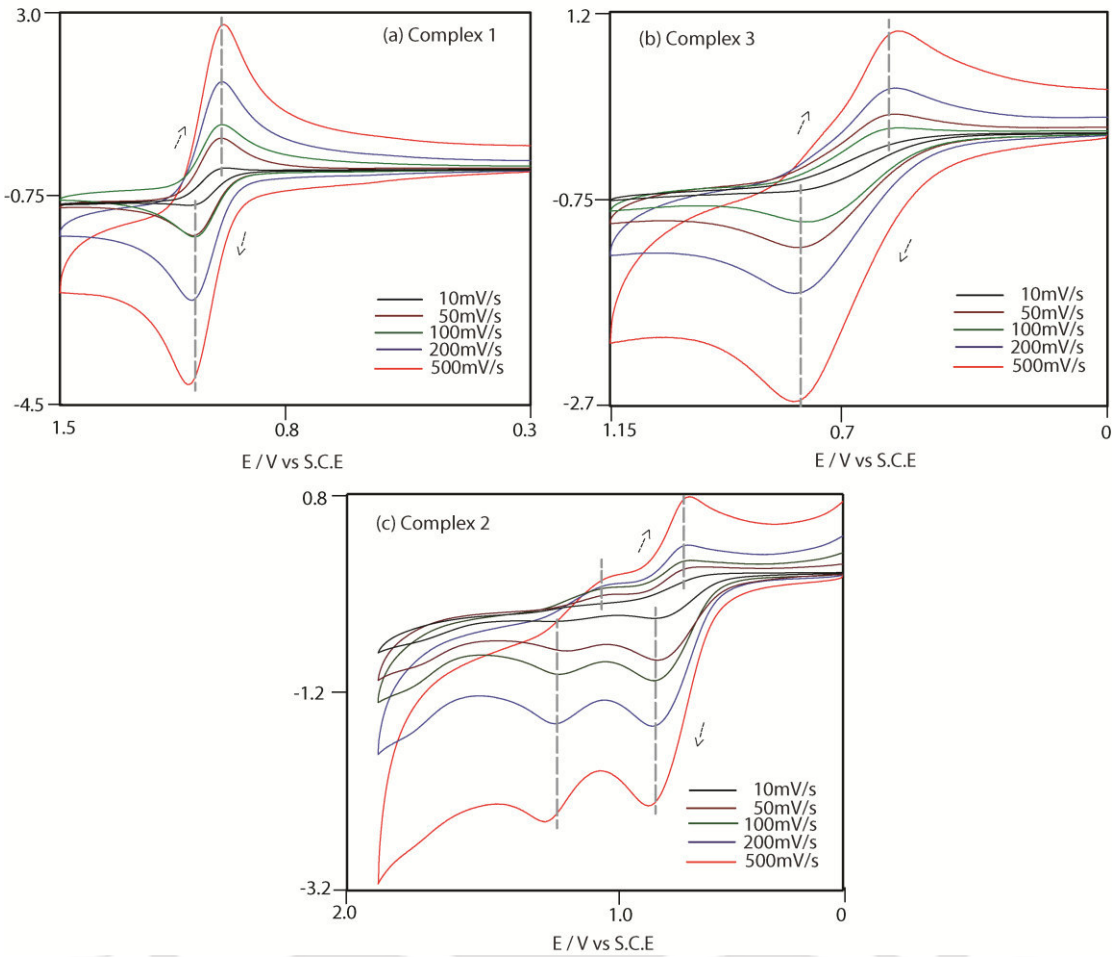

Figure S11. Variable scan rate of the Complexes **1**-**3**.

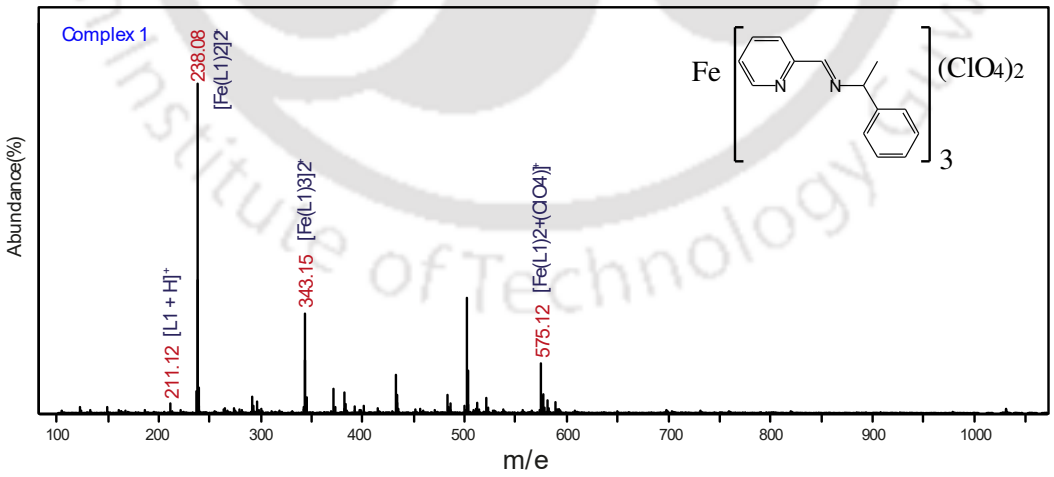

Figure S12. The ESI-MS spectrum of **1** in acetonitrile.

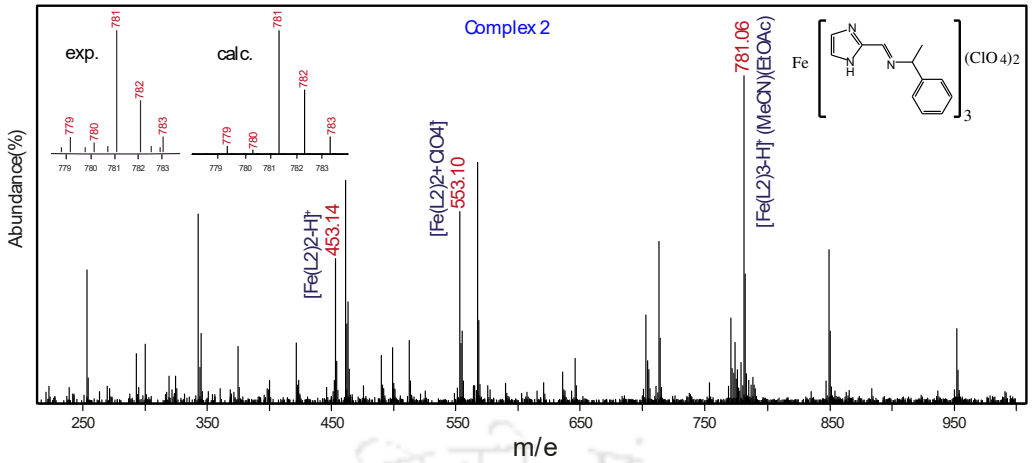

Figure S13. The ESI-MS spectrum of **2** in acetonitrile.

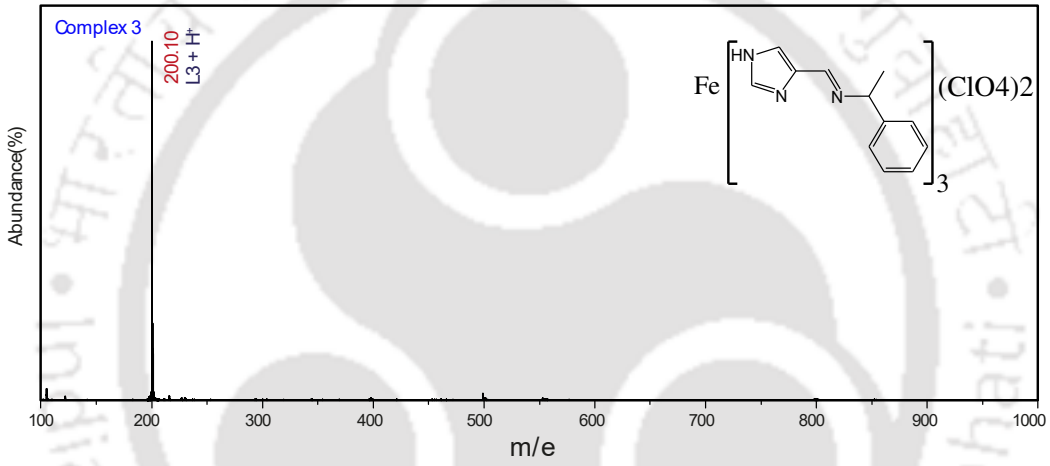

Figure S14. The ESI-MS spectrum of **3** in acetonitrile.

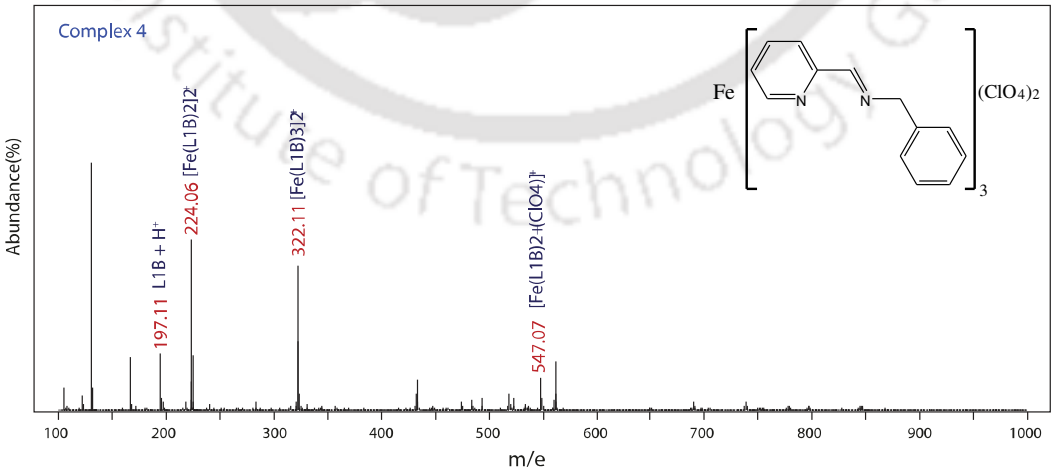

Figure S15. The ESI-MS spectrum of **4** in acetonitrile.

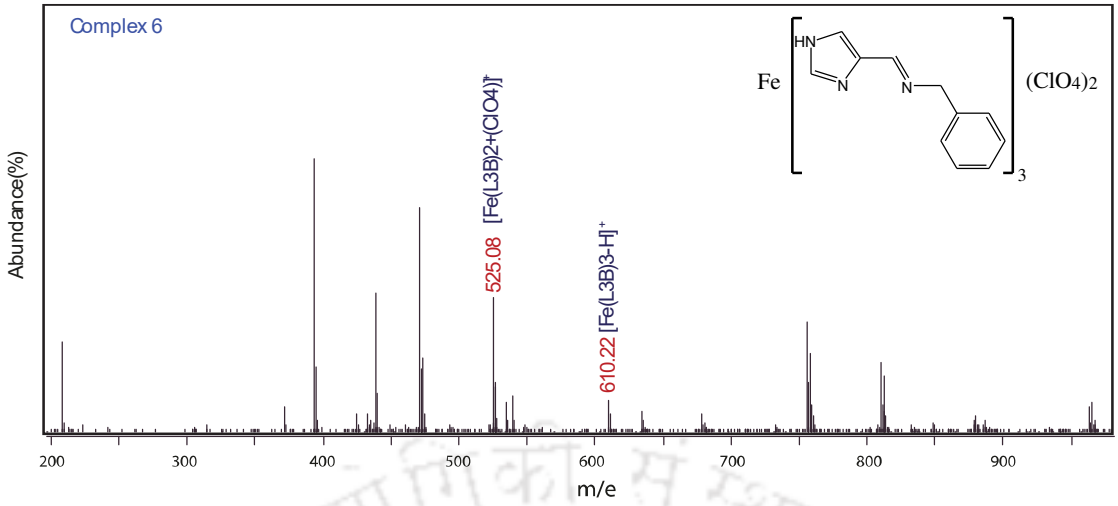

Figure S16. The ESI-MS spectrum of **6** in acetonitrile.

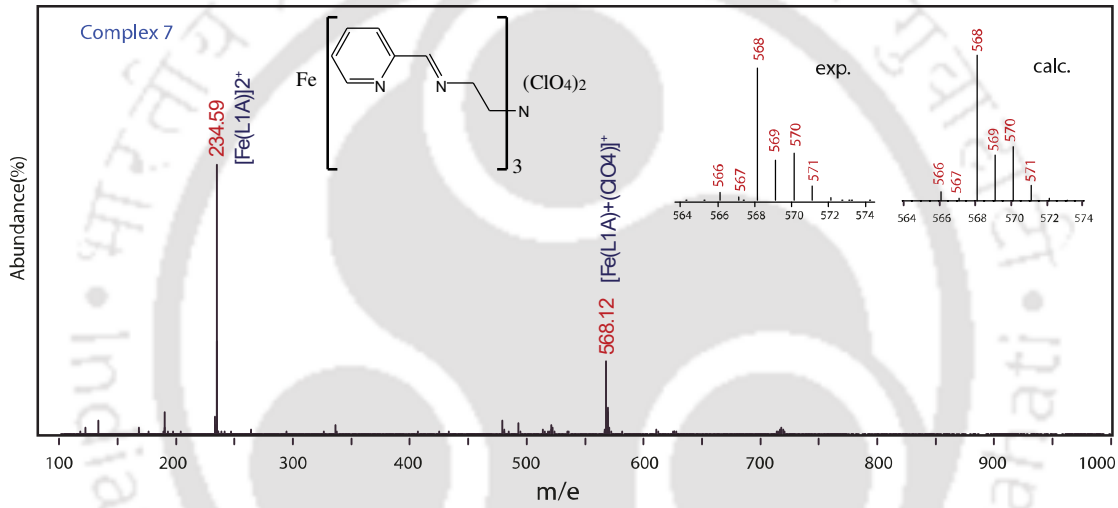

Figure S17. The ESI-MS spectrum of **7** in acetonitrile.

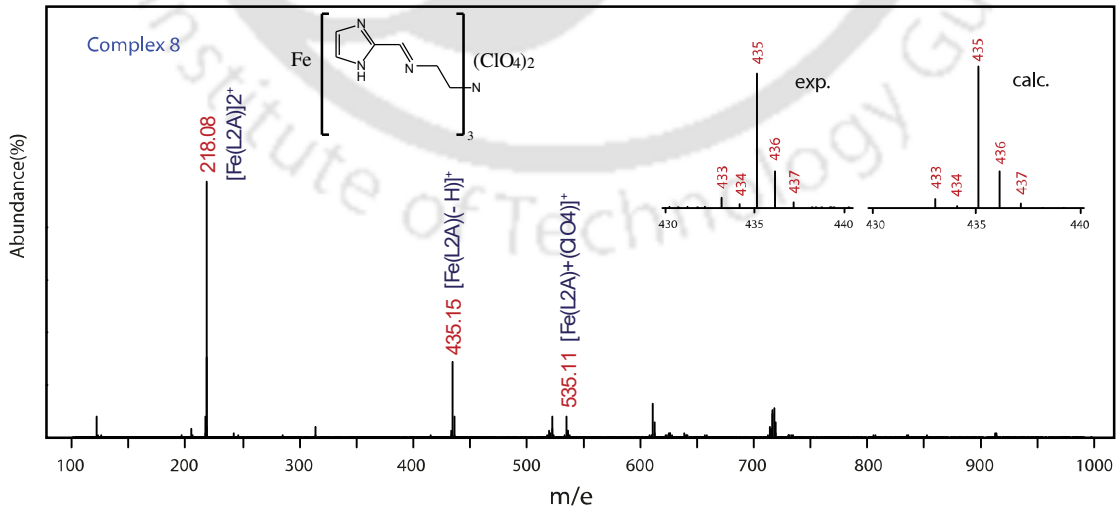

Figure S18. The ESI-MS spectrum of **8** in acetonitrile.

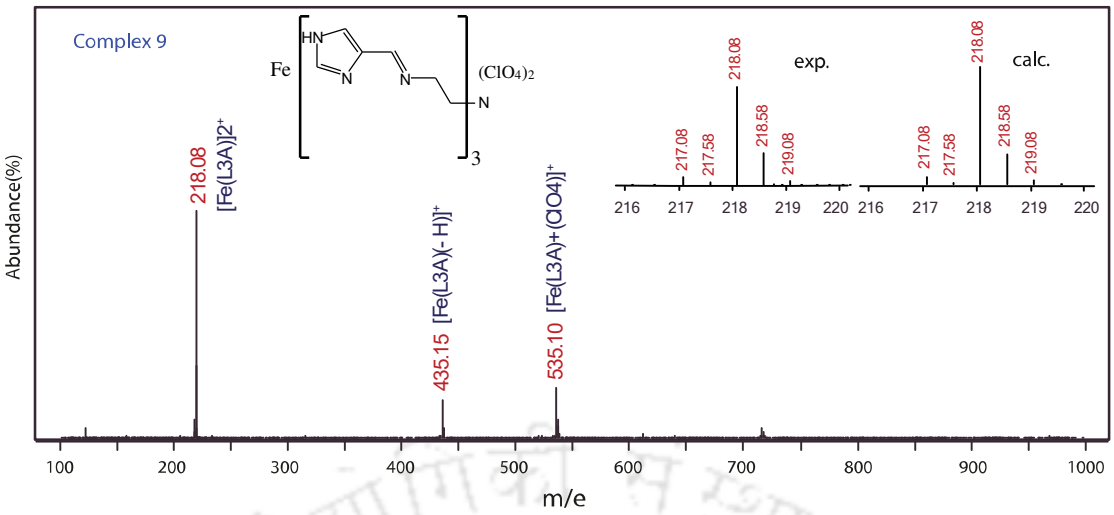

Figure S19. The ESI-MS spectrum of **9** in acetonitrile.

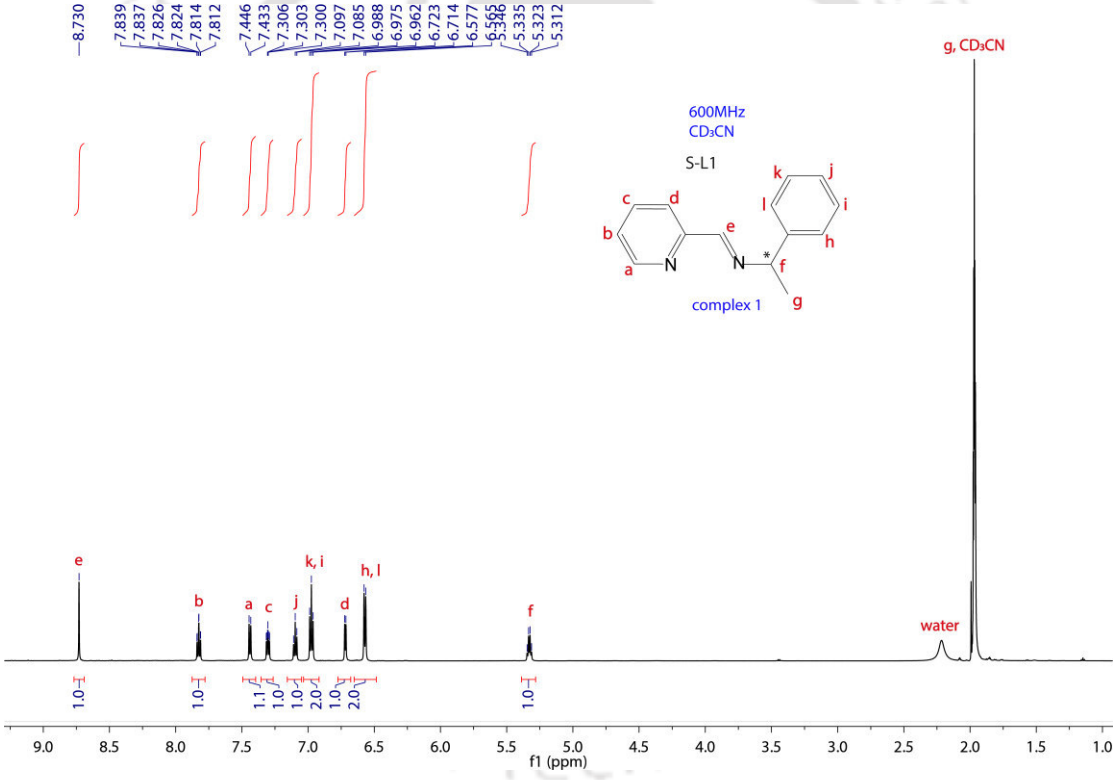

Figure S20. ^{1}HNMR spectrum of **1** in CD_3CN.

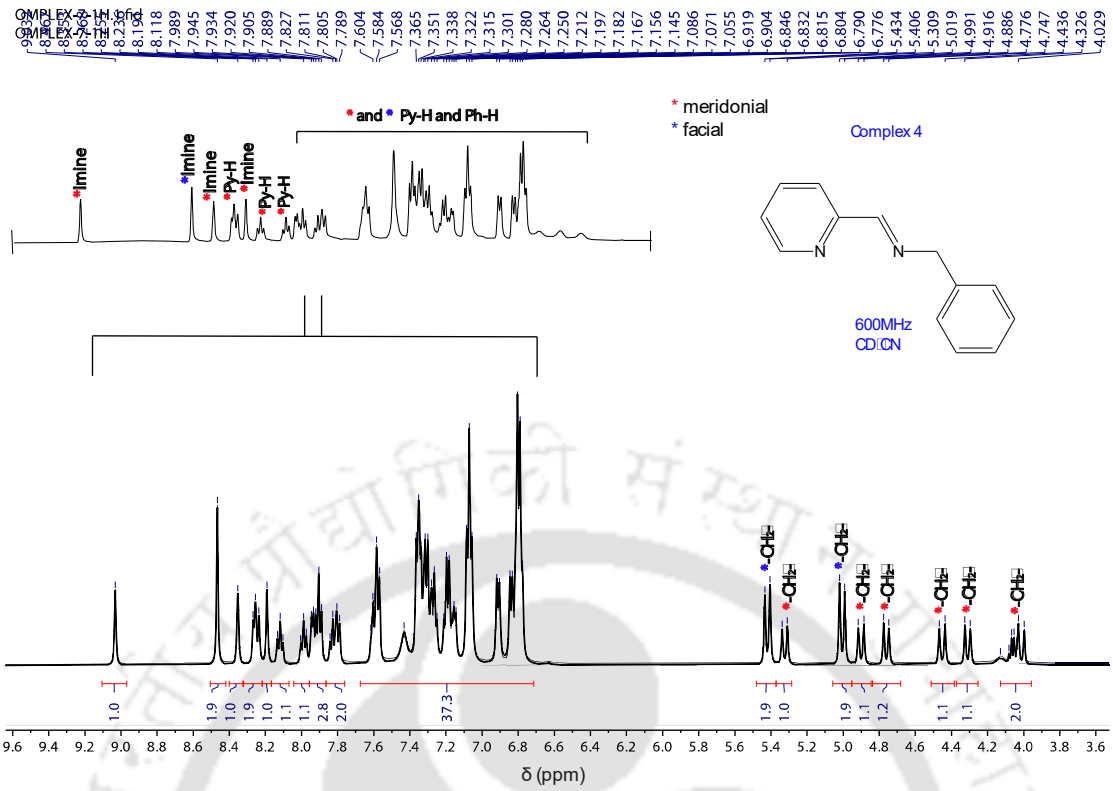

Figure S21. ^{1}HNMR spectrum of **4** in CD_3CN.

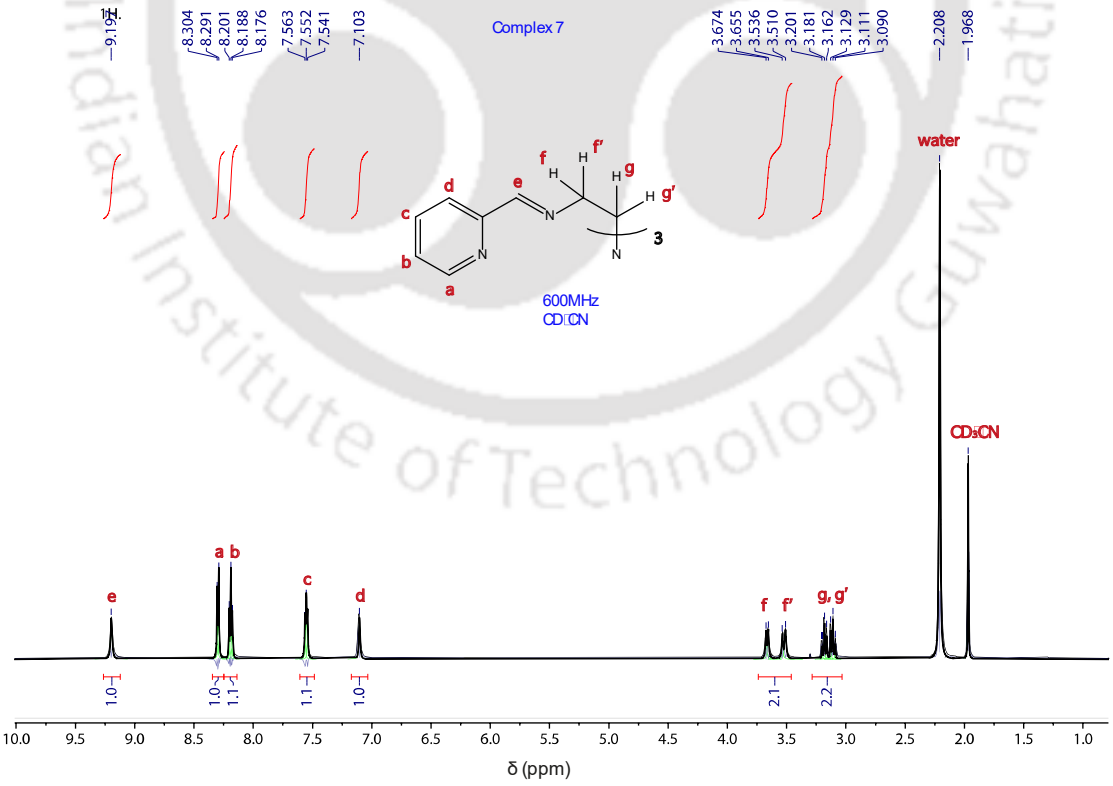

Figure S22. ^{1}HNMR spectrum of **7** in CD_3CN.

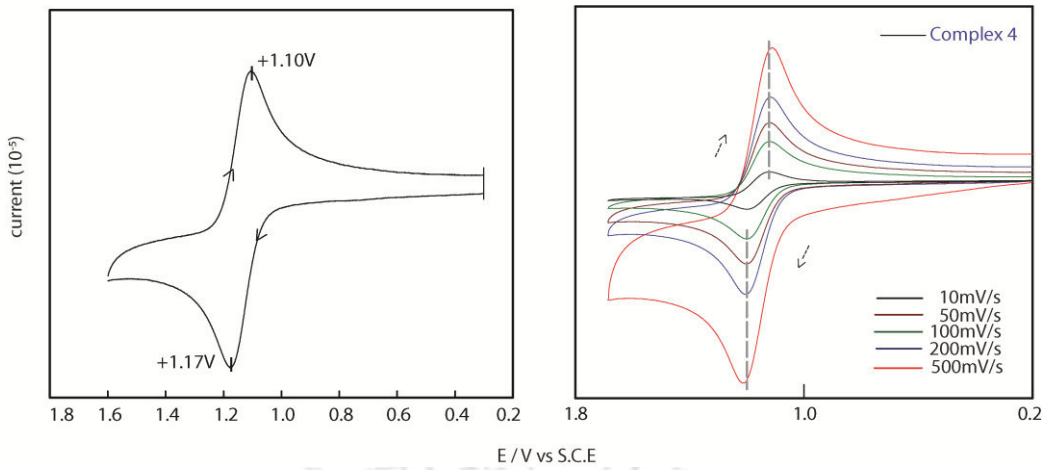

Figure S23. Cyclic Voltammetry diagram plot of Complex **4**. Variable scan rate (mV/s) diagram of the same in acetonitrile.

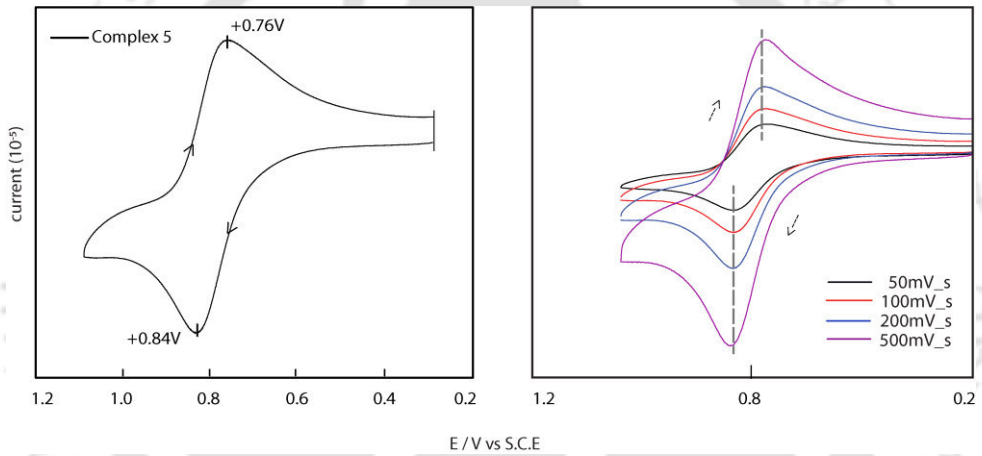

Figure S24. Cyclic Voltammetry diagram plot of Complex **5**. Variable scan rate (mV/s) diagram of the same in acetonitrile.

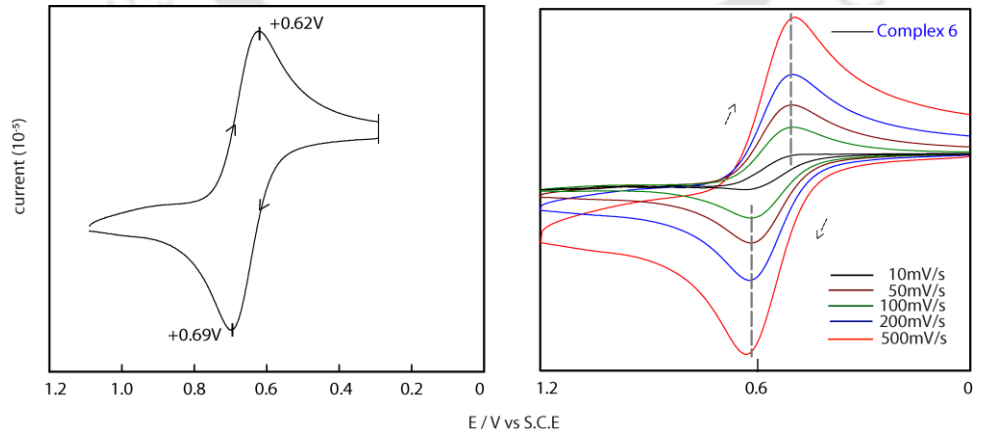

Figure S25. Cyclic Voltammetry diagram plot of Complex **6**. Variable scan rate (mV/s) diagram of the same in acetonitrile.

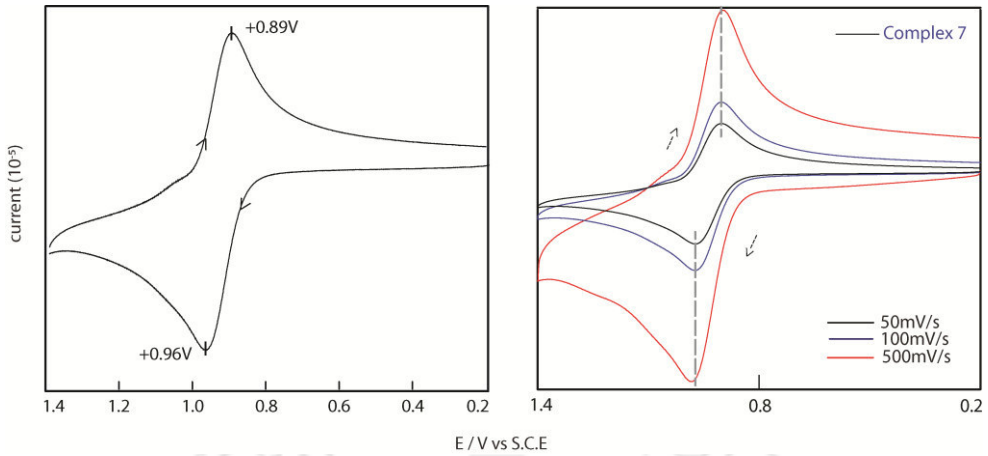

Figure S26. Cyclic Voltammetry diagram plot of Complex **7**. Variable scan rate (mV/s) diagram of the same in acetonitrile.

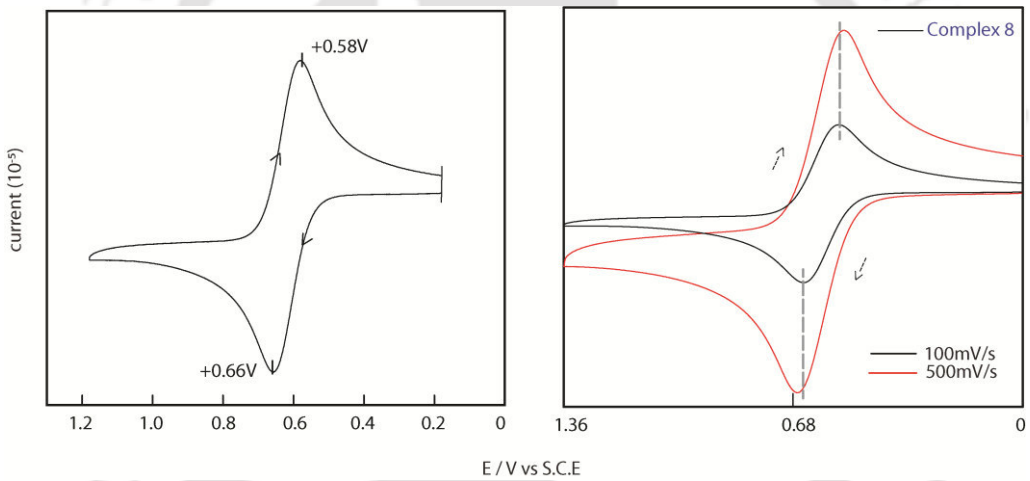

Figure S27. Cyclic Voltammetry diagram plot of Complex **8**. Variable scan rate (mV/s) diagram of the same in acetonitrile.

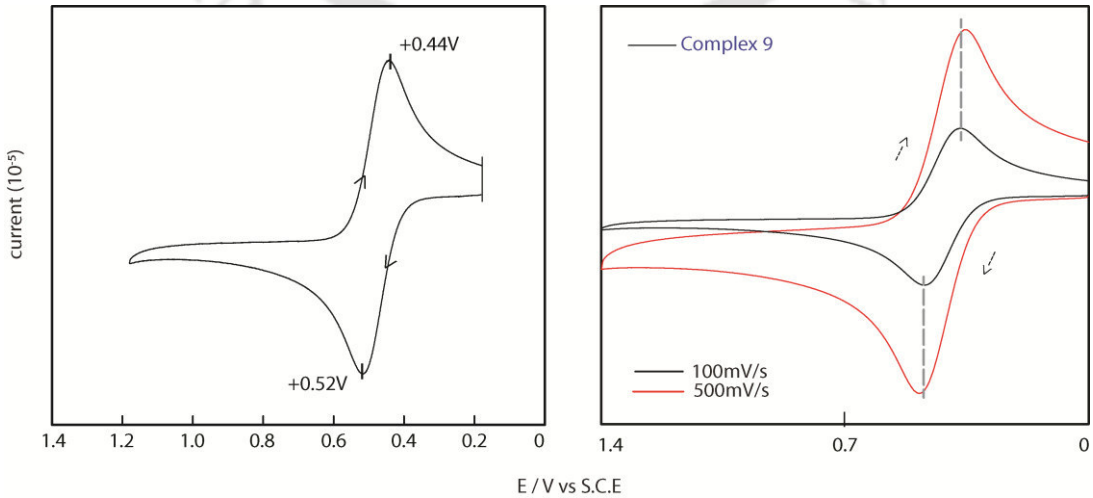

Figure S28. Cyclic Voltammetry diagram plot of Complex **9**. Variable scan rate (mV/s) diagram of the same in acetonitrile.

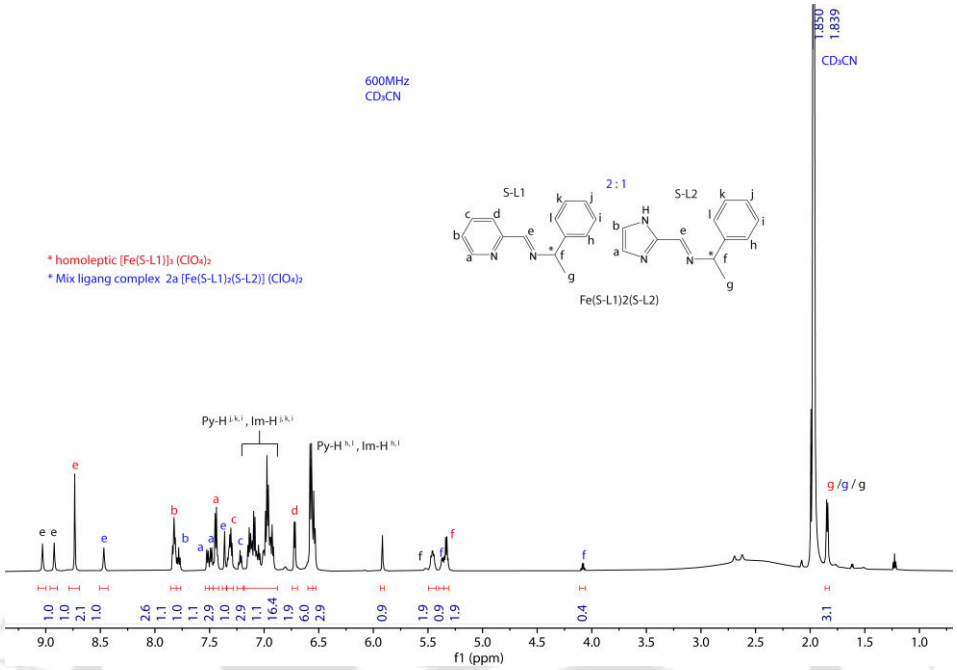

Figure S29. ^{1}H-NMR spectrum of Complex **2b** [Fe(*S*-L1)$_2$(*S*-L2)]$^{2+}$ in acetonitrile.

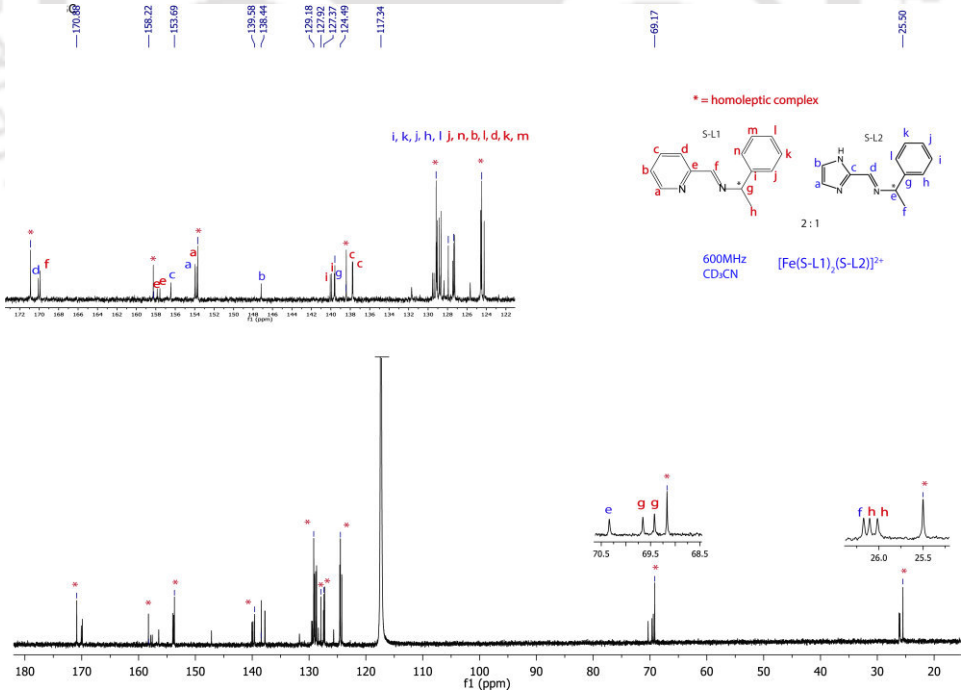

Figure S30. ^{13}C-NMR spectrum of Complex **2b** [Fe(*S*-L1)$_2$(*S*-L2)]$^{2+}$ in acetonitrile.

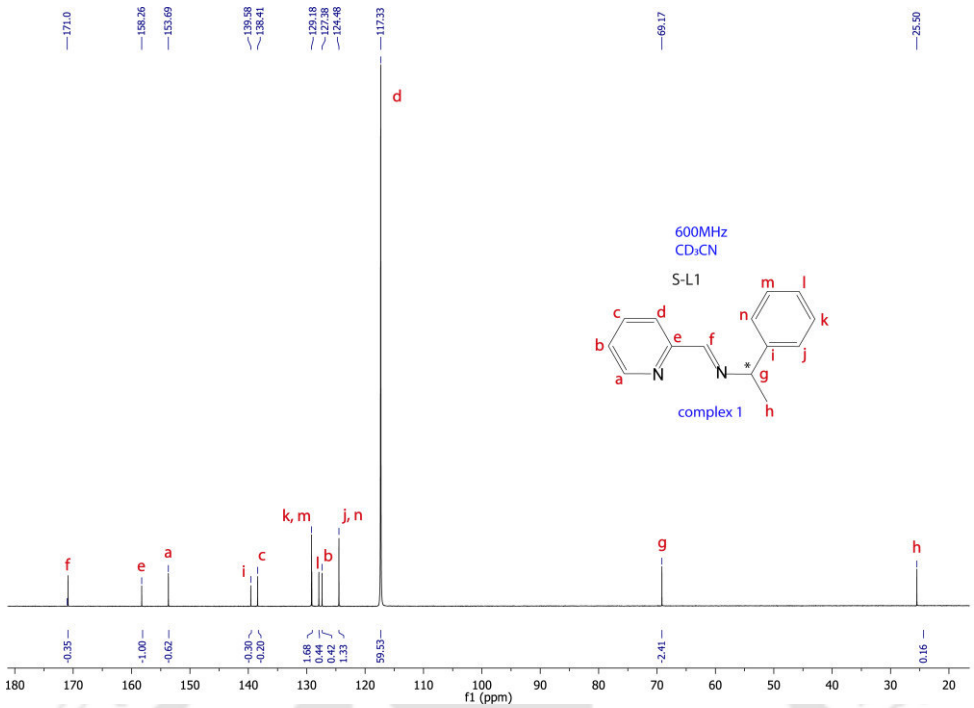

Figure S31. ^{13}C-NMR spectrum of Complex **1** $[Fe(S\text{-}L1)_3]^{2+}$ in acetonitrile.

Publications and Conferences

Research Papers:

(1) "Chiral resolution of 1-phenylethylamine in Schiff base form within a mixed ligand complex of Ni (II)". **Sounak Bhattacharya** and Manabendra Ray. *Inorg. Chim. Acta.,* **2020**, *502*, 119338. *Published.*

(2) Substitution of pyridine with imidazole derivatives within Ni (II) and Fe (II) complexes and their effect on chiral resolution, solution spin state and electrochemical properties. **Sounak Bhattacharya** and Manabendra Ray. *Manuscript submitted.*

(3) Chiral resolution of 1-phenylethylamine in kinetically labile Fe (II) complex and its dependence on its magnetic and electrochemical properties. **Sounak Bhattacharya** and Manabendra Ray. *Manuscript under preparation.*

Conferences:

(1) "FICS 2016", Department of Chemistry, Indian Institute of Technology Guwahati. '*Chiral recognition of 1-amino-2-propanol by a binuclear Ni-complex through non-covalent host-guest interaction'*.

(2) "Chem Convene 2017", Department of Chemistry, Indian Institute of Technology Guwahati. '*Chiral recognition of 1-amino-2-propanol by a binuclear Ni-complex through non-covalent host-guest interaction'*.

(3) "Modern Trends in Inorganic Chemistry, MTIC-XVII, 2017, Pune" held at CSIR-NCL, Pune, IISER, 2017. '*Recognition and Resolution of Multiple Biogenic Amino Alcohols Using Ni (II) Anionic Complex as Host'*.

(4) "Modern Trends in Inorganic Chemistry, MTIC-XVIII, 2019, Guwahati" held at IIT Guwahati, Guwahati, Assam, 2019. "*Chiral Resolution of 1-phenylethylamine in Schiff base form within a mixed ligand complex of Ni (II)*".